POLITECNICO
MILANO 1863

SCUOLA DI INGEGNERIA INDUSTRIALE
E DELL'INFORMAZIONE

Reconstruction of right ventricle morphology and displacements by merging time resolved MRI series

Tesi di Laurea Magistrale in
Biomedical Engineering - Ingegneria Biomedica

Author: **Chiara Gallenda**

Student ID: 953412
Advisor: Prof. Christian Vergara
Co-advisors: Ing. Francesca Renzi
Academic Year: 2022-23

Abstract

In the present work, three-dimensional reconstruction of cardiac ventricles during the entire cardiac cycle in healthy and pathological cases has been carried out with a new effective and accurate reconstruction method: the Multi-Series Morphing (MSMorph) technique is based on merged information from multiple magnetic resonance images to obtain accurate models, with increased automatization of the segmentation and endocardial generation processes that can reduce the reconstruction time. Through these models, shape and motion of cardiac ventricles are at disposal for evaluation of different clinical scenarios.

Analysis of results comprehends a comparison with right ventricle models obtained used a standard reconstruction technique found in literature and the gold standard segmentation method, completely manual.

Reconstruction of right and left ventricles in an healthy case with the two variants of the method, MSMorph II and MSMorph III, were obtained and evaluated through estimation of clinically relevant parameters. The reconstructed models of right ventricle, whose clinical attention is increasingly growing, can represent a powerful diagnostic tool for the assessment of function and dysfunction of the heart, especially in presence of complex shapes of cardiac chambers due to congenital heart diseases. For this reason, the 3D model of right ventricle in a heart affected by Tetralogy of Fallot was generated and analyzed to comprehend the differences with respect to the healthy case.

Keywords: Right ventricle; MRI-series merging; cardiac MRI-based 3D reconstruction; Tetralogy of Fallot

Abstract in lingua italiana

In questo lavoro, è stata ottenuta la ricostruzione tridimensionale di ventricoli cardiaci durante l'intero ciclo cardiaco in caso di cuore sano o patologico tramite una nuova efficiente ed accurata tecnica: il metodo Multi-Series Morphing si basa sulla fusione di diverse serie di immagini, ottenute da risonanza magnetica cardiaca, per ottenere modelli accurati e incrementare l'automatizzazione dei processi di segmentazione e generazione dell'endocardio, riducendo quindi i complessivi tempi di ricostruzione. Con questi modelli, per la valutazione di differenti scenari clinici vi sono a disposizione la morfologia e il movimento dei ventricoli cardiaci.
L'analisi dei risultati è comprensiva anche di un confronto con modelli del ventricolo destro ottenuti tramite una tecnica standard di ricostruzione presente in letteratura e con il metodo di segmentazione di riferimento, completamente manuale.
Le ricostruzioni 3D di ventricoli destri e sinistri di un paziente sano sono state ottenute utilizzando le due varianti, MSMorph II and MSMorph III, del metodo sopracitato e sono state analizzate tramite l'ottenimento di parametri rilevanti dal punto di vista clinico. I modelli tridimensionali del ventricolo destro, la cui attenzione dal punto di vista clinico è in continuo aumento, possono rappresentare un potente mezzo diagnostico nella valutazione della funzionalità o di disfunzioni del cuore, specialmente in casi di morfologie complesse delle strutture cardiache dovute alla presenza di malattie cardiache congenite. Per questo motivo, è stato generato un modello tridimensionale di ventricolo destro di paziente affetto da Tetralogia di Fallot, per essere analizzato in termini di differenze con il caso sano.

Parole chiave: Ventricolo destro; Fusione di immagini MRI; Ricostruzione cardiaca tridimensionale basata su immagini MRI; Tetralogia di Fallot

Contents

1 | Reconstruction of Cardiac Ventricles

Among all, cardiovascular diseases (CVDs) represent the principal cause of death globally: 17.9 million people died from CVDs in 2019, representing 32% of all global deaths [6]. Heart and vessels, constituting the cardiovascular system, can be damaged by multiple risk factors and conditions to culminate in heart attacks and strokes, acute events that have to be detected in time. The impact of CVDs extends also to other clinical scenarios: in the recent COVID-19 pandemic that had caused more than 6 milion deaths worldwide [10], a correlation between severity of the respiratory disease or development of fatal complications in patients infected by SARS-CoV-2 virus and the underlying presence of CVDs was assessed for every group age[16]. Research in the cardiovascular field is increasingly active for the need to investigate the development of CVDs, with tendency for noninvasive personalized medicine.
Specifically, cardiovascular diseases (CVDs) affects the structure and functionality of both heart and vessels: the proper functionality of the heart is necessary for pumping of the blood in circulation, but risk factors of CVDs can bring to heart attacks or heart failures. Indeed, cardiovascular diseases includes various clinical pathological conditions, some of which can affect directly the heart:

- Coronary heart disease affects coronary arteries, that supply the heart muscle: an obstruction in these vessels can prevent the flow of blood that oxygenates the cardiac muscle, causing a myocardial infarction also called heart attack.
- Congenital heart disease, which consists in anatomical defect in the heart structure: the alteration of the structure modifies the physiological function, as they are strictly

correlated, resulting in a modified hemodynamics. The anomalies, present at birth, can be very different with multiple levels of severity.

- Valvular heart disease is related to the malfunctioning, due to aging or defects, of the cardiac valves: with opening and closing generated by pressure levels, they control the blood flow through cardiac chambers and towards principal arteries connected with the two circulation systems. Blood enters in the two receiving chambers, right and left atrium, and is ejected in the corresponding ventricles, that have the essential function of pumping it towards respectively pulmonary artery, connected to lungs through pulmonary circulation, and aorta, the starting point of the systemic circulation. These diseases can be caused by inflammatory factors, representing the rheumatic heart disease.

The functioning of the whole heart can be modified or impeded in presence of CVDs and prevention can improve the management of these pathologies: the estimation from medical imaging of clinically relevant parameters can be useful for diagnostic purposes but lacking of three-dimensional visualization, can be integrated through the use of computational tools. The 3D reconstruction of cardiac chambers, especially ventricles with their essential pumping function, can improve and support the diagnostic and the surgical planning, representing a further enhancement in the research field.

1.1. Cardiac Ventricles

Among cardiac chambers, ventricles are essential for the pumping action of the heart, intended as the ability of the cardiac muscle to inject blood at sufficient pressure value in circulation: with their contraction, at ejection phase in cardiac cycle, right and left ventricles can be considered as mechanical pumps themselves, at service of blood circulation. Their motion and change in shape reflect their functionality, that can be altered in pathological cases: congenital heart diseases as Tetralogy of Fallot (ToF) can impair the structure and function of ventricles, in particular of the right ventricle for ToF. The present work is especially focused on the right ventricle, since the right heart has been less investigated with respect to left heart, even if its functionality has a great impact on the overall heart functioning.

1.1.1. Anatomy and physiology of cardiac ventricles

The heart is the organ responsible for the circulation of blood all over the body: it consists in four chambers, two atria and two ventricles. In particular, atria are smaller and receive the blood, while ventricles are bigger and responsible for the pumping function, as they eject blood in different circulations, as it will be explained.
For this reason, when studying the heart, the most attention is paid to the ventricles: they consist in pumps that leads the blood to circulate, as represented in Figure 1.1. In particular, the left ventricle (LV) has been the most studied with respect to the right ventricle (RV): the oxygenated blood ejected in the aorta during systole by the left ventricle reaches all the tissues of the body through systemic circulation, allowing all cells to have enough nutrients and oxygen to survive and function. At rest, the pumping volume of the heart is 5 l/min in adults. The blood flows towards peripheral vessels to exchange nutrients and gases with all the cells of all tissues through arteries, while it flows back to the heart in veins, entering in the right atrium (RA). Then, the right ventricle pumps, during systole, the non-oxygenated blood in the pulmonary circulation: the blood is sent to the lungs where it becomes oxygenated, leaking the metabolic wastes as the carbon dioxide. It proceeds and enters again in the heart through the pulmonary veins in the left atrium (LA).

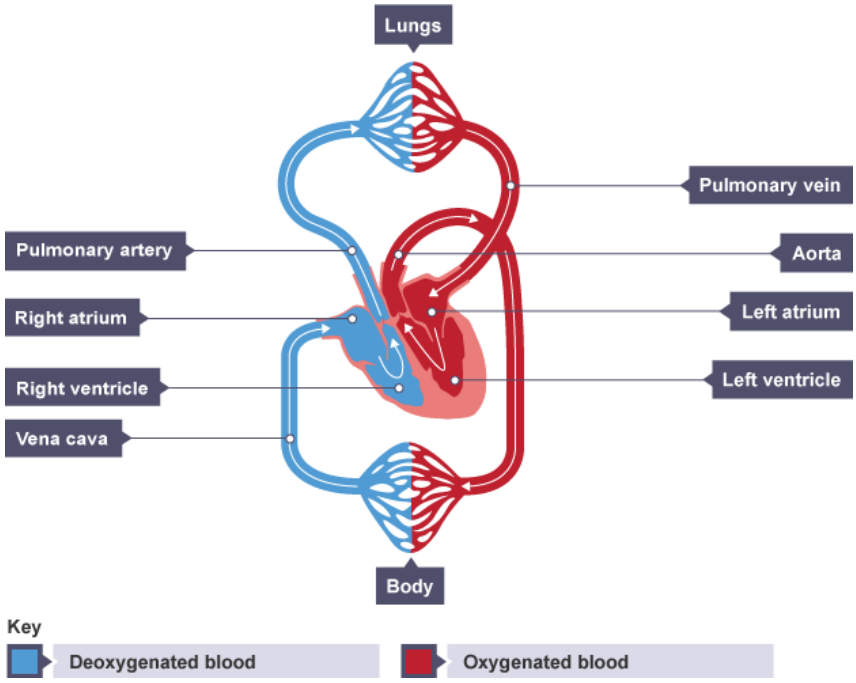

Figure 1.1: Scheme of cardiovascular system: the pulmonary circulation is represented by the network of vessels connecting heart and lungs, the systemic circulation connects heart and body instead.

These blood movements in the cardiac chambers are possible by the opening of the four valves: the mitral and tricuspid valves separates atrium and ventricle of respectively left and right heart, while the aortic and pulmonary valves divides the ventricle from the outlet vessel, respectively aorta and pulmonary artery in left and right heart. A representation of the valves is given by Figure 1.2.

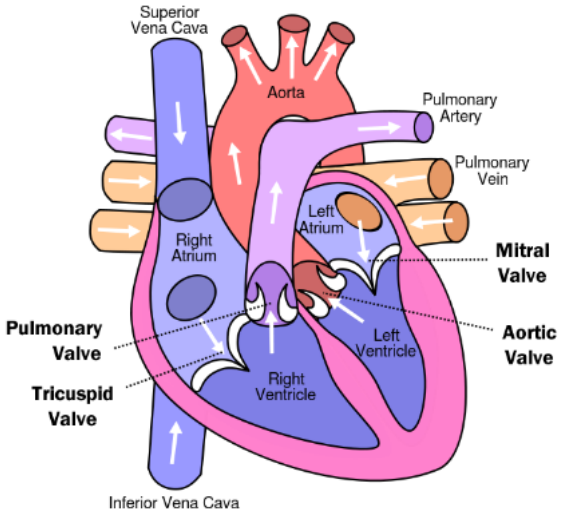

Figure 1.2: Position of heart valves with respect to cardiac chambers

Both ventricles play a major role in the overall functioning of the organism with their blood-pumping action, which is actually carried out in parallel circulations that are loaded with significantly different pressures: the left ventricle generates the higher pressure as it provides the pumping of blood in all the cardiovascular network of vessels, even the peripheral part of it; the right ventricle instead works at lower pressure, as connected only to the lungs through the pulmonary circulation that is characterized by a mean pulmonary artery pressure (MPAP) value of 11-17 mm Hg [58] with respect to the systemic circulation, in which the mean arterial pressure (MAP) is 65–100mm Hg [95]. The difference in pressure is expressed also by the difference of thickness of the two ventricles, since the RV has the thinnest free wall.

In the recent years the importance of the right ventricle has been greatly increased: its crucial role in the clinical scene has emerged, as it was understood to have relevance in different clinical scenarios.

The abnormality of the right ventricle can be a symptom of other pathological conditions: for example, cardiomyopathies usually are considered in terms of impairment of the LV, while they can be characterized in a complete perspective by considering the biventricular involvement. Dilated cardiomyopathies consists in dilation of the LV but actually of both ventricles, that can lower the myocardial contractility also of RV [25] for the ventricular

interdependency and impair the RV diastolic function due to dilation. Hypertrophic cardiomyopathies instead are defined as a thickening of the LV wall, while RV hypertrophy can also occur and if severe can be predictor of different diseases. [25]
Yet, the functional and anatomical difference of right and left ventricles makes impossible to obtain information about the right heart by studying only the left heart, as instead previously was thought to be sufficient.
As an example, considering the heart dysfunctions generated by COVID-19, the right heart was seriously affected in ill patients, while LV seemed to not have clear alterations due to the virus. Non-survivors to COVID-19 was detected to have dilated right heart chambers and reduced RV functionality while size and function of the left heart chambers were in the normal range. [29]
Morphologically, the difference between the two ventricles is related to different parameters: the volume of LV is lower of about 10-15 % with respect to the RV, but the mass of LV is instead higher; the thickness of the free wall in RV is about 4 mm, 1/3 with respect to the LV [95] value, due to the lower pressure at which the right ventricle is submitted. Difference in thickness is displayed in Figure 1.3.

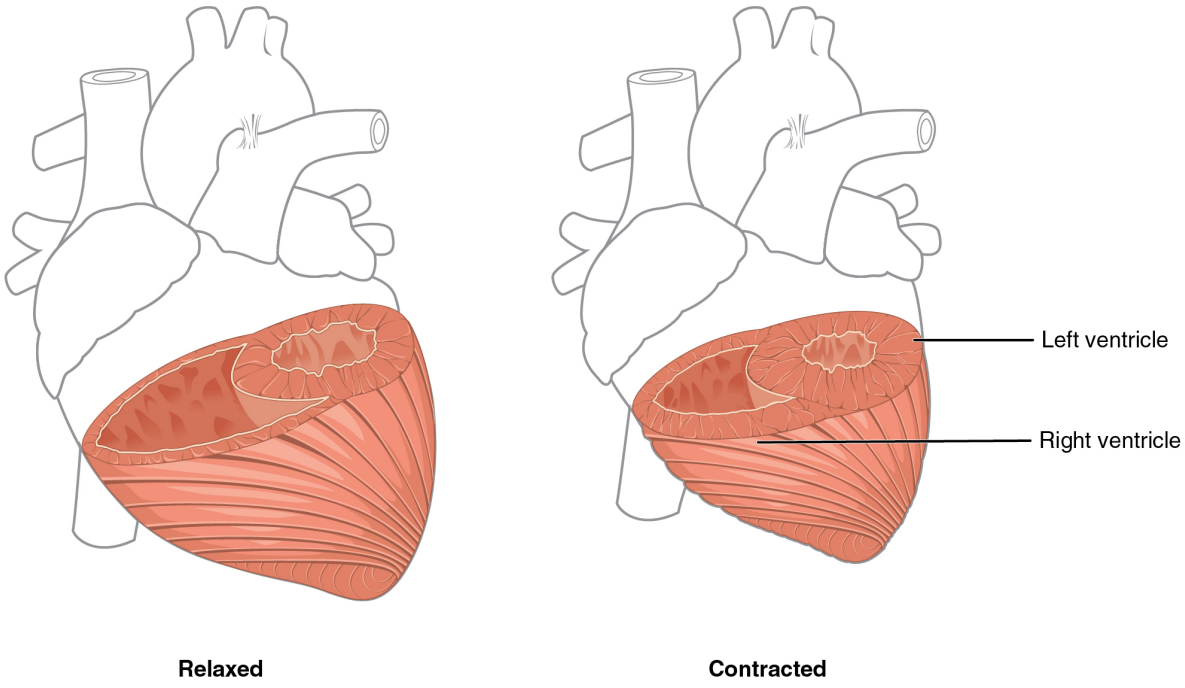

Figure 1.3: Morphology differences between right and left ventricles: thickness is lower in the free wall of RV and cross-sectional shape of RV is more complex and wrapped around the LV [2]

From the anatomical point of view, the RV has presence of uniformly coarse trabeculations, especially at the apex, while LV trabeculations are finer. The outflow tract is fully muscular while in LV there's more continuity with the aorta. Myocardium of both ventricles, formed by smaller cardiomyocytes and more collagen in RV, is layered: the subendocardial layer, with a preferential longitudinal direction of myocytes, and the superficial layer, with a circumferential disposition of myocytes, are common, visible in Figure 1.4, but in the RV the middle layer can not be well distinguished [90], except from the outflow tract.

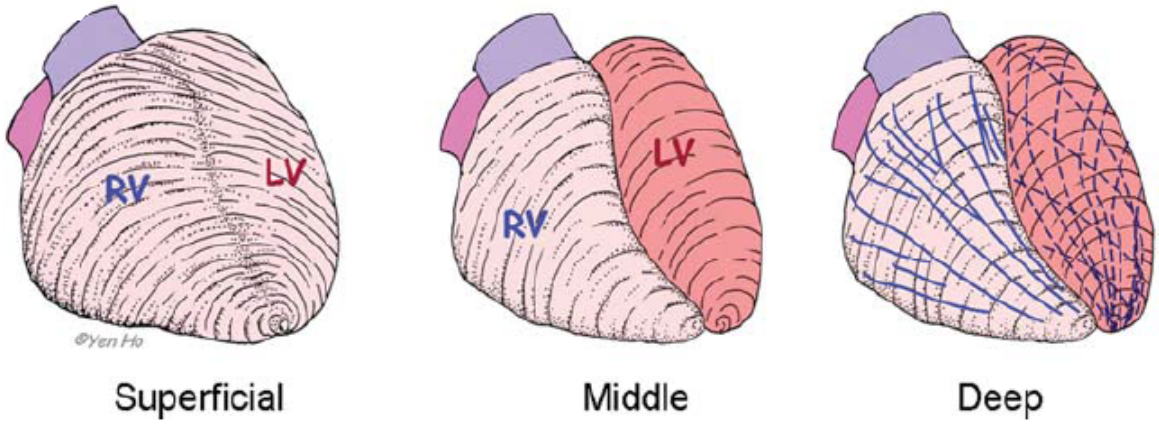

Figure 1.4: Diagrams, from [43], of the myocardial fiber arrangement in right and left ventricles: the superficial subepicardial layer with oblique circumferential disposition of fibers, the middle layer that has a circumferential arrangement of aggregates of myocytes and the subendocardial deep layer, with a longitudinal main direction of fibers

Summarizing the principal anatomical and morphological differences between RV and LV:

- Morphology: with respect to the ellipsoidal morphology of LV, RV has a more complex shape with a triangular geometry if it is seen by side. In a top view, at the base it assumes a convex shape, wrapping around the circular LV while, at the apex level, both are characterized by a circular form. The complexity of RV morphology is related to the irregular shape visible from all views and levels, in comparison with the LV morphology that remains quite constant from apex to base and regular in a three-dimensional point of view.
- Size: RV has an higher volume with respect to LV
- Thickness: RV has a thinner free-wall with respect to LV
- Working pressure: RV works at lower pressure of pulmonary circulation, while LV works at higher pressure of systemic circulation. Since the pulmonary vascular

resistance is also lower, about 10% [19] of the systemic one, the RV consumption of oxygen is lower.

- Cross-section: RV cross-section from apex to base becomes more triangular and wrapped around LV, while LV cross-section remains ring-shaped along the entire longitudinal plane.
- Myocardial architecture: myocardium of RV, in which the middle circumferential layer is not precisely detectable, has more and coarse trabeculations, unlike LV that is less trabeculated. Fiber organization is different and correlated to different muscle contractions: the mayor difference is related to the middle myocardial layer, arranged in circumferential direction: in LV it represents the thickest layer, allowing a mostly circumferential and radial contraction with torsion. Instead, in RV the lack of this layer leads to a ventricle contraction that can be considered as a peristaltic movement from inlet to outlet [36].
- Cardiomyocites: in RV are smaller and more longitudinally oriented.
- Motion: the different fiber arrangement in the myocardium is reflected in different motion of cardiac chambers: the movement of contraction is mostly related to longitudinal shortening in RV [90] for major presence of longitudinally oriented fibers, while shortening in LV contraction is mostly due to circumferential contraction that results in a torsion movement of the ventricle.

The morphological and functional difference among the ventricles can be addressed to different embryological origin of the two ventricles but also for the different hemodynamics. However, the process of excitation and contraction of cardiomyocites of the two chambers is considered equal and there's also a functional interdependence between ventricles in the systolic and diastolic function, as they share pericardial space and circumferential myocytes of the epicardium [90].

1.1.2. Motion of cardiac ventricles

In the assessment of the cardiac ventricles' function, the motion of these cardiac chambers represents an important parameter: there's a relationship between function and structure that links the motion of the heart to its functionality. The capability of narrowing, widening, shortening, lengthening but also twisting and uncoiling can be studied also to predict how they can be affected by diseases.
Considering the left ventricle, a detailed description of cardiac motion correlated to the

anatomical structure can be found in [23]. In particular, the ventricular movements are generated by the contraction and relaxation of overlapping fibers that can move in different directions, resulting in an overall dominant movement of the chambers related to the power of each layer of fibers, with a precise velocity. LV ejection can be addressed to the thickening of the wall and the shortening and narrowing of the cavity in the ventricle, but also torsion happens during this phase. After ejection, the movements are reversed for the heart to recover the original configuration: the cavity lengthens and becomes wider and there's a rotation to recover from the torsion movement. These movements prepare the LV for the rapid filling, that is recognized by cardiologists to be a consequence of the sequence of a torsion during ejection and an uncoiling in the post-ejection phase of the ventricle. Before the opening of the mitral valve, a lengthening of the ventricle takes place. After the rapid ventricle filling, it starts to lengthen and becomes wider but also rotate when the pressure in the ventricle becomes lower than the pressure in atrium.

The connection between motion and structure can be detailed by considering the Wiggers Diagrams for right and left ventricles, that represents different parameters of cardiac physiology and their evolution during the time of cardiac cycle. The alternation of relaxation and contraction of the heart, in the two main phases of cardiac cycle which are respectively diastole and systole, generates the pumping motion able to inject the blood in pulmonary and systemic circulations. These motions generated by conduction of electrical signals in the cardiac muscle result in pressure changes of blood, that define the opening and closure of heart valves. Wiggers diagrams, in Figure 1.5, represents the evolution of pressure and volume during the different phases of cardiac cycle, that certainly have different values from right to left heart: the right heart, as previously mentioned in this work, follows the same pattern of events but working at lower pressure with respect to the left heart. The diagrams represents the cardiac cycle starting from the diastolic phase, representing the ventricular filling: the atrial pressure exceeds the ventricular pressure so the atrio-ventricular (AV) valves are open, generating a passive filling of ventricles.
The consecutive phases of cardiac cycle are:

- Atrial Systole: with *atrial systole*, intended as the contraction of atria chambers, the systolic phase starts and ventricles are actively filled. Contraction of cardiac chambers induce their pressure to increase: with atrial contraction the atrial pressure grows reaching a peak, then it decreases until going below the ventricular pressure value. This reversed pressure gradient generates the closing of atrioventricular valves after which the *isovolumetric contraction* phase begins.
- Isovolumetric Contraction: the ventricular pressure rapidly rises due to contraction

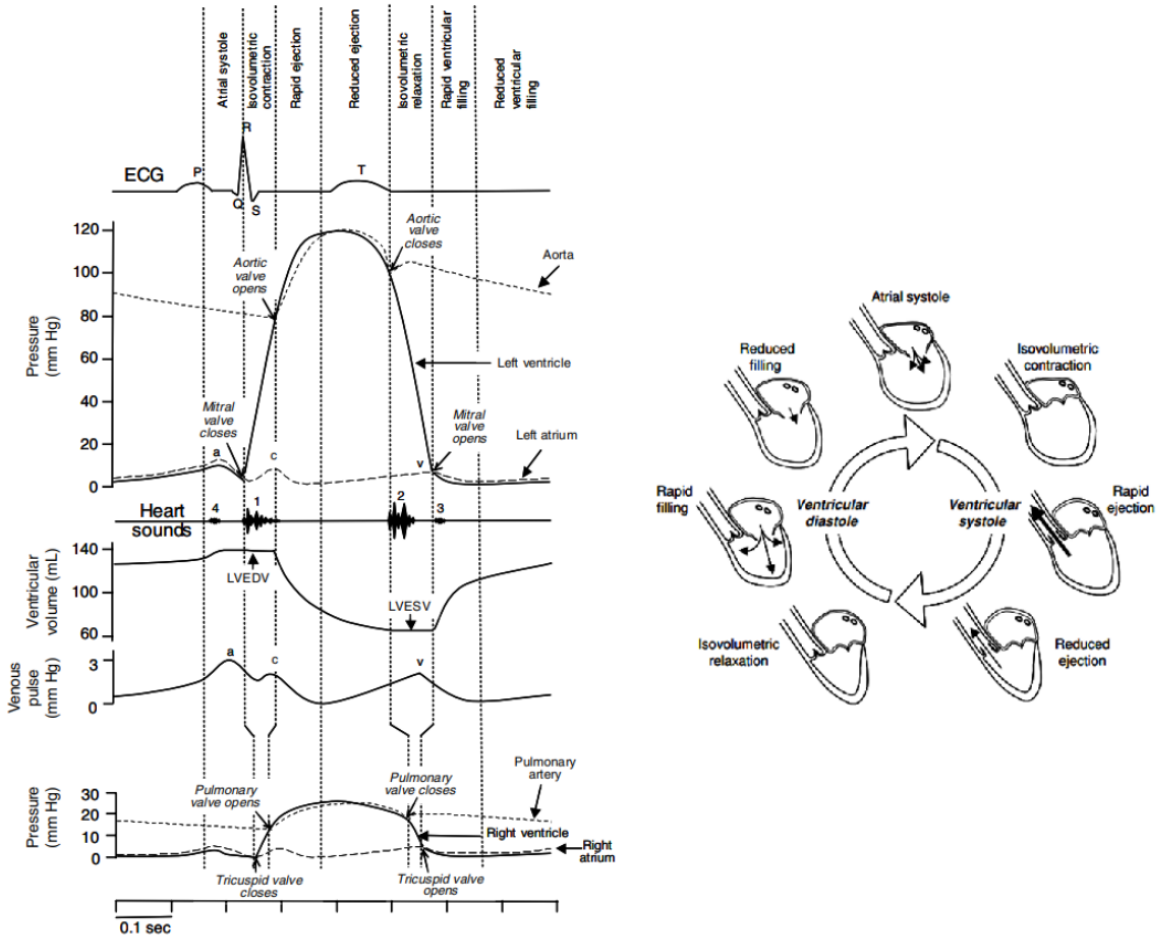

Figure 1.5: Wiggers diagrams for left heart (top, left) and right heart (bottom,left) and scheme of the phases of cardiac cycle (right) [28]

of the chamber, but remains under the aortic pressure or the pulmonary artery pressure keeping semilunar valves to remain closed and so the ventricle's volume constant.

- Rapid Ejection and Reduced Ejection: as the increasing ventricular pressure exceeds the aortic pressure, in left heart, or pressure in pulmonary artery, in the right heart, semilunar valves open and blood is ejected in aorta or pulmonary artery respectively: this phase is called *rapid ejection*, followed by another phase, the *reduced ejection*. In particular, the decrease of ventricular pressure makes the ejection process to be slower in the reduced phase, with the end of the systolic function and beginning of diastole as the semilunar valves close due to the reduction of ventricular pressure below the pressure in the outflow tract.

- Isovolumetric Relaxation: As in case of isovolumetric contraction, where the blood flow was impeded for the closure of the valves keeping the volume constant, the

isovolumetric relaxation phase consists in a rapid decrease of ventricular pressure, not below the atrial pressure value, with relaxation of the cardiac chamber.

- Ventricular Filling: When the atrial pressure, that is slowly rising, goes beyond the ventricular pressure value, atrio-ventricular valves open, allowing the blood to flow and fill the ventricles.

The cardiac cycle, with a physiological duration of 0.8s, starts again with another atrial systole.

In left and right heart the same process of contraction and relaxation happens simultaneously, with difference in pressure values regulating the opening and closing of heart valves: atrio-ventricular valves are respectively mitral and tricuspid valve in left and right heart, while correspondent semilunar valves are aortic and pulmonary valves. As the Wiggers diagram reflects, motion of cardiac chambers is essential to the correct functioning of the heart: considering the increased pressure values under which the left heart works continuously, the focus of research was usually reserved to left chambers, especially left ventricle.

As highlighted, the computational study of the right ventricle was less considered in the past but now the appreciation to its importance is rising, since RV dysfunction can be a sign to determine outcomes of severe diseases. In particular, the RV ejection fraction is a risk factor in patients with moderate left heart failure (LHF) [41]. Also, abnormalities in the right ventricle structure can predict the future development of the right heart failure (RHF), which has recognized impact in the development of pulmonary hypertension and congenital heart disease.
For this reason, the characterization of the right heart has importance in terms of quantification of pulmonary hemodynamics and assessment of the RV function to predict other complications. From this consideration, the need of imaging techniques applied to the RV becomes clear as the RV can not be modeled using a simple geometric shape while LV is long and conical with a circular cross-section. The RV cross section is similar to a triangle at the apex but towards the base it becomes wrapped around the left ventricle with a particular shape.
However, it is important to assess the RV motion since the deformation of the myocardium in terms of shortening and thickening of the free wall results at the end in the RV ejection that we have seen to be key factor in predicting heart failure but also in predicting mortality after infarction of the myocardium [41].
Cardiac MRI represents a technique considered as Gold Standard in evaluation of the RV function and motion, with favorable availability. Moreover, in the assessment of the RV function another interesting parameter is the RV volume, but techniques as echocardiog-

raphy, CT or MRI are used to measure in particular the right atrium size while the use of MRI technique on the right ventricle to obtain the volume is poorly used and need to be eventually further explored [41].
The tridimensional reconstruction of the heart MRI image-based can be a powerful tool to analyse the RV function to obtain both RV volume and EF, but also can be used to analyse the RV motion.

1.2. Tetralogy of Fallot

Among the possible scenarios of right heart hypertrophy, it can occur in presence of a congenital disease called Tetralogy of Fallot (ToF), characterized by an interventricular communication. This malformation can also cause, with different levels of severity, the obstruction of the right ventricular outflow tract: this explains why the Tetralogy of Fallot is called a cyanotic congenital cardiac disease, as the flow of blood to lungs is obstructed. The malformation is actually related to the ventricular septum, which in normal conditions let the ventricles to be perfectly separated: in the case of these patients, a hole is present in the septum, leading also to a biventricular connection of the aortic outlet tract, known as aortic root. The predominance flow of blood goes usually in the right-to-left direction, leading to deoxygenated blood to be ejected directly into the systemic circulation [17]. The difference with respect to a normal heart can be observed in Figures 1.6, 1.7.

The surgical treatment of this malformation consists in ventriculotomy with an eventual transannular patch (TAP) to repair the ventricular septal defect (VSD) or with an atriotomy combined with incision of the pulmonary valve to reduce the right ventricular outflow tract obstruction (RVOTO), as represented in Figure 1.8, and TAP can be still necessary if the annulus of the pulmonary valve is small [99].

ToF represents the most common type of cyanotic congenital heart disease accounting for the 7-10% of all congenital cardiac malformations, with an incidence of 3 of every 10.000 live births[99]. The surgical repair has improved the probability of survival of ToF patients but the need of many re-interventions, especially if using TAP, and the residual problems represents a challenge for future studies.
In particular, the post-surgical factors that can determine the long-term outcomes of ill patients are severity of RVOTO and of pulmonary regurgitation (PR). These problems both leads to a RV dysfunction, that can bring to heart failure: RVOTO usually cause RV hypertrophy while PR can bring to a progressive RV volume overload.

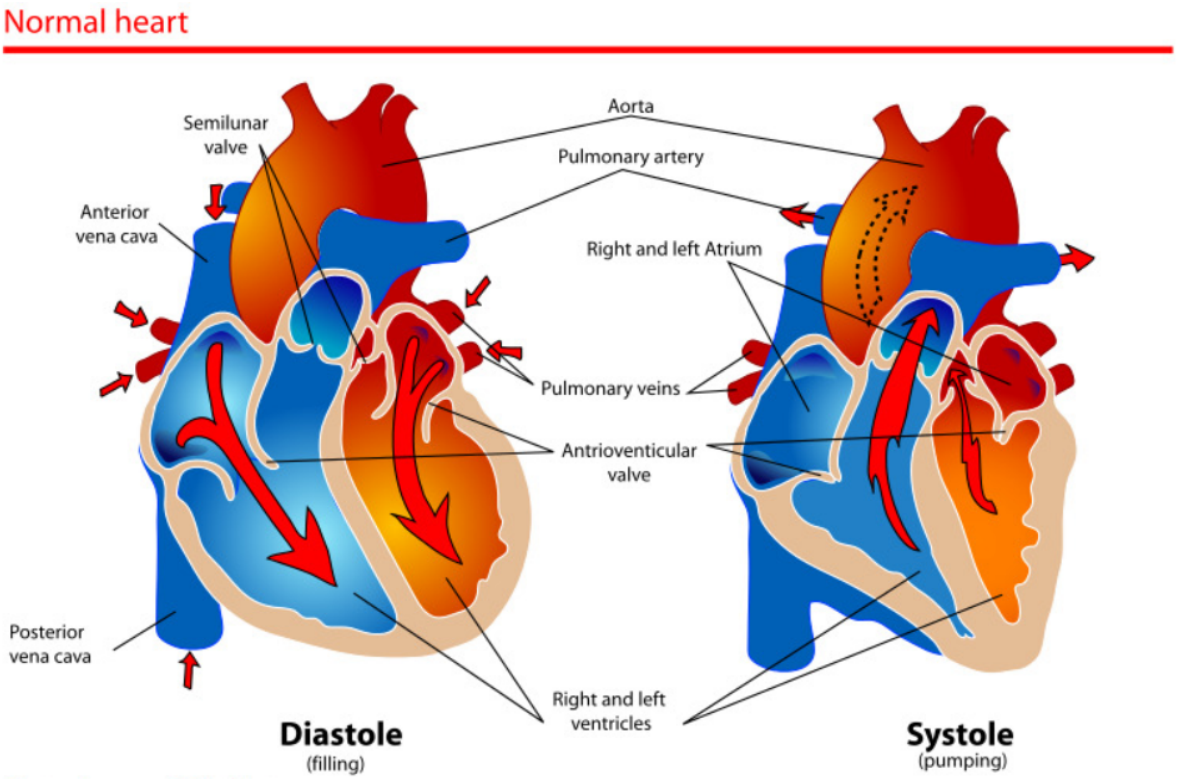

Figure 1.6: Healthy heart during pumping and filling [83]

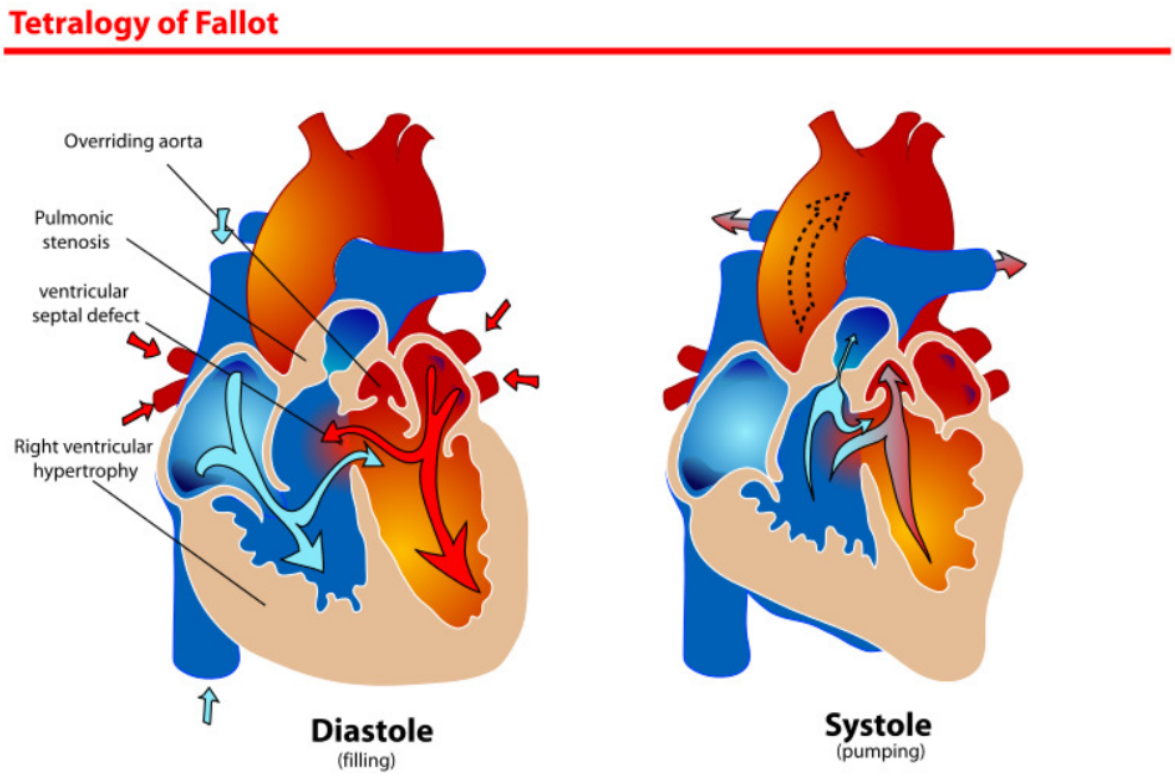

Figure 1.7: Heart suffering from Tetralogy of Fallot during pumping and filling [83]

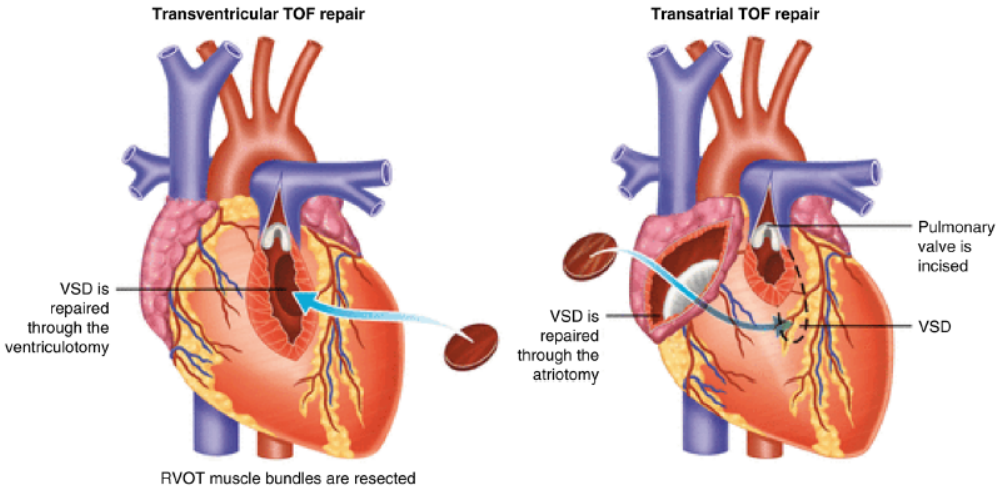

Figure 1.8: Different surgical approaches to ToF repair [99]

Regarding the consequences of PR, the RV is known to be able to adapt in case of volume overload of the ventricle itself, indeed the function of RV is maintained for a certain period of time due to this compensation ability. But the mechanism of this RV remodeling are poorly understood and can fail in some patients, so chronic PR brings in any case to a RV dysfunction. RV dyssynchrony can be also a consequence of repair of ToF and is another factor that can contribute to the dysfunction of the right ventricle.
To assess the RV dysfunction in pathological cases, the motion and the strain of the myocardium can be used: the RV ejection in an healthy subject is usually performed with a longitudinal shortening instead of circumferential contraction. In ToF right ventricles instead a predictive value of longitudinal or circumferential strain is still uncertain [99].
The RV dysfunction after ToF surgical repair comprehends different features that regards the ventriculo-arterial interactions, the atrio-ventricular interactions and the interventricular interactions [11]:

- atrio-ventricular interactions are related to the RV dilations caused by the PR, that can make the RV ejection fraction (RV EF) decrease, sign that the RV systolic function can be altered
- atrio-ventricular interactions are instead represented by the RV diastolic function, intended as the ability to fill the RV which depends on the filling pressure and right atrium functionality: in repaired-ToF signs of RV diastolic dysfunction are the increased RV end-diastolic pressures and the right atrium abnormalities in reservoir and pump action [11];
- interventricular interactions are altered as the presence of the ventricular septal

defect reduces the longitudinally oriented myofibers of RV by impairing the interventricular septum (IVS) in the deep myocardial layer: the RV function can be worsen as it's connected to the longitudinal shortening.

Also, the increased diastolic RV pressure and the geometrical changes of the RV have been discovered to impair also the LV systolic function in 20% of the rTOF patients [11]. The RV dysfunction problem in rTOF patients remains alive as the medical support is not totally effective.

1.3. Reconstruction of Ventricles

The assessment of cardiac chambers' structure and functionality relies on the anatomical knowledge about heart and exploits the use of medical imaging, especially cardiac magnetic resonance (CMR), for visualization and analysis of clinical parameters. A particular process called segmentation can be used to obtain three-dimensional models of cardiac chambers: the diagnostic value of this computational tool has been investigated, with a brief overview on existing segmentation techniques.

1.3.1. Cardiac Reconstruction: a powerful diagnostic tool

Cardiac image-based reconstruction represents, among many others, a diagnostic tool that can be exploit to improve the overall cardiological knowledge. In particular, the three-dimensional reconstruction of the heart or simply of cardiac chambers and valves is a powerful source to have patient-specific clinical information and predictors of several diseases. As reported in [38] the assessment of LV volume can be predictive of some clinical or pre-clinical disease processes: the LV remodeling, intended as the change of its shape, have been recognized to be important for survival after a myocardial infarction and for pre-clinical individuation of diseases in asymptomatic patients when exposed to risk factors. As previously mentioned, the RV is less explored but given the relevance it has in clinical scenarios such as ischemic and non-ischemic heart failure, myocardial infarction, pulmonary hypertension, congenital heart disease and after therapeutic interventions[90], the necessity to generate 3D models becomes inevitable.
The study of the cardiac ventricles' models can be useful to obtain patient-specific clinical

parameters, as End Diastolic Volume (EDV), End Systolic Volume (ESV), Stroke Volume and Ejection Fraction.
The first two parameters are representative of the volume of blood in the ventricle in the diastolic and systolic phase of the cardiac cycle; the Ejection Fraction (EF) represents the percentage amount of blood ejected during contraction of the ventricle, an indicative parameter of the pumping function of the heart; the Stroke Volume (SV), which is defined as $SV = EDV - ESV$, is the volume of blood ejected by the ventricle, usually referred to the left one, in the systolic phase.
The ejection fraction is defined as follows:

$$EF[\%] = \frac{SV * 100}{EDV}$$

Also, three-dimensional reconstructions of shape and motion becomes tools for FSI modeling to combine electro-mechanical properties with fluid dynamics of heart, as done in[22] for the left heart in particular. Other various and less computational-demanding applications can be the use of the reconstructed electro-mechanical models as input of blood flow simulations, as further analyzed in[14], again considering the left ventricle.
Accounting for the right heart, a computational dynamics study where the time-varying RV geometry is extracted by 3D echocardiography is represented by[26]. Despite the acknowledged crucial role of RV function, the left heart remains the focus in cardiological studies while right heart still needs to be further explored.
The reconstruction of the three-dimensional shape of the heart and right chambers can be also useful in terms of collection of of medical data for a population to have a statistical atlas of morphological and functional variations in cardiac models. In particular, these statistical atlases can also be used to exploit patient-specific measurements to individuate different risk factors: an identification of pathological shape features [69] can be performed by analyzing shapes to individuate clinical features that represent the presence or the degree of a certain disease.

1.3.2. Image-based reconstruction

Reconstruction of anatomical portions from medical images consists in different steps that will be progressively described below:

- Choice of the best imaging technique for representation and analysis of the interested portion.
- Segmentation of the anatomical part: generation of contours of the portion on differ-

ent specific medical images, based on the aim of reconstruction. Tracing of contours can be generated manually or automatically in different segmentation approaches.

- Reconstruction of 3D model from the different contours obtained in the previous step. Different reconstruction techniques are available, depending on the anatomical part that have to be modeled.

The medical images that can be used to generate a 3D model of cardiac chambers are different, for example Echocardiography and Computer Tomography (CT) that are both non-invasive and highly used in the field. However, they have limitations that can be overcome by Magnetic Resonance (MR).
Echocardiography is a non-ionizing, available and portable imaging technique that can also provide real-time measurements: for this reason, it represents the first cardiac imaging modality under which patients are submitted. However, it has negative aspects as dependence from the operator, narrow fields of view, limited tissue characterization especially for patients with large habitus or recent surgeries [40].
Moreover, this imaging technique can not detect cardiac findings which are instead captured by Computational Tomography or Magnetic Resonance imaging techniques, as anatomical blind spots: the pericardium detection is limited due to its thin nature, the aorta can be entirely visualized only with a particular combination of views otherwise a lack of accuracy is reported in comparison with MR, small variations in the positioning of transducer can result in a detection of non-true LV apex leading to a wrong morphology of the left ventricle, detection of prosthetic heart valves is also limited and can be overcome by the use of MR and CT [40].
Computer Tomography is an imaging technique that uses an X-ray beam to obtain submilllimeter cross-sectional images [21] of different parts of the body: it provides fast and high-resolution imaging of the anatomy but the downside effect is the exposure of patients to ionizing radiation. CT is requested by specialists, but its use needs to be balanced between risks and benefits: various strategies have been developed to decrease the dose of radiation, that can alter the DNA of exposed cells with extended effects of cancer induction, but it is related to the resolution of images. indeed, increasing the dose of radiation can increase the resolution of CT without affecting image noise [34]. Given the potential risk of development of radiation-related cancer, even if very low, the use of Magnetic Resonance Imaging (MRI) technique is recommended, when possible, as it uses non-ionizing radiation.
Since the present work is focused on the analysis of the Right Ventricle, the comparison between the assessment of its volume and function using CT and MRI in [54] has concluded that results from the two imaging techniques in the evaluation of the ventricle

functionality can be considered comparable.

1.3.3. The use of Magnetic Resonance Imaging

Cardiac Magnetic Resonance (CMR) represents, indeed, the most versatile imaging technique [73]: besides being non-ionizing, it is also non-invasive and can provide quantitative information about cardiac structure and function, both globally and locally related. Magnetic Resonance Imaging (MRI) has increased importance in providing a comprehensive characterization of cardiac functionality, as can be considered the reference modality for morphological and functional assessment of the heart [87]. Indeed, the MRI technique represents the gold standard in the test of cardiac function and evaluation of myocardial volumes and mass [92].

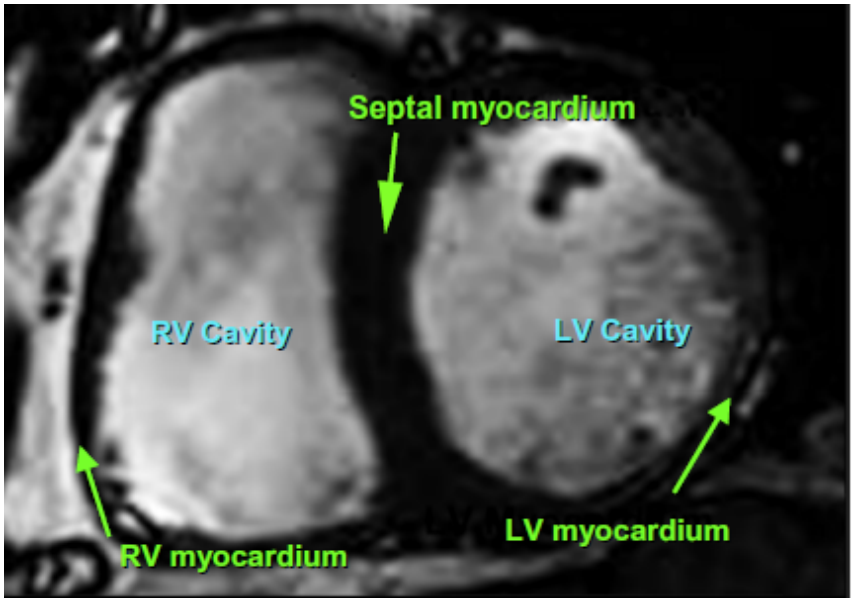

Figure 1.9: Cine-MRI Short Axis image:view of ventricles at end diastole [86]

Clinically, medical MRI images can be non-trivial and time-consuming [73] to be analyzed and computational tools became a real help in accelerating the analysis, but also examine cardiac features to generate quantifiable measurements and provide new parameters about heart diseases' predictors [35].
With image segmentation the contouring of different anatomical parts can be delineated in order to obtain three-dimensional reconstructions: actually, cardiac-MRI represents the gold standard also for cardiac segmentation as both 2D and 3D transthoracic echocardiography (TTE) provides ventricular dimensions which are lower than obtained with cardiac

MRI and they can distinguish less trabeculae from compacted myocardium while MRI allows better endocardial definition [92].
Independently of the segmentation method that is used, that can be manual or automated, the standard and most common MRI image views are the short axis that provides a cross sectional view, example given in Figure 1.9, of cardiac chambers, perpendicularly to the long axis that goes from the apex to the base.
As can be seen in Figure 1.10, the shape of cardiac ventricles is different, with RV having a more complex geometry: the LV remains circular in the long-axis plane creating an ellipsoid, while the cross-sectional area of the right ventricle changes along the longitudinal axis

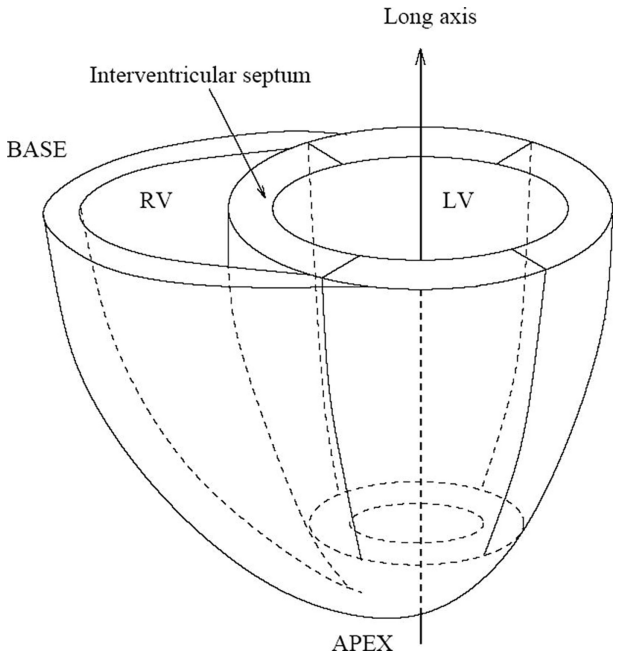

Figure 1.10: Scheme of RV and LV geometry: Long Axis perspective [79]

Also, thickness of the myocardial walls in RV is very low, at limit of the MRI spatial resolution [79], increasing the difficulty of RV segmentation. For these reason, segmentation of cardiac chambers actually is more evolved for the LV reconstruction and analysis with automatic and semi-automatic algorithms, while remains challenging for the automated generation of RV ventricle models. An example of the difference in complexity of endocardial contouring for RV and LV is represented in Figure 1.11.
In presence of Congenital Heart Disease such as Tetralogy of Fallot, where MRI acquisitions are routinely considered as the young age of ill patients requires non-ionizing radiations, the RV shape and its remodeling had been investigated by using statistical ventricular atlases. The geometry of RV of ToF patients, combined with the segmentation of

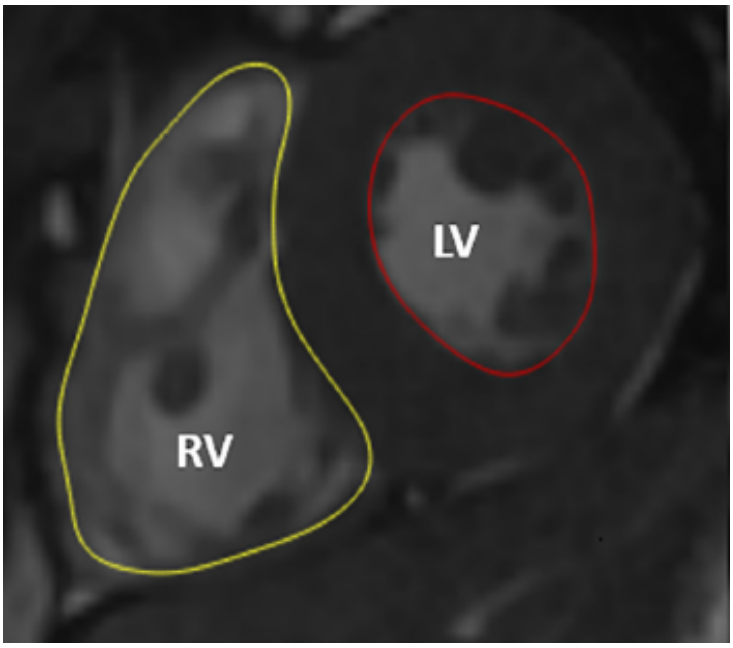

Figure 1.11: Endocardial contouring of the ventricles [82]

healthy cardiac ventricles and ventricles affected by cardiovascular disease, was analyzed to assess the relation between structure and functionality of the heart with cardiovascular risk factors[35]. Cardiac remodeling is, indeed, a long-term feature of the follow-up in case of repaired ToF, along with RV dilation: comparing healthy subjects with rToF cases, considering different anatomical compartments of the right ventricles, different degrees of dilation have been detected to assess the possibility of a non-homogeneous remodeling of RV in case of repaired ToF[20].
Specific MRI acquisitions can be required from clinicians for monitoring of long-term effects of RV dilation in Tetralogy of Fallot: Short-Axis Aortic Valve (SA-AV) and Rotational-TV (TV-R) cine MRI series can be obtained. A description of these specific MRI series is now present, with specification of the utility in clinical analysis of ToF:

- SA-AV cine-MRI series groups acquisitions obtained along the normal direction of plane of Aortic Valve (AV): these specific views allow to see the cross-sectional shape of aortic sinuses and specifically Sinus of Vasalva (SoV), visible in Figure 1.12. Vasalva's sinus represents one of the four widenings between the ascending aorta and the aortic valve cusps: from these dilations arises coronary arteries.
  The importance of these acquisition is related to ad-hoc clinical follow-up in case of repaired Tetralogy of Fallot: a long-term consequence of surgical intervention for repairing anomalies characterizing the Tetralogy of Fallot is dilation of aortic

structures. In particular, among aortic structures, SoV in [55] revealed to be the most susceptible to dilation, with rate of 0.81 mm/year.

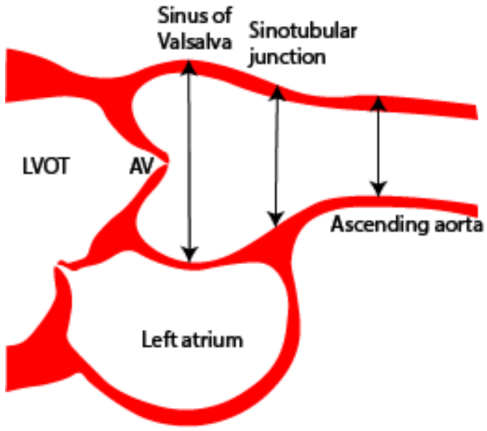

Figure 1.12: Sinus of Vasalva in the anatomical position with respect to Aortic Valve (AV) and Ascending aorta. LVOT :Left Ventricle Outflow Tract.

- Rotational-TV (TV-R) cine-MRI series groups 2D long-axis acquisitions that are specific for analysis of the Tricuspid Valve (TV) annulus. These can be obtained by rotating planes around the axis that connects apex of right ventricle and orifice of TV. A scheme of 18 rotational planes and an example of this rotational acquisition is shown in Figure 1.13.

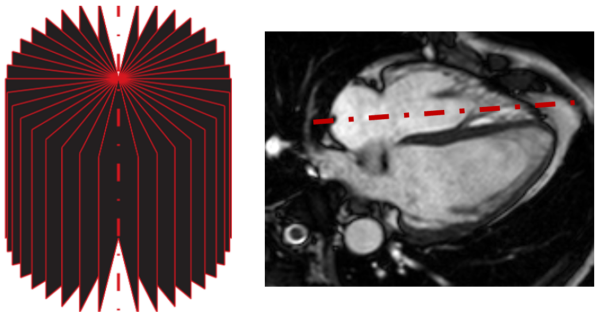

Figure 1.13: Scheme of rotational planes for Rotational-TV acquisitions with correspondent tracing (red) on example of these acquisitions. Figure adapted from [84].

The clinical interest in these specific acquisitions is related to follow-up examinations in case of repaired Tetralogy of Fallot: in case of congenital heart disease, anomalies of the tricuspid valve annulus can be associated with a worsening clinical scenario and the specific condition of repaired ToF can induce a RV dilation with consequence

on the TV [48] : for this reason, monitoring of TV annulus becomes essential for evaluating regurgitation of TV.

As the measurements from medical images can be used by specialists to plan clinical decisions, the use of the most effective imaging technique in the segmentation is required: in this prospective, MRI-based 3D reconstruction of the heart represents a powerful diagnostic tool.

1.3.4. Reconstruction techniques: state of the art

The reconstruction of a 3D model starts from the set of contours delineating the organ under study.
Actually, segmentation can be performed manually, very time consuming but can reach high accuracy, semi-automatic and completely automated by the use of algorithms based on deep learning. The automated segmentation process is instead very fast but it can lack of accuracy, since these algorithms have to be trained with a large image data set: these algorithms are already in use in some CMR image analysis software but they still need to be validated for some regions of the heart that are anatomically challenging, such as RV or right atrium[35].
Manual segmentation can take about 20 minutes [79] for each ventricle if performed by a clinician, but is also affected by inter-variability of the contours traced. This have generated the need to automate the segmentation processes that are able to detect the desired contours, but usually the manual tracing is still needed to improve the accuracy of the results.
The automated and semi-automated segmentation methods have been reviewed in [79] basing on the prior information used in the process to increase accuracy: the need of user interaction or some anatomical and geometrical assumptions can be incorporated into the segmentation process as a weak prior information, while some other process, usually the automated ones, need a strong background to increase robustness, as they use statistical models for the segmentation. Respectively, the methodologies are defined as image-driven or model-driven techniques. Model-driven ones exploits the quite similar shape of the heart among the human individuals, but as said for automated techniques they need a training data set of reconstructions, usually generated manually. The conclusion of the work highlights the higher difficulty in segmentation of RV, with an overall segmentation error of the RV endocardium greater than LV endocardium, and the overall less interest in research for the RV segmentation. The focus in scientific literature regarding LV segmentation techniques over others can be seen in Figure 1.14.

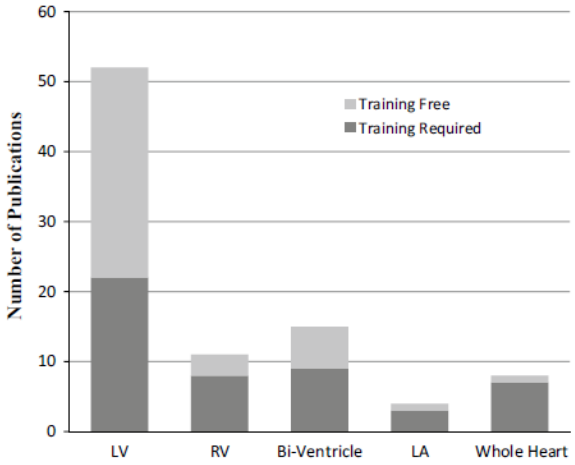

Figure 1.14: Different attention paid to right and left reconstruction in cardiac image analysis: the focus regarding segmentation is given to LV with respect to RV. Training is related to the need for large data set to improve robustness: image-driven methods are training free, while in model-based methods training is required as strong prior knowledge. [76].

Analyzing the state of the heart of the segmentation techniques used for cardiac chambers reconstruction, in case of semi-automated and automated methods, methods related to ventricles reconstruction have been developed mainly for LV application or biventricular reconstructions, while few methods have been developed specifically for right ventricle [30].
A distinction can be done considering:

- Model-driven methods: these are based on statistical shape models and cardiac atlases. Using statistical information to reconstruct cardiac chamber shape or variation, the resulting segmentation becomes more robust to image noise [76].

  Their application on LV can be found in [70], [97], [9], [15] but are also suitable for RV segmentation, treated in [74], [71], [80], [31]. These methodologies benefits from robustness due to strong prior knowledge but requires training data for this advantage: a manually traced large dataset is needed but it requires several time to be built.

- Image-driven segmentation techniques: the identification of voxels for intensity differences belonging to the cardiac chamber or blood is the core of these segmentation processes. This identification can be obtained with different strategies as threshold-

ing combined with region-growing, clustering or voxel classification, active contours or deformable models.

Their application to LV, as reviewed in [76], can be found in [46], [66], [12], [59], [81] with thresholding and region-growing strategies, in [75], [49], [44] with methods based on classification and in [89], [85], [91], [27], [67] for active contours methods. These methods proved to be suitable for LV segmentation and all based on the use of cine-MRI, which provides information about the entire cardiac cycle with fine resolution in space and time and high contrast in intensities related to tissues. Accounting or the RV application, the thresholding method have been applied in [39] to both ventricles as the complexity of RV morphology throughout the cardiac cycle and the more trabeculation in RV wall motion can decrease the effectiveness of this technique. The RV segmentation is performed using deformable models in [104], [103]: these methods can catch the morphological changes of the ventricle, with limitation in their speed when applied to completely different RV shapes [13].

Almost the totality of cited works is based on the use of Short Axis cine-MRI acquisitions: the use of only Short Axis (SA) acquisition can be limiting for reconstruction purpose. The SA view in cine-MRI images requires multiple breath-holds, that can represent an imaging artifact able to decrease the overall accuracy of reconstruction. In particular, the effect of cardiac motion, blood flow and respiratory motion can generate inter-slice imaging defects [42].
On the short axis level, the most complex images to segment are related to the apical and basal parts of the ventricles with respect to the mid-ventricular images: the basal part of the ventricles represents the connection part with the atria, leading to more complex shapes to segment, while in the apex of ventricles the presence of small structures not fully resolved by MRI represents a challenging factor in segmentation [79].

The proposed improvement of this work is to merge information derived from different cine-MRI acquisitions, applied to joint ventricular reconstruction in [65], not only short-axis ones: as described in [101], the contribution of long-axis, basal and apical contours, added to short-axis information, is relevant for geometrical reconstruction of left and right ventricle.

1.4. Aim of the thesis

The recent research on cardiac chambers segmentation and particularly on reconstruction of Right Ventricle models presents these limitations:

- underestimation of the clinical importance of Right Ventricle and major focus on the study of left heart
- morphological complexity of Right Ventricle and consequence on the segmentation process
- automated segmentation processes developed and validated especially for the Left Ventricle
- use of only Short Axis MRI acquisitions for segmentation purposes

The purpose of the work is the three-dimensional reconstruction of right ventricles using the Multi-Series Morphing (MSMorph) method [84]: the application of this reconstruction technique, in the two variants of MSMorph II and MSMorph III, for the right healthy ventricle and for the right ventricle affected by rTOF were analyzed in terms of accuracy, efficiency and reconstruction-time. In every reconstruction, shape and displacement field of the cardiac chamber were obtained. 3D Reconstructions of left ventricles of the healthy heart was also obtained using the two variants of the technique, above mentioned, allowing the visualization of the bi-ventricular motion.
MSMorph reconstruction method relies on the exploitation of different views of cine-MRI acquisitions to overcome the possible defects in the reconstructions related to the only use of SA images and improve the accuracy of cardiac ventricles 3D models by merging information from all the possible MRI-series of images.
The reconstruction results will be compared with manually traced contours which are considered the gold standard for the comparison of the automatic contours generation [84] and with models obtained with standard technique of reconstruction that uses only SA-MRI images, inspired by the one used in [37] for the left ventricle.
The method can also improve the automatization of the RV segmentation, as the manual contouring of the endocardium is applied on a slice of cine-MRI only for a frame, while the remaining contours of the set are obtained by registration of the manually traced contour over the cardiac cycle despite the morphological complexity of the right ventricle.
This analysis can provide further research on the assessment of right ventricle function through three-dimensional reconstruction of the RV shape and motion using segmenta-

tion based on of multiple views of MRI images that can improve the overall accuracy. Clinically relevant parameters can be obtained to evaluate the RV function, especially in comparison with the pathological heart affected by Tetralogy of Fallot.

Summarizing, the objectives of the present work are:

- Reconstruct the complex right ventricle morphology for an entire cardiac cycle, reducing computational time employed.
- Obtain a pathological right ventricle reconstruction: a 3D model of repaired Tetralogy of Fallot ventricle is generated and compared to healthy case.
- Merge different acquisition of medical imaging, to integrate more information in the reconstruction process.
- Acquire clinically relevant parameters from RV reconstruction to assess the RV functionality.
- Achieve the wall motion of the right ventricle.
- Improve the automatization of the reconstruction process, without loosing accuracy of reconstructed models.
- Analyze and compare the MSMorph technique used for reconstruction with the reference technique, completely manual.

The outline of the thesis is as follows:

- Chapter 2 presents an overview over the most classical strategies for shape and motion reconstruction based on acquisitions of short-axis type only, which have been defined in Chapter 1. One general standard method is described for reconstruction of shape and motion of right ventricle.
- Chapter 3 describes the specific MSMorph reconstruction technique, based on the merging of information given by multiple types of MRI acquisitions.
- Chapter 4 contains results obtained in the present work: delineation of patients and corresponding types of MRI acquisitions at disposal is carried out, then to show difference in application of a classical technique, based on use of only short-axis acquisition, and MSMorph technique. Accuracy and efficiency of the innovative MSMorph technique are analyzed.

2 | Standard Reconstruction Techniques

In this Chapter, standard procedures for cardiac ventricles' reconstruction are considered. Accounting for the endocardial surface reconstructions, a brief overview of classical methods based on short-axis (SA) acquisitions is given, to focus then on the specific approach used in this work for generation of 3D surfaces of right ventricle endocardium, with exclusive use of short axis images. In particular, a semi-manual segmentation is performed on SA images to obtain contours that through interpolation generates a 3D surface. Successive adaptations of endocardial surfaces are carried out, with later generation of the corresponding epicardial and myocardial surfaces. Myocardial surfaces, obtained for the entire cardiac cycle, are used for the reconstruction of the wall motion of the right ventricle. Summarizing all these steps of the standard technique:

- Segmentation of short-axis MRI images and reconstruction of the endocardial surface
- Generation of the epicardial surface to obtain myocardium
- Reconstruction of wall motion of the ventricle

2.1. Geometrical Reconstruction of Right Ventricle endocardium

Standard reconstruction techniques, based exclusively on Short-Axis images, are usually applied to left ventricle, with few exceptions for application on the right ventricle only, that are identified in this Section. After having identified a more general reconstruction technique for segmentation of SA images, all the steps for reconstruction of endocardial surfaces are detailed in each paragraph.

2.1.1. Reconstruction based on Short Axis cine-MRI series

As previously mentioned in Chapter 1, the majority of reconstruction methods are based on use of short-axis images with aim to reconstruct the LV. Among image-driven techniques used, few works are focused on reconstruction only of RV: a low-level method combined with use of a model-based algorithm in [63] was used for extraction of endocardial contours in SA images, with need of a final adjustment due to the complex shape of RV, not circular as LV; semi-automatic surface detection with level sets is used in [18] to generate 3D models of right ventricle, with difficulties in delineation in the apical region of RV. Given these considerations, it is clear how automatization of reconstruction techniques on RV encounters different difficulties when only SA images are employed: the standard approach detailed in this chapter is inspired by the more general and manual strategy based on segmentation of SA images used in [37] only for LV. In this view, a semi-manual segmentation for RV reconstruction is carried out to obtain accurate models of RV endocardium.
In particular, in terms of MRI types of acquisitions for RV reconstruction, Short-Axis (SA) cover the right ventricle main axis: they are considered standard in clinical practice, as also Long-Axis (LA) images that instead cover the perpendicular direction of the RV main axis. When considering complex RV structures instead, for example in case of a patient affected with Tetralogy of Fallot (see Section 1.2), specific acquisitions can be required by clinicians: two of these can be represented by Short-Axis Aortic Valve (SA-AV) acquisitions, obtained in the normal direction with respect to the plane of aortic valve, and Rotational-TV (TV-R), acquired in particular rotating planes around the axis that connect tricuspid valve (TV) and RV apex. A detailed description of SA-AV and TV-R acquisitions is given in Section 1.3.3. Examples of different acquisitions are displayed in Figure 2.1. Among all types of MRI acquisitions listed, standard reconstruction methods are based on segmentation exclusively of Short-Axis images.

2.1.2. Segmentation of the endocardium: use of Medical Imaging Interaction Toolkit (MITK)

For right ventricles' image-based reconstructions, slices of the SA cine-MRI series are visualized and segmented with the use of MITK, the Medical Imaging Interaction Toolkit [8] and in particular of MITK Workbench, which is the related free application. Indeed, the semi-manual segmentation technique considered for purpose of explanation is based on an algorithm implemented in MITK that was proposed in [33]. MITK represents a free

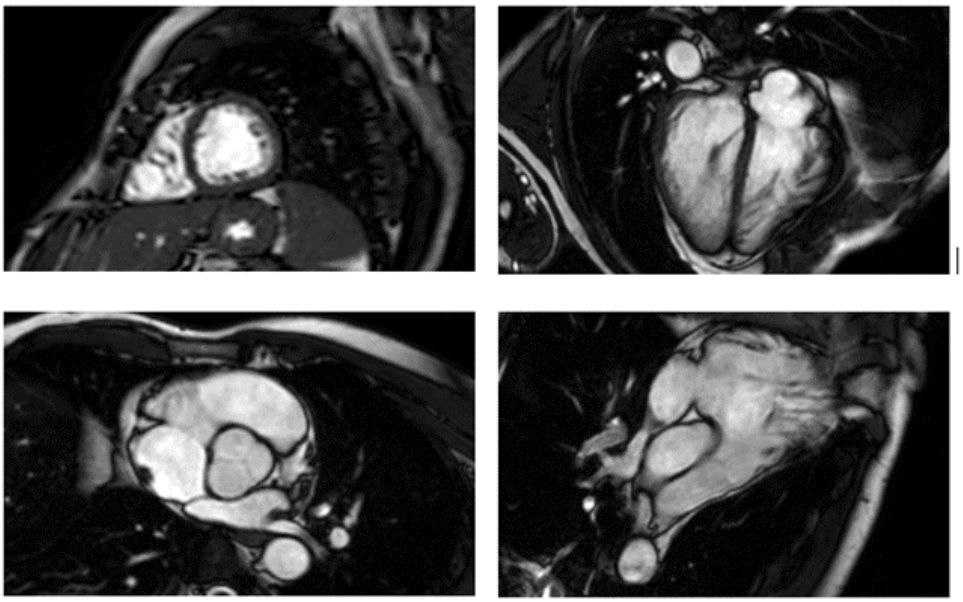

Figure 2.1: End-diastolic views of different cine MRI-series: Short-Axis (top, left), Short-Axis Aortic Valve (bottom, left), Long-Axis 4 Chambers (top, right), Rotational-TV (bottom, right)

open-source software that is dedicated to the interactive processing of medical images: the visualization and segmentation of the Cardiac Magnetic Resonance (CMR) images can be performed using the MITK Workbench application, that provides powerful functions for image processing.
CMR images can be uploaded in the application as DICOM files grouped in frames: example of visualization of the medical images in a fixed frame is represented in Figure 2.3. Three anatomical planes are used for visualization: axial, sagittal, and coronal plane. A scheme is represented in Figure 2.2.

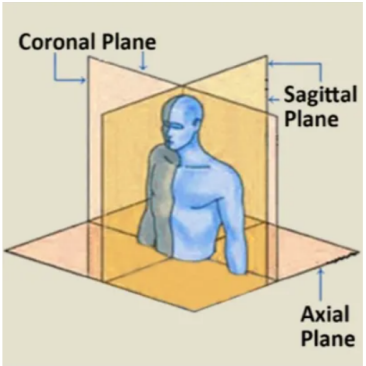

Figure 2.2: Anatomical planes represented: axial, sagittal and coronal

Axial plane is horizontal and cross-sectional, dividing the body into superior and inferior

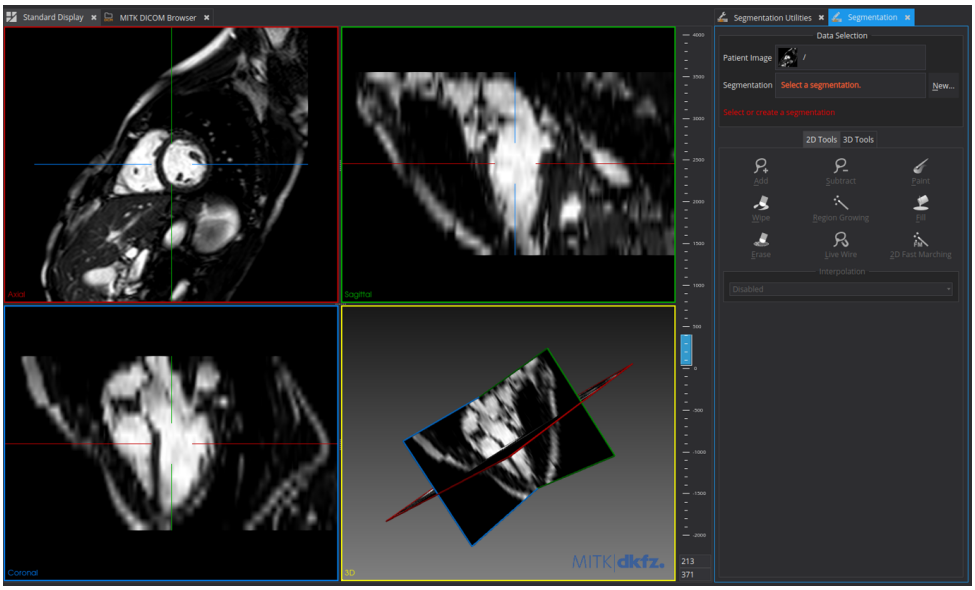

Figure 2.3: Visualization of the MITK Workbench with uploaded the desired DICOM images: anatomical planes are represented and combined in a 3D representation in the yellow square (bottom, right). The axial plane is represented in red (top, left) contoured square, coronal plane in blue (bottom, left) and sagittal in green (top, right). For a better image visualization, the Texture Interpolation feature can be applied. The panel for segmentation functions can be seen on the right part of the image.

portions, while sagittal and coronal planes are longitudinal ones. They differ since the sagittal plane divides the body into left and right portions, while anterior and inferior portions of the body are obtained by coronal plane division.
By using cine-MRI volumetric series, this visualization can be obtained, based on anatomical planes: the combination of them can be seen in the 3D view.

The segmentation technique exploits the contouring tool which can be used in the described anatomical planes of reference for the manual tracing of the endocardium of the ventricle, considering in particular right ventricle. Using the 2D segmentation tools the manual contouring of the endocardium of RV can be generated on many 2D slices with Add and Subtract tools that allow the user to delineate or eliminate the voxels representing the anatomical part in which one is interested: In Figure 2.4 the approach, based on voxels, for segmentation used by MITK can be observed: unlike other approaches based on contours that can cut voxels, voxels are selected or not to generate the corresponding segmentation. After manual contouring of the endocardium is executed multiple times on different anatomical planes and slices, which represent a time demanding part of the segmentation process, the 3D interpolation of the contours, visible in Figure 2.5, is per-

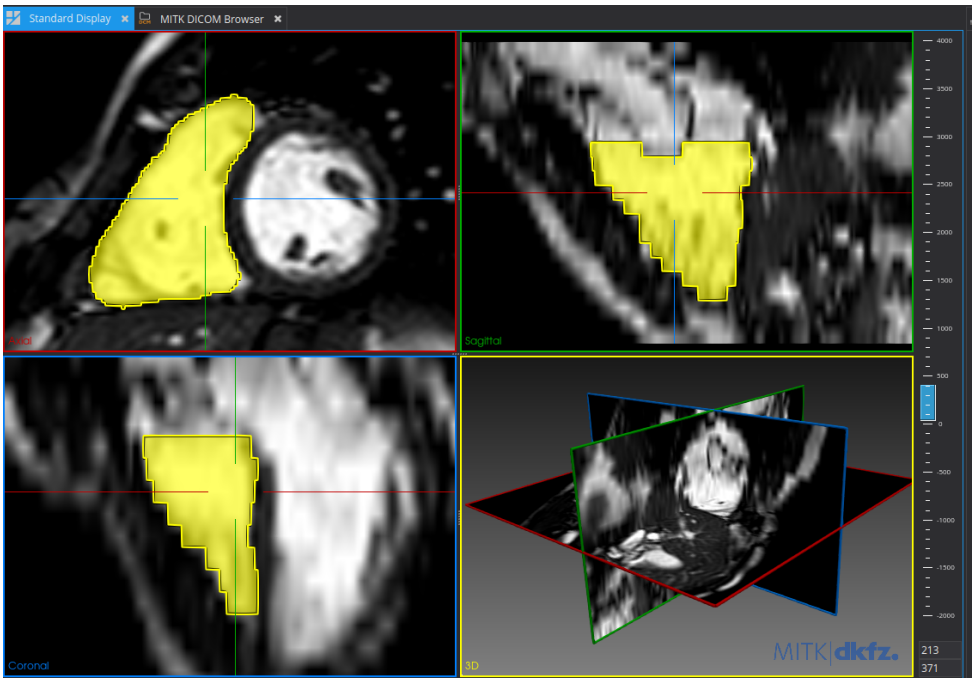

Figure 2.4: Example of manual contouring voxel-based performed on MITK Workbench

formed with a designated tool in MITK: the generation of a 3D surface from contours is performed more accurately when sparse contours are generated in arbitrary slices, instead of parallel-slice wise segmentation. The interpolated surface consists in a vtkPolyData, defined as a concrete dataset represents vertices, lines, polygons, and triangle strips.

2.1.3. Reconstruction of the endocardium surface: improvements for adaptation to images

The 3D surface extracted from interpolation can be compared to the medical images to evaluate the accuracy of segmentation by the use of 3D slicer, a free open-source software for visualization and analysis of medical images [1]: this application can be exploited by uploading both DICOM images used for segmentation and the resulting 3D surface obtained by interpolation in MITK. The correspondence between the surface contour and medical images of the endocardium can be visually assessed, with examples given by Figures 2.7, 2.8.

To increase the correspondence, the *Sculpt* tool of Autodesk Meshmixer [7] application can be used, in combination with visualization in 3D slicer: local spatial deformations can be performed on the surface using Volume Brushes, in particular *flatten* and *drag*, to manually adapt the endocardial surface to the endocardium visualized in the short-axis MRI images.

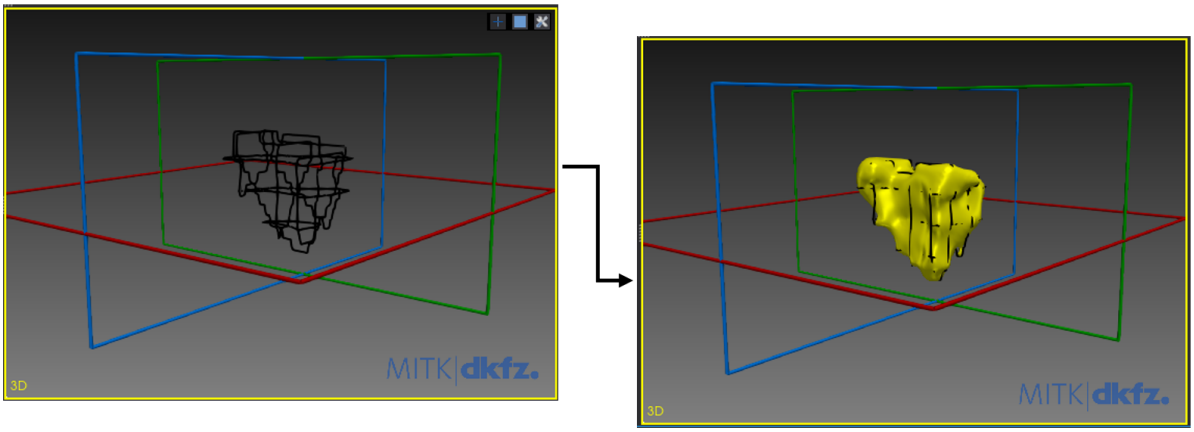

Figure 2.5: Example of a surface (yellow) derived from 3D interpolation of contours (black lines), performed by MITK with sparse contours manually traced in arbitrary planes: an optimal interpolation result derives from this method, while creating parallel contours only on one plane can generate an interpolated surface lacking of the three-dimensional representation of the other planes.

Illustration of surfaces' differences before and at the end of adaptation process are shown in Figure 2.6. This manual improvement of the surface accuracy represents another part of the process that can take several time to be executed: if cine-MRI series covers the entire cardiac cycle, it has to be repeated on all the three-dimensional surfaces for each frame. Surfaces can also be prepared to be eventually used in CFD simulations by applying filters in VMTK, the Vascular Modeling Toolkit [4], that represents a collection of tools and libraries for 3D reconstruction, geometric analysis and mesh generation, specific for modeling of blood vessel. The surfaces can be smoothed removing artificial bumps that can affect the simulation results, with *vmtksurfacesmoothing* filter that implements Taubin's non-shrinking algorithm for optimal surface smoothing. Then, they can be also remeshed, resizing the triangle edges of the surface, with *vmtksurfaceremeshing* filter.
At this point, as the surfaces of right ventricle endocardium, obtained and accurately adapted to the real anatomical morphology by comparison with medical images, are closed and without valve orifices, another manual process is necessary for this purpose, especially regarding the tricuspid valve: the pulmonary valve can be obtained by cutting the outflow tract of the right ventricle at the valve level, again with comparison with medical images at disposal. The orifice of tricuspid valve, which is the atrio-ventricular valve in RV, have to be manually generated instead using Autodesk Meshmixer application erasing the manually selected area in correspondence of the orifice of the valve: the identification of the area is obtained visually, always with comparison in 3D slicer with all cine-MRI series for better identification of the valve position.

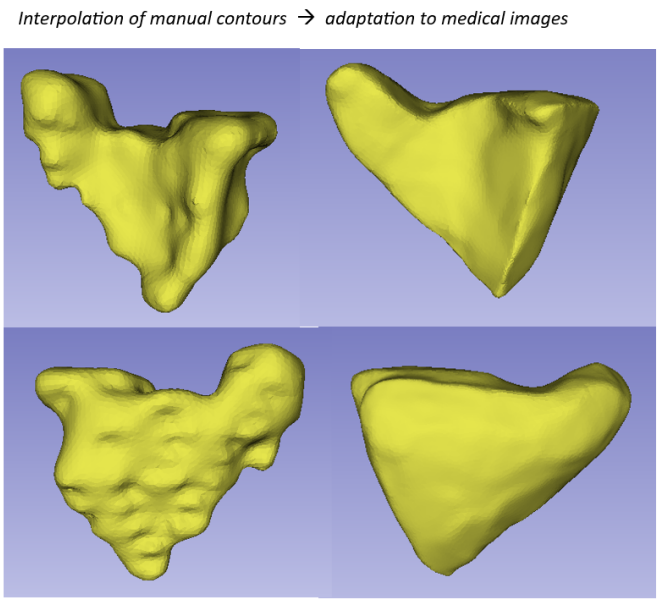

Figure 2.6: Illustrative comparison between a 3D surface obtained by interpolation in MITK and final adaptation of the surface to images through Autodesk Meshmixer application

2.2. Generation of myocardium

At this point, a fictitious myocardium can be obtained starting from the endocardial surfaces and extruding them to have a certain thickness.
The procedure consists in extrusion of the endocardial surface with valve orifices to obtain the corresponding epicardial surfaces: the extrusion can be performed with the Paraview [3], open-source application for visualization and data analysis. In particular, generation of the correspondent normals on each surface have to be performed, then to warp by vector the models: a tentative epicardial surface can be obtained.
Then, smoothing and remeshing of the epicardial surfaces can be performed, as earlier described for the endocardial ones. A connection between endocardial and epicardial surfaces, of which an illustrative Figure 2.9 is shown, can be carried out by use of surface-connection algorithm: it connects two open surfaces separated by a gap producing an output continuous surface by smoothly connecting the boundaries of the two [32]. Indeed, the algorithm is based on triangles generation between boundaries of the surfaces with a minimum distance criterion, as it chooses triangles with shortest connecting edge between rings of connection, preserving the smoothness in the connection. This algorithm is implemented in VMTK through the *vmtksurfaceconnector* command.

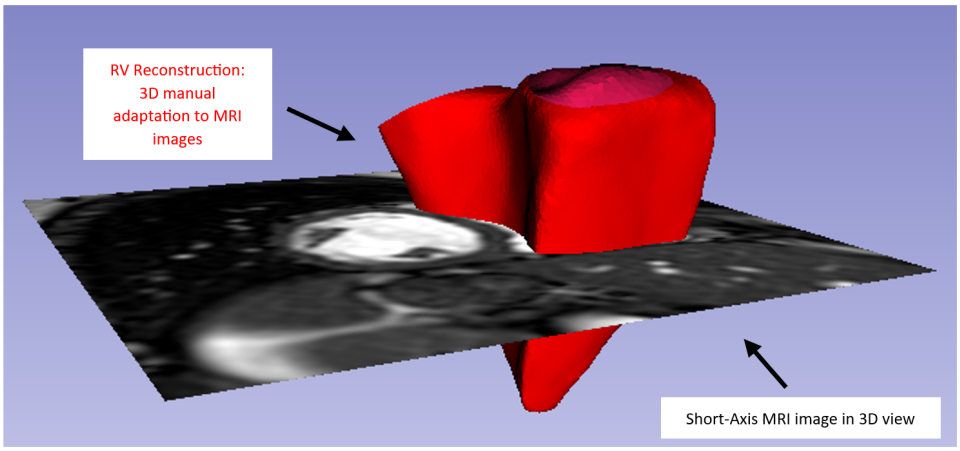

Figure 2.7: 3D view in 3D Slicer representing the RV endocardium surface (red) cut by short-axis MRI image: high accuracy can be reached with manual adaptation between surface and medical images at disposal

2.3. Reconstruction of ventricle's motion

As previously assessed in Chapter 1, the RV motion reflects the RV overall functionality and visualization and quantification of the morphological and geometrical changes over the cardiac cycle could be significant for assessment of the ventricle function or dysfunction. RV motion over the cardiac cycle can be reconstructed using the 3D surfaces obtained as described above. The steps for wall motion achievement consist in

- generation of artificial level-set images of the 3D myocardial surfaces
- registration of the level-set images
- achievement of displacement field along cardiac cycle

2.3.1. Registration of artificial level-set images

Consequently to the generation of the myocardial surfaces, as described in the previous section, the generation of the corresponding artificial level-set images can be carried out. Example of artificial level-set images for RV is given in Figure 2.10. The level-set images represent in binary type the information of the three-dimensional structures: they function as binary masks for image processing, as registration procedure. Image registration consists in a process for alignment of multiple images in case valuable information can be

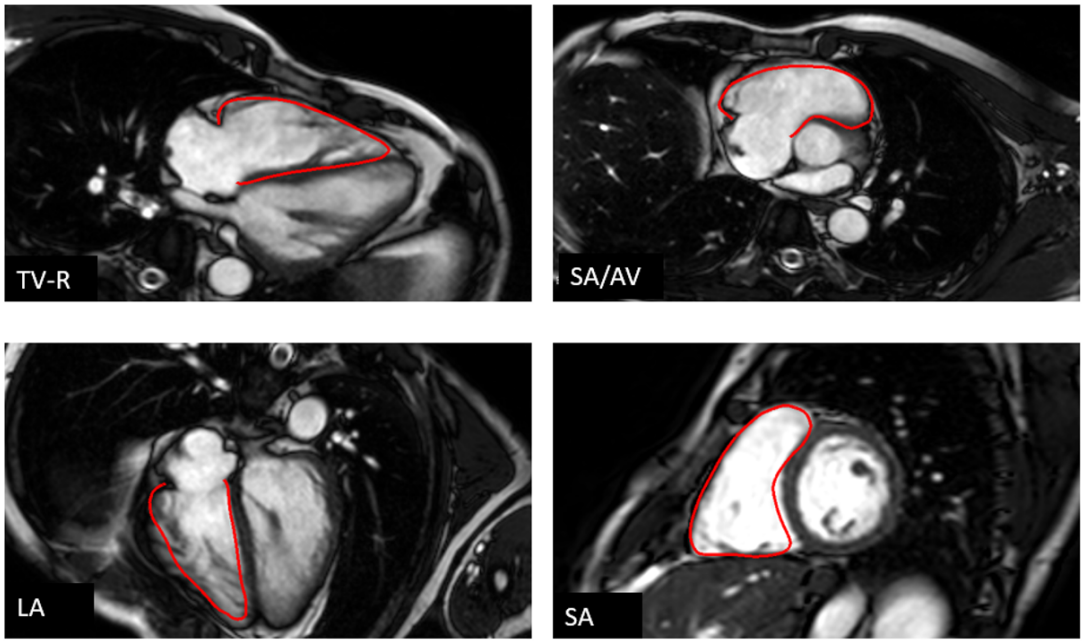

Figure 2.8: Examples of contours (red lines) corresponding to manual adapted surface with respect to multiple MRI acquisitions: Rotational-TV (top, left), Short-Axis Aortic Valve (top, right), Long-Axis (bottom, left), Short-Axis (bottom, right). The 2D projections of the surface are cut in correspondence of tricuspid valve at the level of connection with right atrium.

obtained by considering more than one image. Considering cine-MRI series for example, image registration can be exploited to obtain information from images acquired at different times covering the cardiac cycle: for completeness in the description, we refer to this case in the following description.
The aim of these level-set images generation is to register the motion only of the ventricle's reconstruction over the heartbeat, not all the information contained in the SA cine-MRI series actually. In fact, the registration process can be applied to the artificial level-set images of myocardial surfaces, including information about the myocardial motion, but it is usually applied to medical images for clinical track of events [68]: diagnostic investigation of medical images or surgical planning are two examples of application for image-registration.
This particular type of images functions as deformable surface representation not through points and triangles but with 3D functions contained in images of binary type.
Registration process of the level-set images consists in a spatial alignment of a moving image $I_m(x)$ with respect to a fixed image $I_f(x)$: the fixed image represents the reference configuration, chosen by the user as an endocardial surface at a fixed frame. The moving image is deformed with a transformation $\mathbf{T(x)}$, described in Figure 2.11, to be spatially

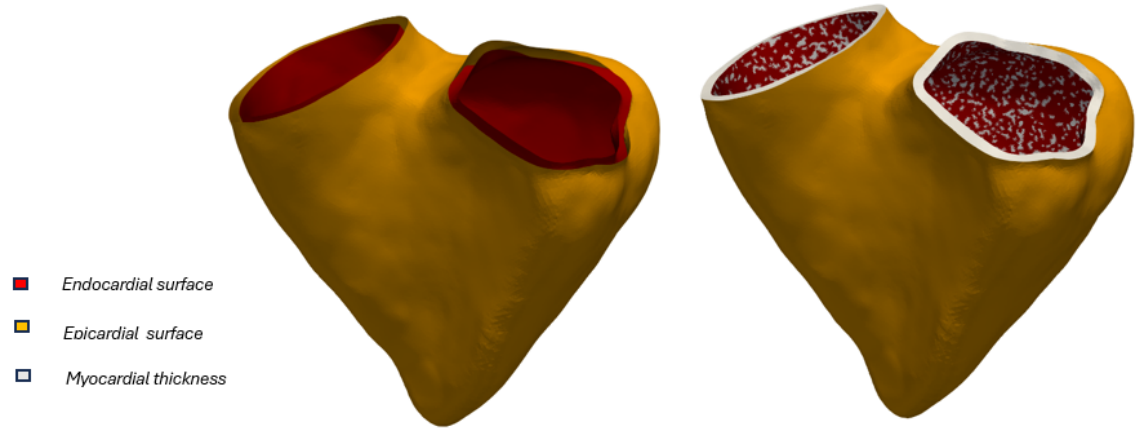

Figure 2.9: Illustration of tentative myocardium generation process: the endocardial (red) surface is extruded to obtain the epicardial one (orange) and the connection between them (white thickness) is generated to create the tentative myocardium

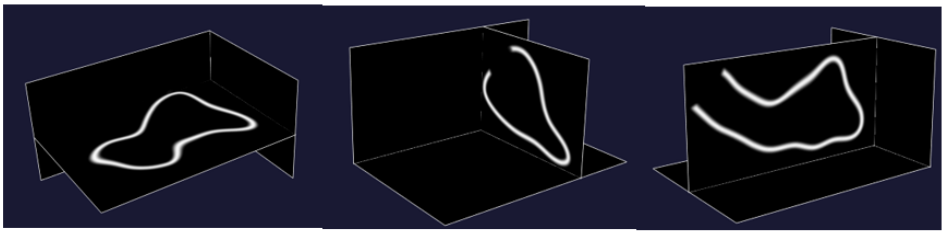

Figure 2.10: Illustrative figure of artificial level-set images of 3D right ventricle reconstructions

aligned to the reference configuration: quality of the alignment is determined by a cost function **C(T(x); Im(x); If(x))** that have to be minimized with respect to **T(x)**.

Cost function represents a similarity measure between the fixed and the transformed moving image. For aim of minimization, a suitable optimization method allows to have the optimal choice for *coordinate transformation* ***T(x)*** [57].
Minimization of cost function **C** with respect to transformation **T** for alignment of Fixed Image I_f and Moving Image I_m is represented by the following expression:

$$T_\mu = argmin_{T_\mu} C(T\mu; I_f, I_m),$$

The vector μ represent the transformation parameters, since parametric approach is

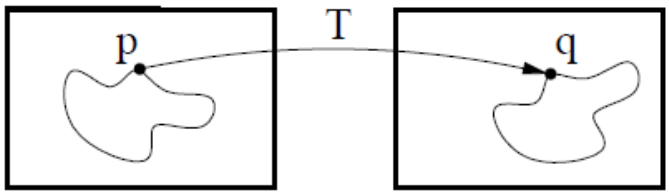

Figure 2.11: Spatial transformation T generates a mapping from the fixed image (left) to the moving one (right): the registration problem consists in finding the transformation for the spatial alignment between the two images [56]

adopted: the elastix software, exploited for the registration step, is based on this approach that consists in limitation of the possible transformations by use of a parametrization. Elastix sofwtare, based on widely used open source library for medical image processing as the Insight Toolkit (ITK) [57], is an open-source image-registration toolbox that has implemented different algorithms for image registration. Among all, non-rigid registration algorithms are recommended adopted for the exposed registration procedure. A multi-resolution approach can be adopted.
Suggested choices for the registration components are:

- Transformation: non-rigid B-spline-based transformation is suitable. Non-rigid transformations are characterized by a varying size of μ and corresponding degrees of freedom of the deformation applied by the coordinate transformation $T_\mu(x)$. As B-spline based, the transformation is modelled as a weighted sum of B-spline basis functions placed on uniform control point grid [57].
- Cost Function: Mutual Information (MI) between the reference level-set image and the moving one, that assume a statistical relation between images' intensities. When a nonrigid transformation model is used, a regularization term is added to the cost function for penalization of undesired deformations: in the specific procedure, constraint is preferably represented by bending energy, supported by Elastix.
- Image sampler: the described procedure accounts for a grid with four values of spacing ranging from 22.4 mm to 8.0 mm as a suitable choice is related to the subset of voxels on the fixed image to be considered in similarity with the moving image, instead of considering all voxels of the reference image that can be time-consuming. As the size of the grid is a down-sampling factor without prior smoothing, a Gaussian smoothing filter without down-sampling is applied.
- Optimizer: adaptive stochastic gradient descent optimizer represents an optimal

choice for reducing computational times using a subset of voxels of fixed image [57].

Output of the registration procedure is given by the displacement field that can be evaluated on endocardial surfaces of right ventricle.

2.3.2. Acquirement of displacement field over the heartbeat

The resulting displacement field after the registration process consists in a 3D vector field representing the transformations of artificial images with respect to the reference image. The 3D vector field can be evaluated on every point of the endocardial surface of reference to compute the endocardial displacement during the entire cardiac cycle considered. Endocardial morphology and displacement can be visualized in Paraview, as Figure 2.12 displays: in this way, local changes in the endocardial configuration are quantified and wall motion is obtained.

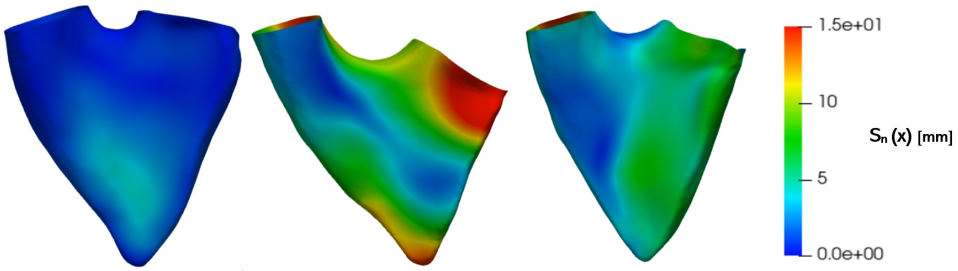

Figure 2.12: Illustration of RV endocardium displacement field for different phases: motion is expected to be more consistent in systolic phase (center) rather than diastasis (right) and diastolic phase (left). The coloured legend gives a quantification of the displacement of endocardium, where red represents maximum values and blue the zero values.

3 | Multi-Series Morphing technique

As discussed in Chapter 2, standard segmentation techniques for the ventricles relies on the use of Short Axis images solely. Here we present a new strategy, Multi-Series Morphing (MSMorph), developed at LABS, Department of Chemistry, Materials and Chemical Engineering "Giulio Natta" of Politecnico di Milano, in particular by F. Renzi.
The underlying principle of MSMorph technique is the use of merged clinical data to obtain an accurate three-dimensional surface of the endocardium of cardiac chambers. In particular, focusing on the use of cardiac cine-MRI data, all the available series of acquisitions can be used in synchrony to reconstruct the desired cardiac chamber, overlapping the use of only Short Axis MRI-acquisitions which represents a limitation for accuracy of reconstructions: this would represents a valuable enrichment with respect to classical strategies described in Chapter 2 that utilize only one type of acquisitions.
Since MSMorph technique exploits multiple cine-MRI series, different variants of this innovative technique are defined basing on the level of merged information used. MSMorph technique, as the name suggests, also employs morphing to generate surfaces from sets of contours, which represent another key step of the method, to improve efficiency in terms of time used for reconstruction. The time employed for generation of models is also reduced as the MSMorph technique involves semi-automatic generation of the contours of the endocardium: a further improvement is included with respect to classical techniques of Chapter 2 for the decreased dependency on the manual activity of the user. Sequentially, the steps of MSMorph reconstruction technique are:

- Semi-automatic segmentation of multiple cine-MRI series: for a fixed frame, the manual contours are traced on each slice and for remaining frames contours are obtained automatically through a registration process. Multiple sets of contours are generated and combined for each frame to obtain desired level of merging data.

- Generation of the endocardial surfaces by morphing templates with respect to sets of contours, previously combined.

The outline of the Chapter is as follow:

- *Introduction* in Section 3.1: some considerations about the importance of using of merged data are carried out.
- *Contours generation* in Section 3.2: first step of the MSMorph technique.
- *Definition of Multi-Series Morphing variants* in Section 3.3.
- *Definition of morphing concept* in Section 3.4.1
- *Surface generation by morphing* in Section 3.4.2: second step of the MSMorph technique.

3.1. Merging of information from multiple cine-MRI series

The majority of techniques used for three-dimensional reconstructions of cardiac chambers utilizes only short-axis images, as highlighted in Chapter 1. Few works focus instead of the use of multiple types of MRI acquisitions: merging information from multiple series represents a valuable tool to obtain a model that reflects the real anatomy of cardiac chambers. Considering the left ventricle reconstruction, combination of scans from different orientations, exploiting also fewer contours for the generation of ventricle's models, had resulted in [72] to generate a better and more precise geometrical reconstruction, with respect to conventional techniques exploiting only SA stack of images.
Starting from this consideration, for right ventricle reconstruction another point to note is the complexity of morphology: in Chapter 1 the different shape of ventricles has been described. For the crescent moon-shaped morphology of the right ventricle that has great variations according to the imaging slice level, high accuracy in the geometrical model obtained is essential for a real 3D characterization of it. This need is instead lowered in case of left ventricle, having a cross-section that maintains its ring shape across SA slices and its ellipsoidal shape in long-axis views.
Right ventricle application of merged data sets is considered in [102], with use a statistical shape model to obtain data for the models of both right and left ventricles: results show how long-axis contours bring structural information that should be incorporated

when complex geometries are reconstructed, to capture all relevant anatomical features. For these reasons, the use of contours traced in sparse and arbitrarily oriented slices can represent a great improvement in the accuracy of 3D reconstructions of right ventricle. Cardiac cine-MRI acquisitions as explained in Chapter 2, can be of different types: Short-Axis and Long Axis acquisitions, that are routinely obtained for standard procedures but also Short-Axis Aortic Valve (SA-AV) and Rotational-TV (TV-R) cine-MRI series that are both specific acquisitions, not usually considered in standard clinical practice.

3.2. Generation of contours: automatic process from manually traced reference

We present here the first step of *contours generation* in Multi-Series Morphing technique. In particular, segmentation has to be performed on each slice of cine-MRI series and for each acquisition time to reconstruct models for the whole cardiac cycle. Indeed, for each cine-MRI series it is possible to identify the number of slices that composes the series and the time resolution as the number of frames per cardiac cycle. Number of slices and number of frames for each cine-MRI series, are identified in this section for explaining purposes as:

- k index: represents the total number of slices characterizing all cine-MRI series considered.
- n index: number of frames characterizing each cine-MRI.
  n is defined as the ratio of the acquisition times t_n of each cine-MRI and the time resolution of cine-MRI τ_{cMRI}
  $$n = \frac{t_n}{\tau_{cMRI}} \tag{3.1}$$
  with t_n varying from 0 to T, where T is the heartbeat duration.
  The index n can vary from 0 to N= T/τ_{cMRI}, which corresponds to the maximum value.

Starting from all the considered cine-MRI series, the procedure involves the manual tracing of the contours of the endocardium for only one acquisition time t_n of the cine-MRI: for simplicity in the description of the procedure we consider, as a suitable choice, the diastasis phase, in which the passive filling of the ventricle is slowed with partial closure of tricuspid valve, before atrial contraction that completes the active filling of the ventricle. Diastasis represents the mid portion of diastole in which ventricular and atrial pressure

equilibrate [62]: as there is no atrioventricular pressure gradient, there is no net wall motion in the ventricle [94]. Also, volumes in atria and ventricles assume an intermediate value in this phase.

For every cine-MRI series, the manually traced contour at diastasis phase, identified as $t_{\tilde{n}}$ in the fixed frame $\tilde{n}$, is generated on each slice k. The 3D slicer software can be used for the tracing: it includes a Markups module that can be used to define point sets. To trace the manual contours, points can be used, then interpolated in a smooth curve by using Kochanek spline by the software.

The union of contours traced at diastasis phase $t_{\tilde{n}}$ for each slice k creates an initial set of contours $\Gamma_{\tilde{n}}$, which corresponds to the reference configuration of the registration process to obtain all the other contours $\gamma_{n,k}$ for every n different from $\tilde{n}$ on every slice k. In particular, each physical slice $\Omega_{n,k}$ of cine-MRI series is characterized by grey-level functions $\Upsilon_{n,k}$ on which contours $\gamma_{n,k}$ are traced, as can be seen in Figure 3.1.

For the registration process, a non-rigid registration algorithm can be used. The algo-

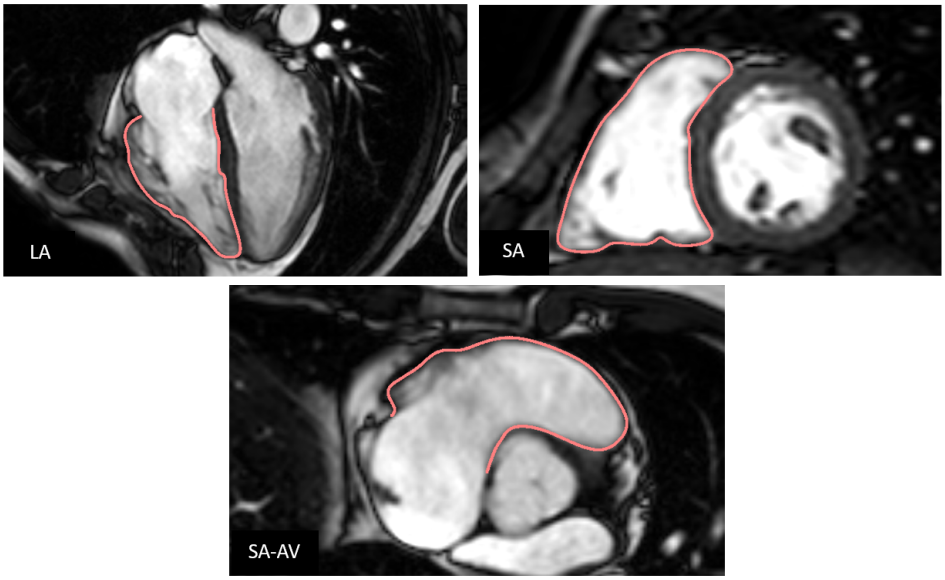

Figure 3.1: Examples of manually traced contours at diastasis phase $\gamma_{\tilde{n},k}$ in three possible types of acquisitions: Long-Axis (top,left); Short-Axis (top, right); Short-Axis Aortic Valve (bottom, center). Each square represents a physical slice $\Omega_{\tilde{n},k}$, the images define the grey-level function representation $\Upsilon_{\tilde{n},k}$ and the pink lines traced represent the contours $\gamma_{\tilde{n},k}$.

rithm is implemented in the Elastix software, considered in Section 2.3 for the wall motion achievement, and specific for registration of slices that are time-consecutive: the principle remains the same, with the aim here to find the Transformation $T_{n,k}$ that spatially align the grey-level functions $\Upsilon_{n,k}$.

Choices of registration components are listed:

- Non-rigid B-spline based transformation for $T_{n,k}$, suitable due to large deformations. As non-rigid transformations require a regularization term, a smoothness constraint can be adopted: the transformation T is constraint to be smooth by incorporating a specific energy term into the energy function, which maximization determines the deformation of the model, as described in [64].
- Cost function is given by the definition of Mutual Information defined in [96]: the criterion proposed is based on a continuous differentiable function of the parameters of registration using Parzen windows.
- Image sampler: Grid-spacing which can vary in a specific range in the two dimensions with Gaussian smoothing filter without down-sampling applied due to the lack of prior smoothing in the down-sampling, that is generated by the grid itself.
- Optimizer: standard gradient descent is most suitable for the application.

A multi-resolution approach with 4 levels is suggested: the use of hierarchical strategies with levels of increased complexity, in case of complex structures of images, is advised to avoid local minima traps in the optimization surface. Hierarchical approach is indeed considered as 'coarse to fine' strategy: to obtain a global optimum match, the global matching precedes calculations of finer details of the deformation [61].
Differently from the registration process to achieve endocardial displacement, described in Section 2.3, the alignment performed by the $T_{n,k}$ is performed on each slice k backward and forward in terms of the evolution of n with respect to the $\tilde{n}$, where contours are already defined.
For this reason, the transformation can be split into forward and backward type as defined below:

- $T_{bn,k}$ for backward alignment with n = 0, ... , $\tilde{n}$ - 1
- $T_{fn,k}$ for forward alignment with n = $\tilde{n}$ + 1, ... , N

Spatial alignment is performed on grey-level functions $\Upsilon_{n,k}$ of each slice backward and forward applying the previous transformations for respective n parameter evolution:

$T_{fn,k}$: $\Upsilon_{n,k} \rightarrow \Upsilon_{n+1,k}$
$T_{bn,k}$: $\Upsilon_{n,k} \rightarrow \Upsilon_{n-1,k}$

From the registration process, trasformation $T_{n,k}$ is obtained and applied to the initial set

of endocardial contours for each cine-MRI series.

The scheme of application on a single endocardial contour is given by:

$$\gamma_{0,k} \xleftarrow{T_{b\,n,k}} \gamma_{\tilde{n},k} \xrightarrow{T_{f\,n,k}} \gamma_{N,k}$$

An illustrative representation of the application of backward and forward transformation is given in the Figure 3.2 for an endocardial contour of right ventricle. At the end of

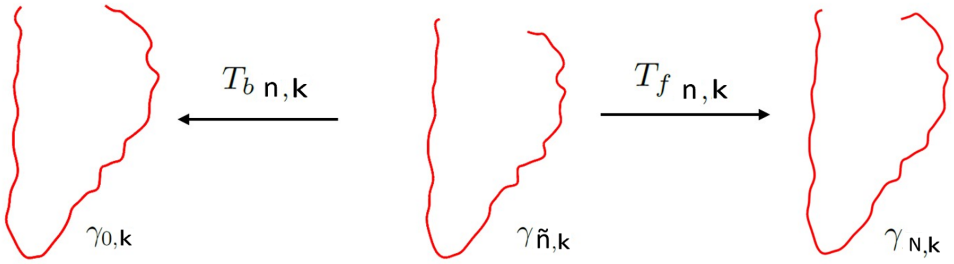

Figure 3.2: Scheme of application of the forward and backward transformations, respectively $T_{f_{n,k}}$ and $T_{bn,k}$, in the procedure for automatic registration (see Section 3.2) of contours $\gamma_{n,k}$ (red lines). The backward transformation is applied for each k with n varying from $\tilde{n}$ back to zero. The forward transformation instead for each k is applied with n varying from $\tilde{n}$ to the maximum value, N.

the registration process, N total contours sets are obtained: for each n, a contours set is represented by the sum of all contours $\gamma_{n,k}$ generated for each k. Depending on the types of cine-MRI series included in the registration process, the k index assumes a different value corresponding to the total number of slices for all cine-MRI considered: in this way, contours set are generated with different level of merged contours. Examples of contours set of right ventricle with different merging level are shown in Figure 3.3

3.3. Variants of Multi-Series Morphing technique

The different merging of imaging data generates multiple variants of the Multi-Series Morphing reconstruction technique: segmentation of multiple cine-MRI series generate contours sets defined by all the slices characterizing the series, with a specific value of k index, as highlighted in Section 3.2. In consideration of different cine-MRI series listed in

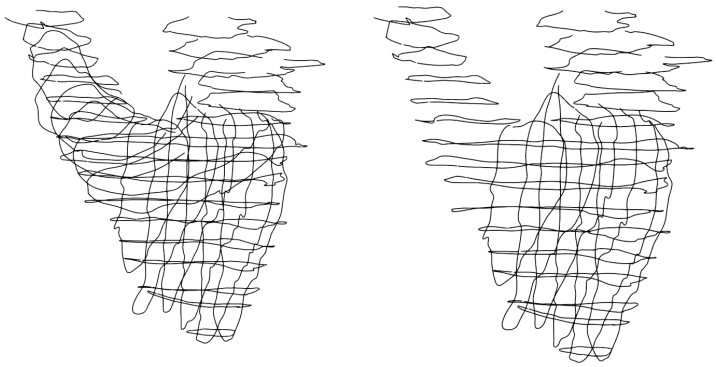

Figure 3.3: Two examples of contours sets $\gamma_{n,k}$, obtained with automatic registration (see Section 3.2) for each slice k at a fixed acquisition time t_n, are displayed. Different level of merging is determined by different contents of contours: on the right, two types of contours are combined, while on the left the combination of contours exploits three different kind of contours.

Section 3.1, the definition [84] is given:

- **MSMorph I**: use of contours obtained by all available cine-MR images
- **MSMorph II**: use of contours obtained by all available cine-MR images, excluding TV-R.
- **MSMorph III**: use of contours obtained by short-axis and long-axis acquisitions of cine-MRI type.

It is important to note that all different variants of the technique represents an attempt to overstep the limiting use of exclusively short-axis acquisitions of standard techniques (see Chapter 2): exploitation of different acquisitions of cine-MRI series is carried out at different levels in every variant of the method for this specific purpose.

3.4. Generation of the endocardial surface by morphing

In this section, the concept of morphing with general examples of its applications are delineated. Then, the use of morphing for surface generation in the Multi-Series Morphing technique is described.

3.4.1. Concept of morphing and different applications

The concept of morphing is represented by the transformation of one object into another object: it can be applied to 2-dimensional objects, as images, and to 3-dimensional objects. The effect of morphing or metamorphosis is the shape transformation from a source object into a target object. An example is shown in Figure 3.4. The most well-known application of the technique is found in computer animation: new shapes can be created by blending existing shapes in order to fill animations [60].
Actually, morphing as a graphic application have gained recognition in medical research field: in [77] different application of digital image morphing are detailed, for example analysis of healing processes, reconstructed as videos with medical images, that are shown for clinical or educational purposes or the surgical planning by using a reference image morphed on a specific scan of a patient. These 2D metamorphosis are generated basing on the same principle as 3D morphing techniques, where the objects are instead three-dimensional, allowing to transform them basing on features of the original template.

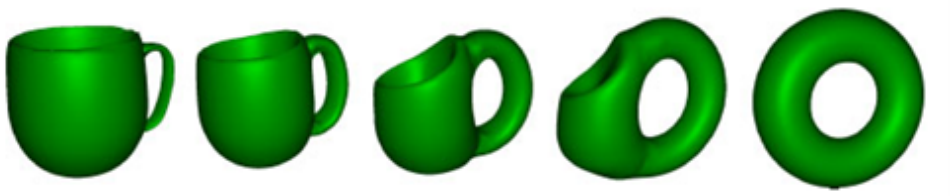

Figure 3.4: Taken from [45], a representation of morphing procedure applied to triangular meshes: from a mug shape, a torus shape is obtained.

In particular, with term object is intended any entity that has a 3D surface, as defined in [52]: morphing is applied to the mesh generated from the three-dimensional model. Of the mesh, we consider the topological elements as faces, edges and vertexes, combined in a network.
Considering the source mesh that has to be transformed accordingly to the target mesh, shape transformation is acquired with two processes [24]:

- Vertex correspondence problem: individuation of mapping, with specific functions, between the two meshes since a link between vertices of target and source objects must be established
- Vertex path problem: generation of intermediate models using the correspondences

between vertices, with their alignment in source and target object along trajectories where a transformation is applied

Different methods can be used to solve both problems, inter-related as one the consecutive of the other. When morphing takes place, deformation is generated with warping filters, that are topological filters used to change shapes of the images of objects, combined with amplitude filters [100].

3.4.2. Specific application of morphing in Multi-Series Morphing technique

In this section, the second step of Multi-Series Morphing technique, *surface generation by morphing*, is described.
Contours represent the starting point of the surface generation obtained by morphing: each set of contours, obtained as detailed in Section 3.2, is used as a target to morph a source template Σ towards its configuration. An improvement of the procedure, that is performed similarly in [98] with a reference heart model as template, is represented by the possibility to choose any surface for Σ, independently of the phase of cardiac cycle and so of n, defined along with k in Section 3.2. For right ventricle reconstruction, a sphere can be utilized as template surface, with minimal modifications for aim of best adaptation to contours.

In particular, the morphing procedure consists in implementation of an iterative algorithm, shown in Figure 3.6 where steps, corresponding to numbers in figure, are now detailed:

1. *Projection of points cloud of data, target object, onto the initial surface, source object*
   The projection of points cloud Γ_n generates a points cloud Θ_n defined on the source surface Σ, chosen as already mentioned to be a sphere.

2. *Computation of the distance of corresponding points of the source and target objects*
   The sphere is considered as an initial surface where the vtkPointLocator filter is initialized to search the closest points: points are analyzed in the 3D points cloud of the contours set. An algorithm for point location is implemented in the *vtkPointLocator* filter. Then, with use of the locator, the closest points in the template surface with respect to points cloud Γ_n can be found and stored in a double array where both the ID for point identification and the corresponding distance from contours

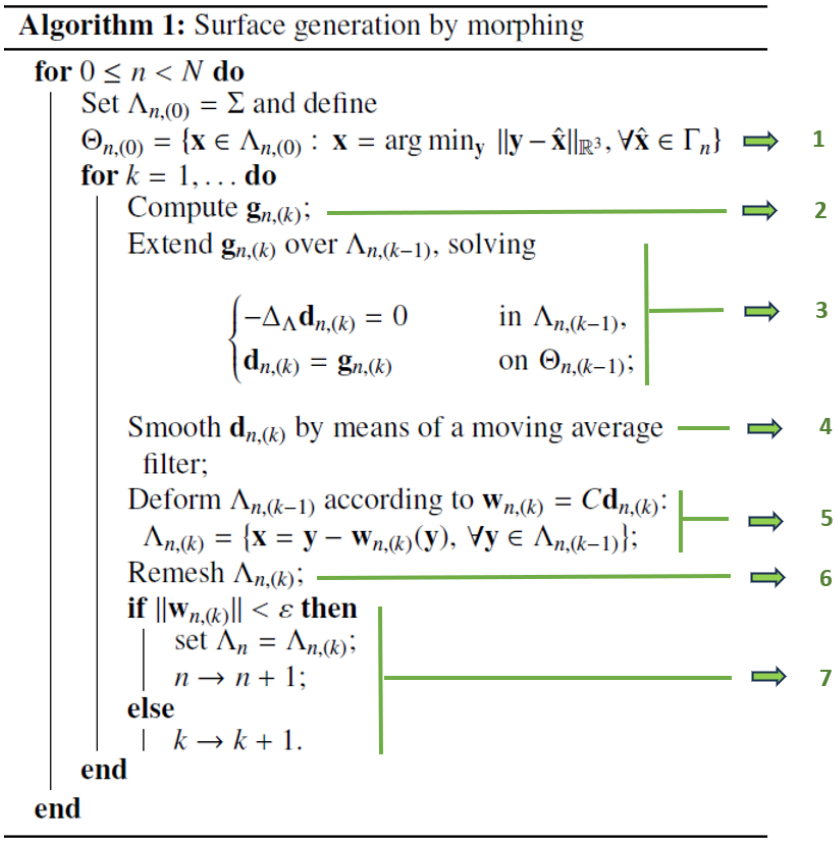

Figure 3.5: Adapted from [84], the different parts of the algorithm for generation of a surface by morphing are numbered for description: each green number represent a step of the procedure detailed in the numbered list of Section 3.4.2. The parameters n and k are defined in Section 3.2.

set are inserted. The calculation of the distance $g_{n,k}$ is performed with vtkMath filter: the difference of the coordinates for points located in the array referred to the surface and closest points in the cloud is computed.

3. *Extension of the distance field over the whole surface*
   A harmonic function is built on the distance field $g_{n,k}$, generated as a vectorial array, with use of *vtkvmtkPolyDataHarmonicMappingFilter*: this allows the resolution of the vectorial Laplace-Beltrami problem to extend the solution to the entire surface. In this way, the distance $g_{n,k}$ calculated, that has a value stored for each component as a vectorial array, is defined as a boundary condition for the equation that is solved for each component. The result is stored into another vectorial array, that represents the harmonic distance computed $d_{n,k}$.

4. *Smoothing of the distance field*
   A smoothing of the harmonic distance $d_{n,k}$ array defined on the surface is per-

formed of the point array defined on the surface: the *vmtksurfacearraysmoothing* filter is applied, that performs a moving average smoothing on data. For this type of smoothing method applied to the array of the surface points, a subset size is needed to compute the moving averages of data: this size coincides to the element patch of each node in the Finite Elements representation. The resulting harmonic array is then projected onto the source surface with the interpolation based on a minimum distance criterion performed by *vmtkSurfaceProjection* filter. At this step, a mapping for vertex correspondence is created with vertex path defined between the points cloud of target and source object.

5. *Deformation of the surface according to the vector field*
   The deformation is generated by use of a warping filter: this kind of filter is based on the use of the mapping generated in the previously steps. By use of the map, given by correspondences between the target and the source objects, a topological transformation is performed according to a scaling factor. In particular, the warping process can be executed with the *vtKWarpVector* that allows the deformation of the geometry with the use of vector data: the projection of the vectorial array of the smoothed harmonic distance is used for this purpose, to obtain $w_{n,k}$. The VTK [5] filter permits to choose the scaling factor, C, for the transformation process, as it is user-defined. In this step, the source object is transformed towards the target configuration by generation of intermediate models $\Lambda_{n,k}$.

6. *Remeshing of the intermediate model created, needed for adjustment of the surface mesh connectivity*

7. *Checking the stopping criterion*
   As an iterative method, the described numbered steps are executed for each n for a certain number of k iterations in relation to the stopping criterion based on the maximum square distance value of $w_{n,k}$, as defined in point 7 in Figure 3.6.

As a result, since the parameter n ranges from 0 to N value, N endocardial surfaces are morphed basing on the combination of contours set, eventually for each variant of the technique, detailed in Section 3.3. A superimposition of contours set and final morphed endocardial surface in two cases are represented in Figure 3.6.

From this point, the procedure for myocardial achievement and obtaining of the displacement field for corresponding surfaces can be repeated equally as described in Chapter 2 for standard reconstruction techniques: orifices of valves can be generated on the endocardial surfaces, from which the respectively epicardial surfaces can be obtained by extraction. Connection between epicardial and endocardial surfaces results in myocardial ones, of

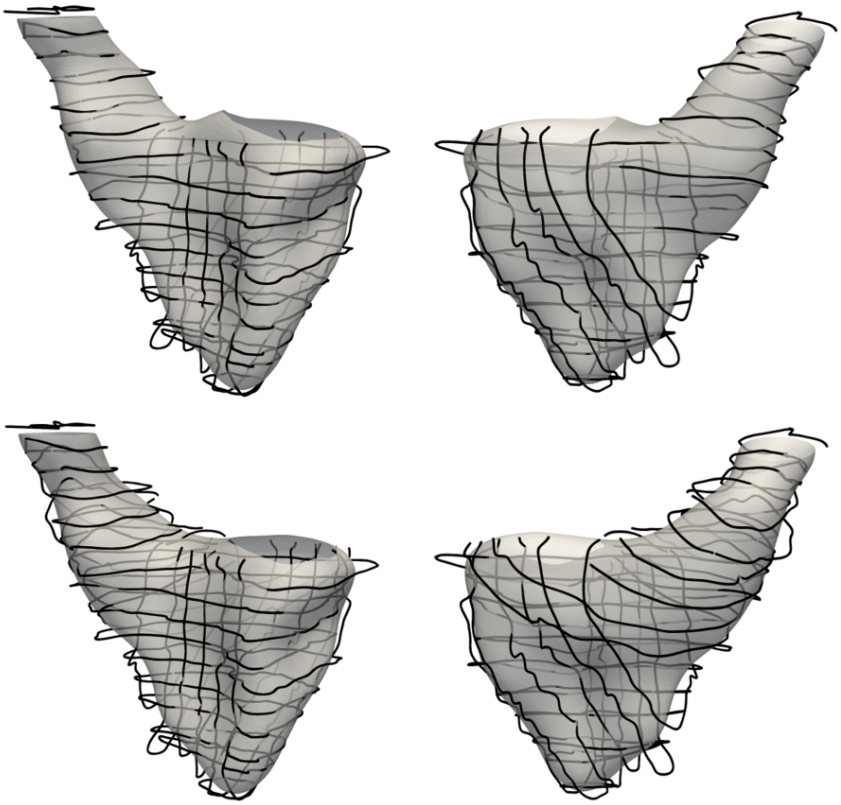

Figure 3.6: Two examples, for each row in two views, of final endocardial models (white surfaces) obtained for a fixed n at the end of the k iterations performed by the morphing procedure, described in Section 3.4.2. Contours sets (black lines), used as target in the morphing procedure, can contain different types of contours: the first row shows a set composed by two types of contours, while in the second row three contours types are included in the set. From contours sets, successive morphing iterations applied on the template generates intermediate models until best correspondence is obtained between contours sets and corresponding endocardial model, as can be seen in these examples.

which the wall motion can be calculated by generation of artificial level-set images: their registration allows to obtain the displacement field.

4 | Results and Discussion

Results of the present work and their analysis are now presented. Specifically, analysis of right and left ventricle for an healthy patient A and analysis of right ventricle for a patient B affected by Tetralogy of Fallot (see Section 1.2) are carried out in the chapter. The outline of the Chapter is as follows:

- Data sets of the patients analyzed in this work are detailed in Section 4.1, in terms of cine-MRI series at disposal and reconstruction techniques applied to obtain 3D models of ventricles.
- Projections of 3D models obtained for each type of reconstruction technique for each patient (see Section 4.1) are displayed in Section 4.2 at end-diastolic phase for visual assessment of the precision in the reconstruction process of *surface generation by morphing* (see Section 3.4.2).
- Three-dimensional reconstructions of ventricles for each patient are shown in Sections 4.3 for right ventricle's models of Patient A, 4.4 for left ventricle's models of Patient A and 4.5 for right ventricle's models of Patient B: shape and motion are displayed and analyzed regarding differences related to different reconstruction techniques used, both standard reconstruction (see Chapter 2) and Multi-Series Morphing technique (see Chapter 3), with models as result of the obtainment of endocardial morphology and motion of the ventricle, as described in Section 2.3. Representation of morphology and displacement fields is shown in three characteristic phases of cardiac cycle, chosen as end of systole, diastasis and end of diastole. These three phases correspond, in terms of volume, of minimum and maximum ventricular volume respectively at end of systole and end of diastole, while diastasis represents the phase in which ventricular volume and atrial volume are intermediate.
- Analysis of ventricular volumes is carried out in Section 4.6 with computation of

clinically relevant parameters and comparison with reference values, according to scientific literature.

- Analysis of accuracy and efficiency of the MSMorph technique, described in Chapter 3, is carried out in Section 4.7.

4.1. Patients of the present work: data sets and techniques applied

In the present work we analyze the 3D reconstructions of ventricles, considering two patients, with relative cine-MRI series at disposal are:

- **Patient A**: healthy patient.
  Cine-MRI series at disposal for patient A are now presented:
  - Short-Axis cine-MRI volumetric series made of 21 slices.
  - Long-Axis cine-MRI volumetric series made of 6 slices.
  - Short-Axis Aortic Valve cine-MRI volumetric series made of 6 slices.
  - Rotational-TV cine-MRI volumetric series of 18 slices.
- **Patient B**: patient affected by Tetralogy of Fallot, that have been surgical repaired (rToF).
  Cine-MRI series at disposal for patient B are:
  - Short-Axis cine-MRI volumetric series made of 18 slices
  - Long-Axis cine-MRI volumetric series made of 6 slices

Delineations of characteristics for different types of cine-MRI series above listed can be found in Section 1.3.3.
Cine-MRI series at disposal were provided by the Division of Radiology of University Hospital of Verona, Verona, Italy. The achievement of all acquisitions was carried out using the Achieva 1.5T (TX) - DS (Philips, Amsterdam, Netherlands) technology: the in-plane homogeneous space can vary in the different types of acquisitions from 1.15 mm to 1.25 mm while thickness ranges from 5 mm to 8 mm [84]. Time resolution of all the cine-MRI series is given by 30 frames/cardiac cycle.
Considering the data sets above described, the definition of the variants of the MSMorph

reconstruction technique (see Section 3.3) are detailed specifically for the application in the present work as follows:

- MSMorph II technique is generated with use of Short-Axis, Long-Axis, Short-Axis Aortic Valve cine-MRI series.
- MSMorph III technique is generated with use of Short-Axis and Long-Axis cine-MRI series.

Reconstruction techniques have been applied differently for the two different patients:

- Patient A:
  - right ventricle's models have been obtained with a standard reconstruction, described in Chapter 2, and with variants II and III of the MSMorph reconstruction technique, described in 3.
    The comparison between the application of MSMorph technique with respect to the standard reconstruction methods, which uses only short axis acquisitions, is carried out from differences considering models related to patient A.
  - left ventricle's models have been obtained with MSMorph II and MSMorph III variants, defined in Section 3.3, to obtain then a biventricular model in both cases when considered with the corresponding right ventricles models obtained with same variants.
- Patient B: right ventricle's models have been obtained with MSMorph III technique, defined in Section 3.3.
  The comparison with respect to the right ventricle's models obtained for the healthy patient A, obtained with the same MSMorph III variant, gives information about the morphological difference in ToF right ventricles with respect to an healthy case.

Specifically for Patient A, gold standard contours were provided by Ing. Francesca Renzi. Indeed, Manual Gold Standard contours are represented by the result of manual segmentation of each slice of cine-MRI series, for all the frames covering the cardiac cycle. The delineation of the endocardial contours for every frame of all the slices of each considered cine-MRI series, obtained with the Markups module of 3D Slicer [1], represents the reference method for segmentation of the right ventricle and allows the analysis of accuracy that is included at Section 4.7.1.

4.2. Visual assessment of correspondence between models and MRI-images

All the 3D endocardial reconstructions that have been obtained for each patient undergone a visual assessment for evaluation of the correspondence with medical images at disposal for each patient (see Section 4.1).
For simplicity of exposition, the projections of 3D models, obtained for the entire cardiac cycle, are shown only at one phase of cardiac cycle, chosen as end-diastolic phase.
Focusing on Patient A, the projections on MRI images at disposal of 3D models are contained in Figures 4.1, 4.2, 4.3: respectively generated with a standard reconstruction technique, with MSMorph II and MSMorph II techniques. In particular, it is important to note that as described in Section 2.1.3, projections of models obtained with standard techniques represent the result of a manual adaptation of the surface derived from interpolation of contours. Instead, for the application of the MSMorph techniques, projections represent the results of the morphed surfaces with respect to contours sets, obtained semi-automatically as detailed in Section 3.2. In particular in this work, for the registration process of contours the grid-spacing could vary from 48 mm to 6 mm in all the applications of the contours registration procedure of MSMorph technique.

Considering the projections of models obtained with MSMorph technique and standard reconstruction technique, it can be seen that great correspondence is obtained also with surfaces obtained by morphing, on which manual improvement is not performed.
For patient A, as described in Section datasets, also left ventricle's reconstruction have been carried out with MSMorph II and MSMoprh III variants: related projections of models on each cardiac MRI image at end-diastolic phase are displayed respectively in Figures 4.4 and 4.5.
Also for these representations, correspondence was found between projections and medical images considered. Again, in this case manual improvement of the models obtained with MSMorph techniques was not performed.
Considering Patient B instead, the reconstructions with MSMorph III variant of the technique projected onto medical images at disposal is shown in Figure 4.6. Great correspondence can be found also in this more complex RV structure, as can be seen comparing these image to projections shown above in this section of Patient A.

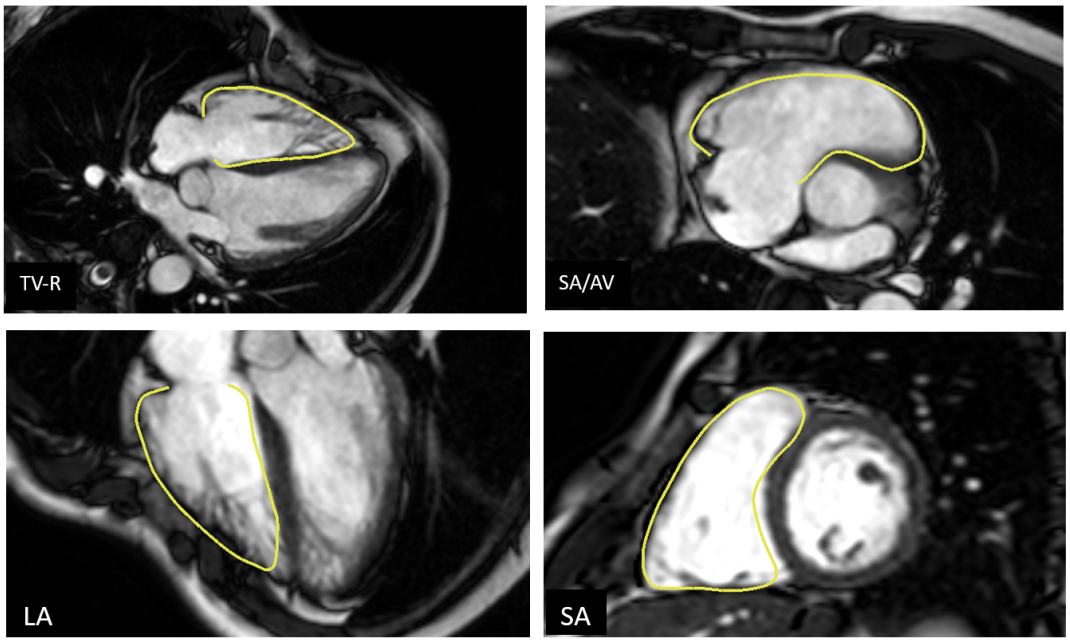

Figure 4.1: Patient A, right ventricle: projection of the 3D end-diastolic model obtained with standard reconstruction technique (see Chapter 2) onto Rotational-TV (TV-R) acquisitions (top, left), Long-Axis (LA) acquisitions (bottom, left), Short-Axis Aortic Valve (SA/AV) acquisitions (top, right), Short-Axis (SA) acquisitions (bottom, right).

4.3. Patient A: reconstructions of right ventricle

Cine-MRI images of Patient A were used for segmentation in different combination for reconstructions through MSMorph II and MSMorph II (see Section 3.3) techniques, as previously detailed in Section 4.1. Reconstructions of the right ventricle of Patient A obtained with a standard reconstruction method are also displayed for comparison with application of MSMorph variants. Furthermore, endocardial displacement fields of surfaces obtained with each technique have been obtained: given the description of the procedure to obtain the displacement field in Section 2.3, for all the applications of this work the artificial level-set images were built with homogeneous space resolution of 1 mm along each direction and their registration process was carried out considering the first frame as reference image.

The consequential succession of endocardial surfaces of Patient A from end-systolic phase through diastasis until end-diastolic phase for the different techniques are shown in Figures 4.7 and 4.9: the increasing volume throughout these phases is representative of the ventricular filling from end-systole to end-diastole.

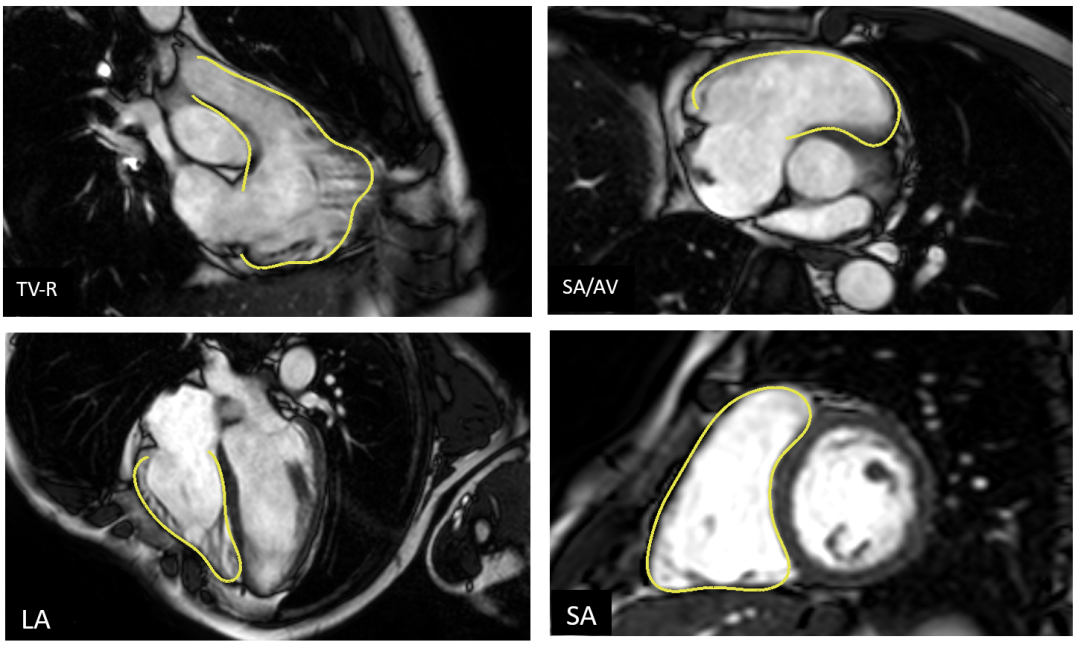

Figure 4.2: Patient A, right ventricle: projection of the 3D end-diastolic model obtained with MSMorph II technique (see Section 3.3) onto Rotational-TV (TV-R) acquisitions (top, left), Long-Axis (LA) acquisitions (bottom, left), Short-Axis Aortic Valve (SA/AV) acquisitions (top, right), Short-Axis (SA) acquisitions (bottom, right).

Differences in reconstructions obtained with the two MSMorph variants can be seen in small adjustments of the MSMorph II reconstructions due to the use of more contours, from the SA-AV cine-MRI series segmentation. However, the complex shape of right ventricle have been obtained also in the application of the technique with only SA and LA acquisition: this can be an advantage since these acquisitions are routinely acquired in standard clinical practice. With respect to the standard reconstruction technique, the application of MSMorph method in both variants had resulted in smoother surfaces: surface irregularities are evident in the standard models, while the use of the MSMorph technique seems to be helpful in preventing them as do not require great amount of manual manipulation of the surfaces obtained. Indeed, for the displayed morphed surfaces manual manipulation resulted to be not necessary: overlapping the surfaces on all the available MRI acquisitions, great correspondence was found (see Section 4.2) in the correspondence between projections of models and medical images.

From the quantitative displacement field representation in Figures 4.8 and 4.10, it can be noticed that the ventricular motion in case of application of standard reconstruction techniques is much greater while in the application of MSMorph techniques it becomes more attenuated. However, as expected, the most accentuated wall motion in every model can be found at the systolic phase where the ventricle is contracted, while displacement

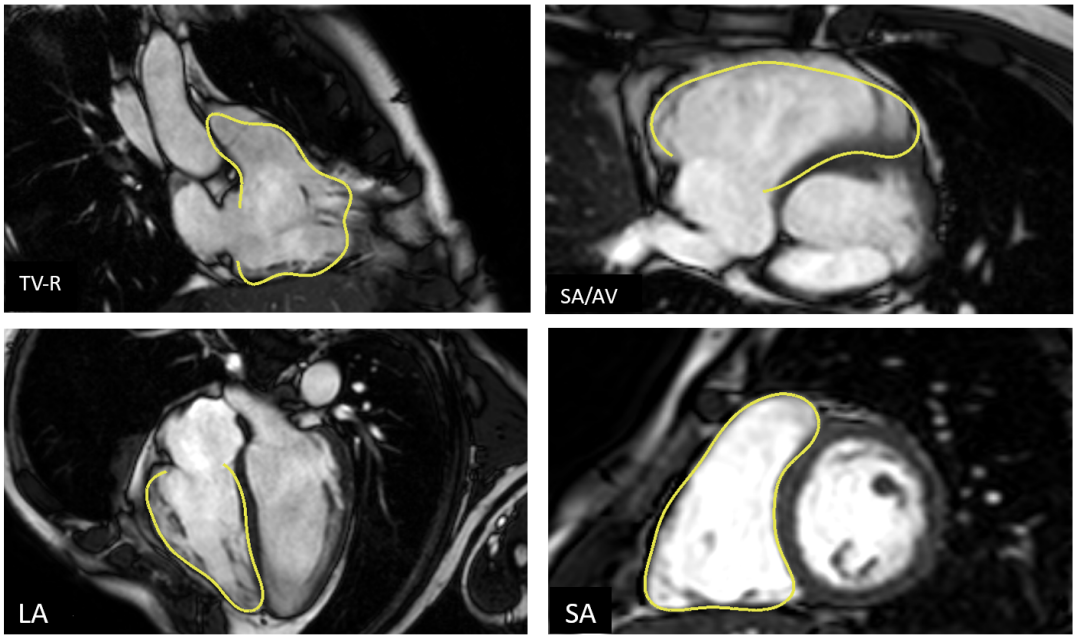

Figure 4.3: Patient A, right ventricle: projection of the 3D end-diastolic model obtained with MSMorph III technique (see Section 3.3) onto Rotational-TV (TV-R) acquisitions (top, left), Long-Axis (LA) acquisitions (bottom, left), Short-Axis Aortic Valve (SA/AV) acquisitions (top, right), Short-Axis (SA) acquisitions (bottom, right).

becomes lower or null in different portions towards the diastolic phase.

4.4. Patient A: reconstructions of left ventricle

First, a description of the specific procedure for obtainment of 3D models of left ventricle of Patient A is given. Then results of the reconstructions, in terms of shape and endocardial displacement, are presented.

4.4.1. Procedure for achievement of left ventricle reconstructions

The application of the MSMorph reconstruction technique (see Chapter 3) on left ventricle of Patient A, presented in Section4.1, had yielded endocardial surfaces comprehending the aorta: in particular, the left ventricle reconstruction had been separated from the generation of models for the aorta, since this revealed to be the best way for the applica-

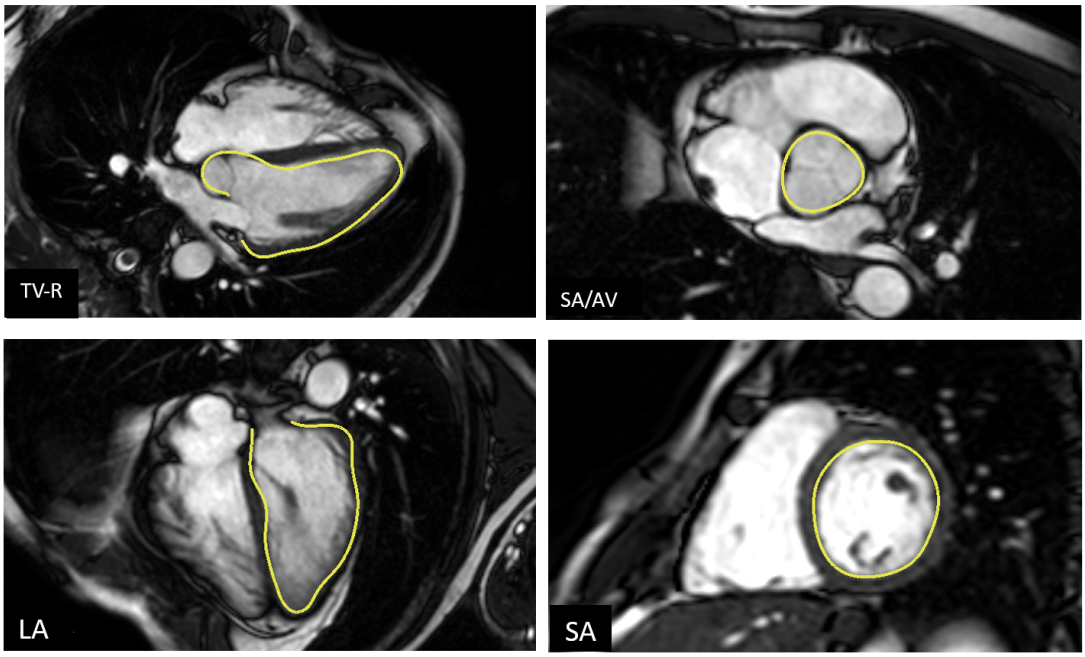

Figure 4.4: Patient A, left ventricle: projection of the 3D end-diastolic model obtained with MSMorph II technique (see Section 3.3) onto Rotational-TV (TV-R) acquisitions (top, left), Long-Axis (LA) acquisitions (bottom, left), Short-Axis Aortic Valve (SA/AV) acquisitions (top, right), Short-Axis (SA) acquisitions (bottom, right).

tion of the MSMorph technique for left reconstruction. In all the processes of generation of surfaces by morphing, a sphere was used as a template surface, with reference to the description in Section 3.4.2. The aortic reconstruction and the ventricle one have been processed performing an intersection of the distinct morphed surfaces obtained with *vmtksurfacebooleanoperation* command in VMTK: the intersection is then used for calculation of the implicit distance in the aortic and ventricle reconstruction with respect to the intersection itself. Then, with application of a *Threshold* filter on Paraview[3] a maximum and minimum value for the distance computed was selected to obtain the desired output, where intersection have been removed. The lower and upper threshold was selected to be 0.1 and the maximum value possible respectively. Lastly, the connection between the two new surfaces, where intersection have been removed in each, was performed with *vmtksurfaceconnector* filter of VMTK.

As for right ventricle, the generation of mitral valve was performed manually with Autodesk Meshmixer application [7] by comparison with cine-MRI images. The aortic valve was obtained with a *clip* filter in Paraview application.

Epicardium and myocardium generation was carried out with the same procedure as in right ventricle, with obtainment of endocardial shapes and displacements with the proce-

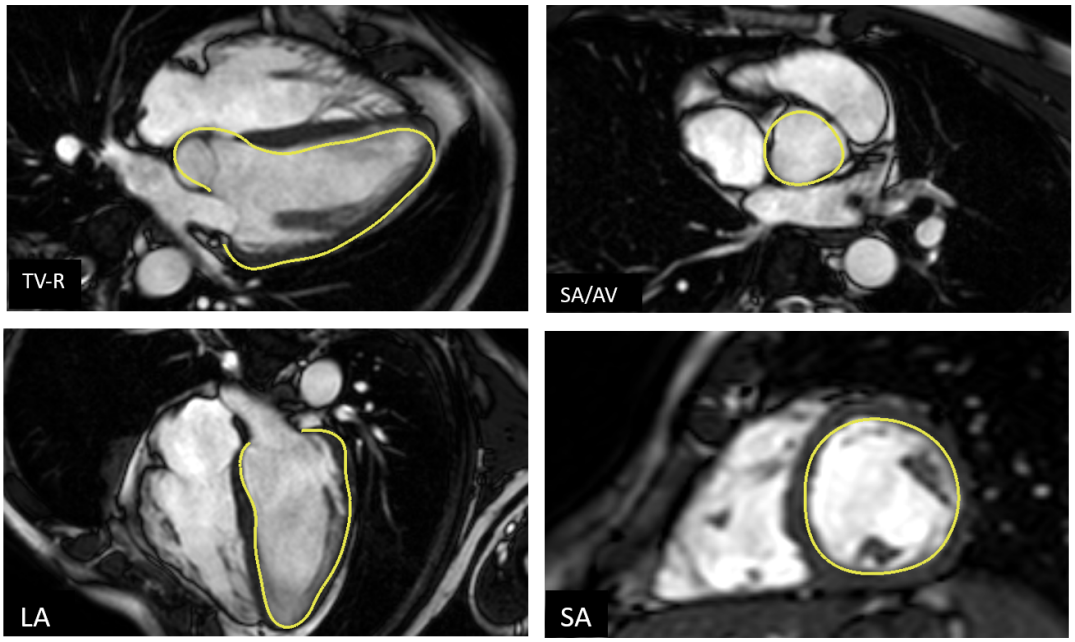

Figure 4.5: Patient A, left ventricle: projection of the 3D end-diastolic model obtained with MSMorph III technique (see Section 3.3) onto Rotational-TV (TV-R) acquisitions (top, left), Long-Axis (LA) acquisitions (bottom, left), Short-Axis Aortic Valve (SA/AV) acquisitions (top, right), Short-Axis (SA) acquisitions (bottom, right).

dure described in Section 2.3.

4.4.2. Result of left ventricles reconstructions and biventricular models

Respectively surface and displacement field visualizations of the left ventricle reconstructions of Patient A are shown in Figure 4.11 and Figure 4.12. As obtained for the right ventricle reconstructions, ventricular volume increases from the systolic to the diastolic phase, as can be seen in the morphology representation. In addition, the quantification of the displacement of the endocardial wall motion is provided, showing a peak in systolic phase and decrease towards diastolic phase, as expected.

The left ventricle's reconstruction can be used in combination with the right heart representation to obtain a biventricular model, as shown in Figure 4.13. The representation of morphology and displacement field can be useful for evaluation of ventricular interdependence. Indeed, the interaction between cardiac ventricles has been assessed to have

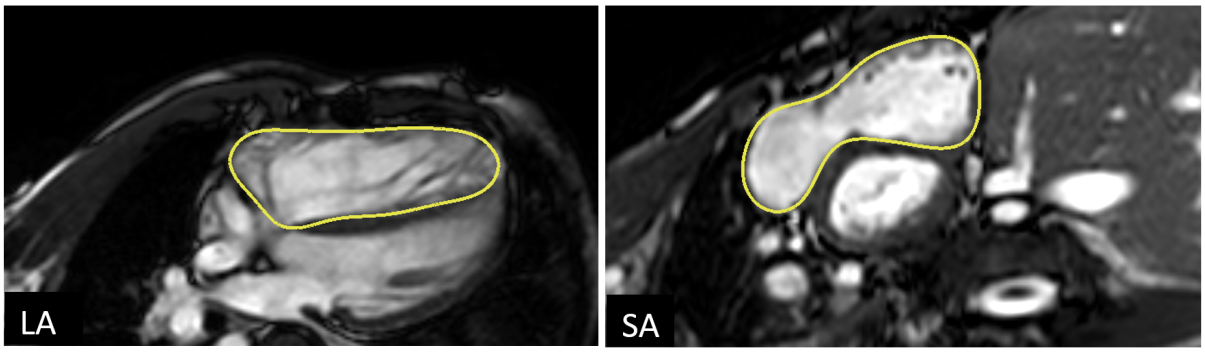

Figure 4.6: Patient B, right ventricle: projection of the 3D model obtained with MSMorph III technique, (see Section 3.3), onto Long-Axis (LA) acquisitions (left), Short-Axis (SA) acquisitions (right).

a clinically relevant role: the forces exchanged between pumping cardiac chambers, due to their anatomical proximity and the fact that they share a septal wall, determines that alterations on one ventricle can result in effects on the other.

In particular, for the present work the focus have been kept on the right ventricle: the left ventricular contraction have effects on the right ventricular one in terms of pressure and volume of the outflow for about 20%-40% [88] and the right ventricular response in presence of pathological conditions can be linked to this dependency on left ventricle movement. The interaction between ventricles can have diagnostic relevance, as for example an increased ventricular interdependence can be related to respiratory-driven changes in left and right ventricular filling [47].

4.5. Patient B: reconstructions of right ventricle and comparison with Patient A

The reconstruction of the right ventricle of Patient B, affected by Tetralogy of Fallot as introduced in Section 4.1, was compared with representation of right ventricle of Patient A obtained with the same variant of the Multi-Series Morphing technique, MSMorph III (see Section 3.3), most simple and fast variant of the reconstruction method, to analyze cases in which clinically atypical acquisitions such Rotational-TV and Short-Axis Aortic Valve series, are not available. As for previous cases in Sections 4.3 and 4.4, the visualization of shape and displacement field are represented in the three characteristic phases of cardiac cycle: end-systole, diastasis, end-diastole. Results of reconstructions for Pa-

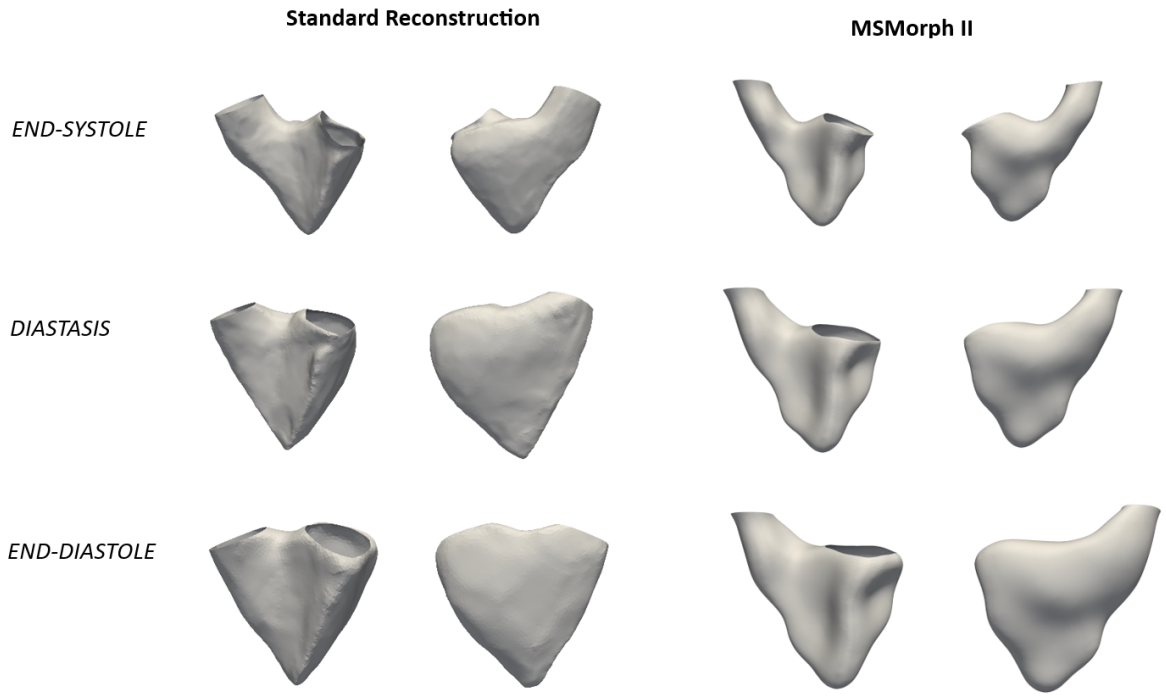

Figure 4.7: Patient A, right ventricle : comparison of morphology between reconstructions of right ventricle with standard reconstruction technique (left double column) and MSMorph II technique (right double column). Two views for each model are displayed in the three chosen cardiac phases defined by the three rows: from top to bottom are end-systolic phase, diastasis phase and end-diastolic phase.

tient B, compared with ones of Patient A, are now shown in Figure 4.14. Considering the surface visualization, shape differences between healthy and pathological cases can be observed:

- Broader and rounder apex for the ToF model
- Bulging RV apex laterally at the level of the tricuspid valve annulus: it can be observed in the right view in columns, where the basal portion of the ventricle is more pronounced towards the left, with respect to the healthy case.
- Tilted TV annulus

These variations were found also in [93] where an analysis of the ventricular shape in ToF patients is carried out. Moreover, in the paper, end-systolic variations were found to be less visible, tendency that remains true for the present work.

The RV dilation observed in the pathological case of Patient B has impact also on the endocardial displacement field in Figure 4.15: compared to healthy Patient A, the ventricular wall motion of right ventricle in case of Tetralogy of Fallot is highly lowered. The

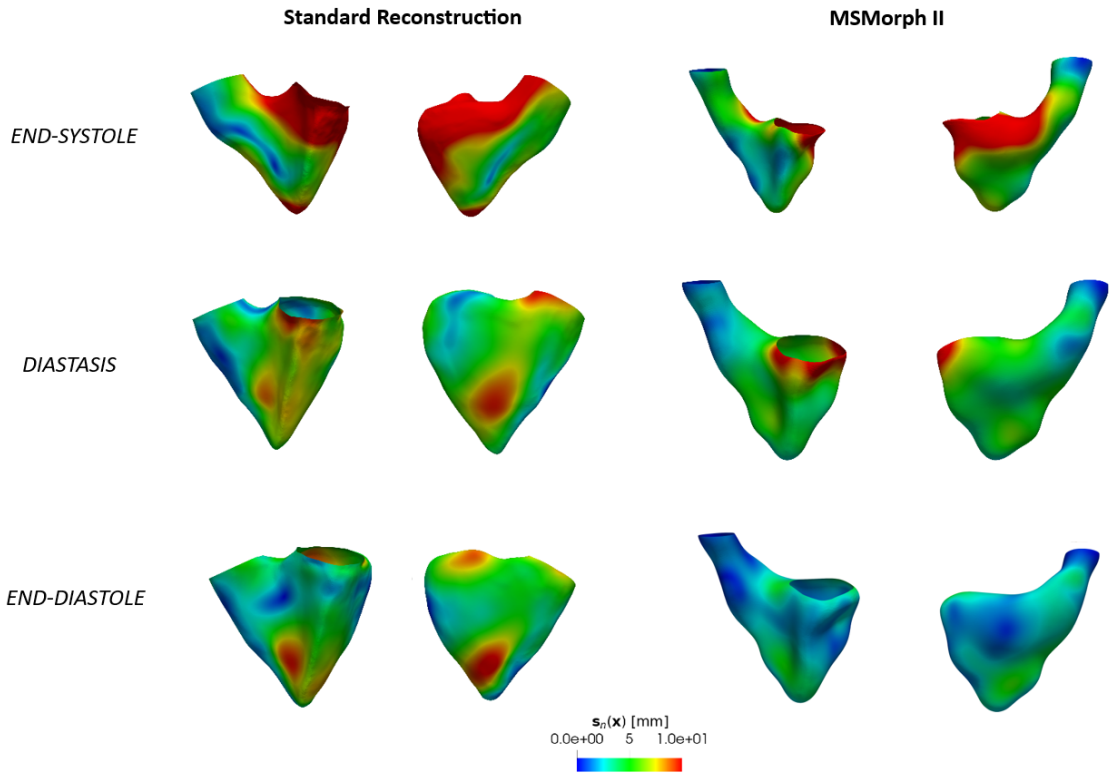

Figure 4.8: Patient A, right ventricle: comparison of displacement field between reconstruction of healthy right ventricle with Standard Reconstruction technique (left double column) and MSMorph II technique (right double column). Two views for each model are displayed in the three chosen cardiac phases defined by the three rows: from top to bottom are end-systolic phase, diastasis phase and end-diastolic phase. The colored legend (top, left) defines values of endocardial displacement.

difference can be observed in particular at the systolic phase, where the decreased contraction of the ventricular wall for models of Patient B is evident from the displacement. As mentioned in Section 1.2, the RV systolic function in this particular pathological scenario can be altered by the dilation of the ventricle. The consequence can be a decreased value of Ejection Fraction, that is assessed in Section 4.6.

4.6. Analysis of ventricular volumes

Ventricular volumes are clinically relevant parameters of the cardiac functionality. The evolution in time of ventricular volumes and their flowrate have been achieved: the evaluation of fluctuations is used for comparison for different techniques. Ranges of physiological values for right and left ventricular volumes are given by [51], [78], [50]. The obtaining

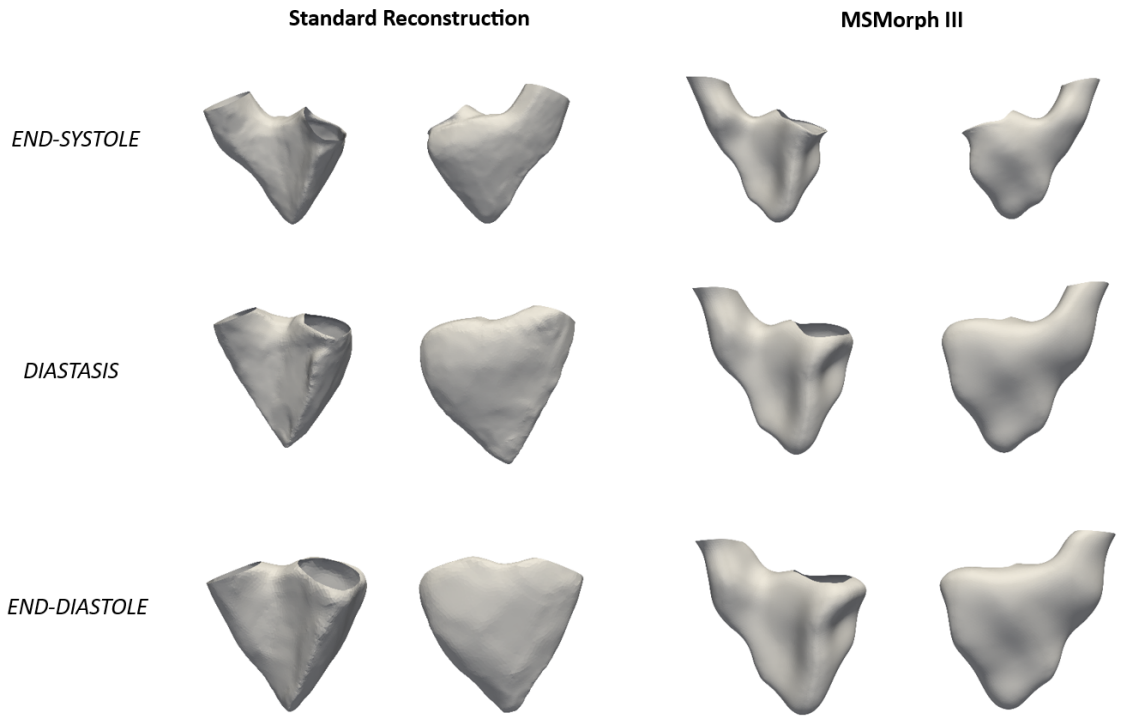

Figure 4.9: Patient A, right ventricle: comparison of morphology between reconstruction of healthy right ventricle with Standard Reconstruction technique (left double column) and MSMorph III technique (right double column). Two views for each model are displayed in the three chosen cardiac phases defined by the three rows: from top to bottom are end-systolic phase, diastasis phase and end-diastolic phase.

of volumes, in terms of End-Systolic (ESV) and End-Diastolic (EDV) volumes that are corresponding minimum and maximum ventricular volumes, can be exploited to evaluate other key parameters for the assessment of correct functionality of cardiac ventricles. For this purpose, the calculation of Ejection Fraction and Stroke Volume values have been carried out with EDV and ESV obtained by the obtained models. The description of these parameters and their expression have been detailed in Chapter 1.
For simplicity of exposure, the current analysis is carried out divided by left ventricle and right ventricle models: in particular, left ventricle volumes are related to Patient A, while right ventricle volumes are achieved both of Patient A and Patient B, defined in Section 4.1. Indeed, two subsections are now followed: respectively, left ventricle volumes and right ventricle volumes.

4.6.1. Left ventricle volumes

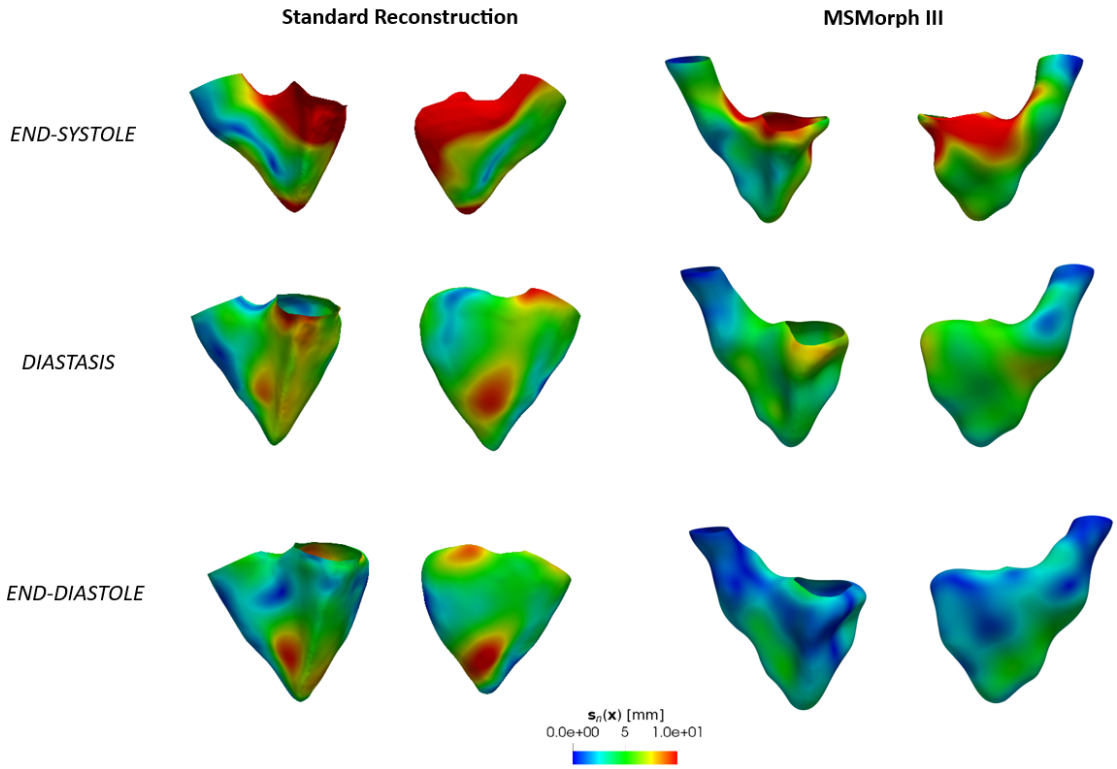

Figure 4.10: Patient A, right ventricle: comparison of displacement field between reconstruction of healthy right ventricle with Standard Reconstruction technique (left double column) and MSMorph III technique (right double column). Two views for each model are displayed in the three chosen cardiac phases defined by the three rows: from top to bottom are end-systolic phase, diastasis phase and end-diastolic phase. The colored legend (bottom, center) defines values of endocardial displacement.

For the left ventricle reconstructions of Patient A (see Section 4.1), the evolution in time of the ventricular volume in case of MSMorph II and MSMorph III variants is shown in Figure 4.16. The evolution in time of the LV volume shows the expected tendency of decreasing values in systolic phase, reaching a minimum value representing the ESV, then reversing in increasing values corresponding to the ventricular filling in diastolic phase. The fluctuations of values are attenuated by the use of MSMorph II variant with respect to the other: this reflects the importance of merging more information using a higher number of cine-MRI series to reduce abrupt changes in ventricular volume that do not reflect the real physiology of the heart.
The attenuation of fluctuations in the MSMorph II variant with respect to the other is confirmed also by the evolution in time of the LV volumes flowrate, represented in Figure 4.17. The LV volumes were then used for the calculation of EF and SV parameters, to be compared to reference range values found in scientific literature: parameters values and

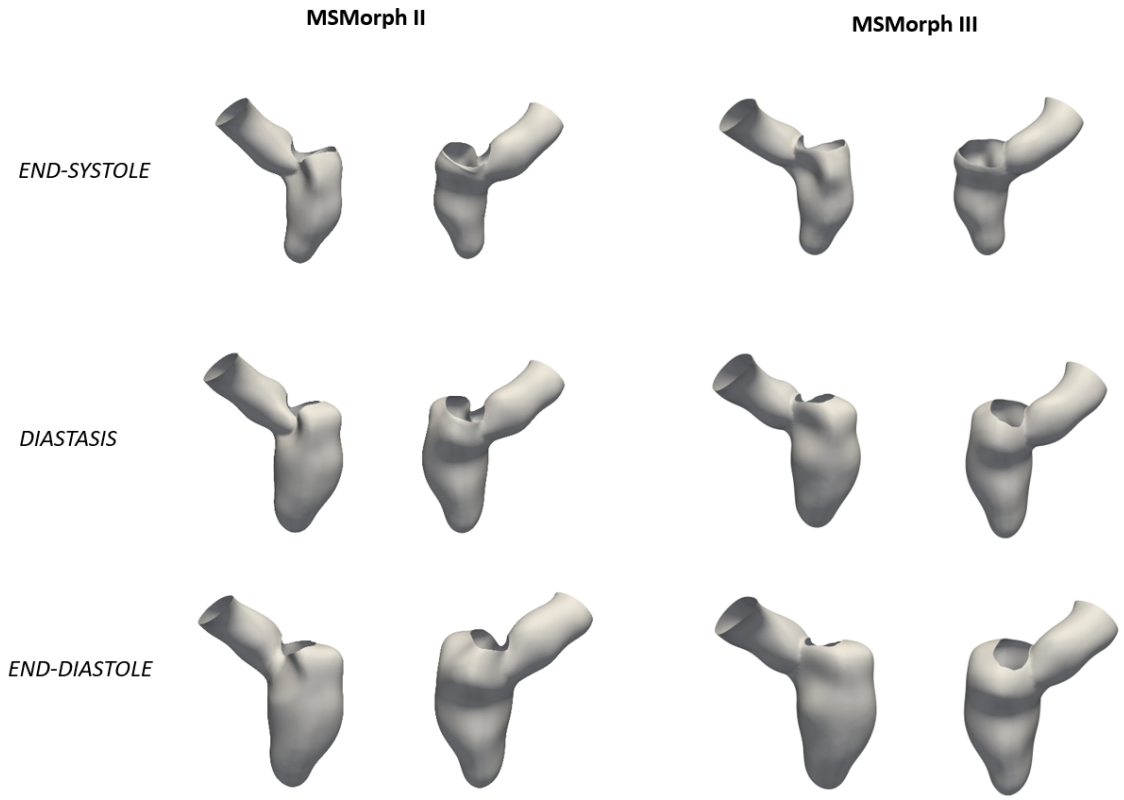

Figure 4.11: Patient A, left ventricle: comparison of morphology between reconstruction of healthy left ventricle with MSMoprh II technique (left double column) and MSMorph III technique (right double column). Two views for each model are displayed in the three chosen cardiac phases defined by the three rows: from top to bottom are end-systolic phase, diastasis phase and end-diastolic phase.

comparison can be found in Table 4.1.

Values of EDVi and SVi are in line with reference values from literature, while ESVi and EF differs from the reference values: ESVi is about 32% above the Upper Limit (UL) value, while EF is 22% lower with respect to the Lower Limit (LL). Accordingly to literature [53], EF and ESVi are related through an inverse, non-linear relationship: the tendency is for high values of ESVi to have corresponding low EF values, which is reflected by the data we obtained. This discrepancy can be due the portion in which aortic tract and left ventricle volumes have been artificially connected.

4.6.2. Right ventricle volumes

The evolution during the cardiac cycle of the volumes of right ventricle models of both

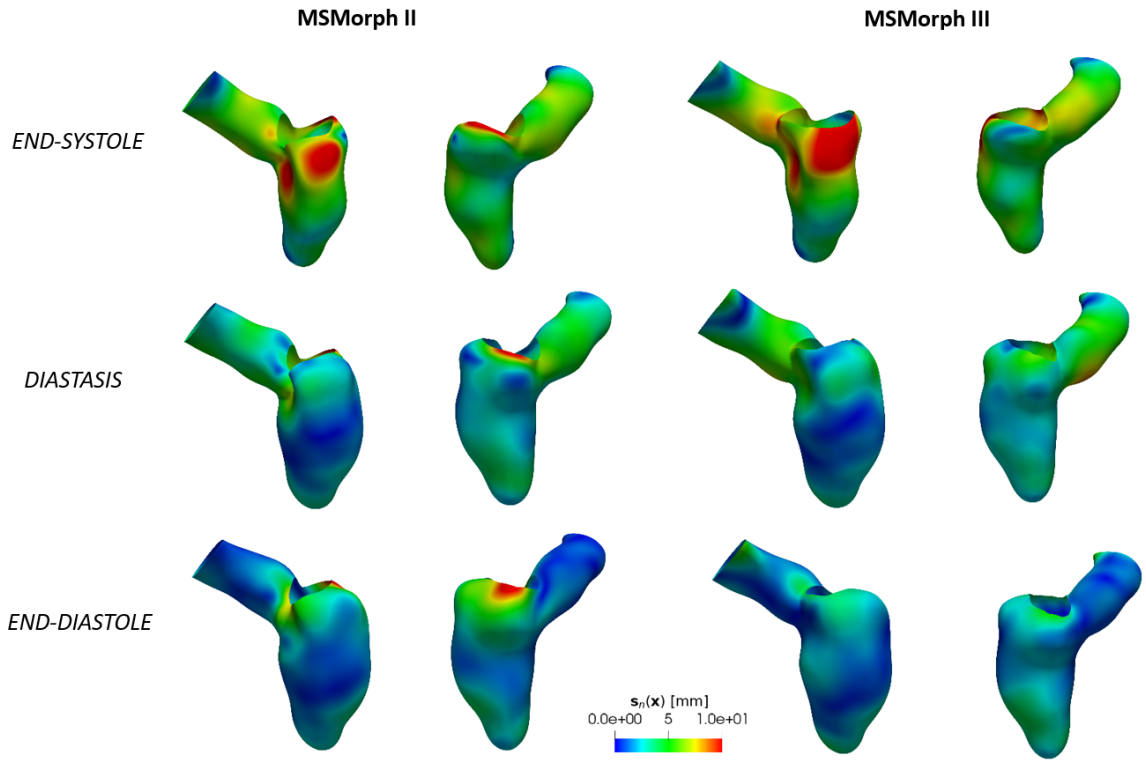

Figure 4.12: Patient A, left ventricle: comparison of displacement field between reconstruction of healthy left ventricle with MSMorph II technique (left double column) and MSMorph III technique (right double column). Two views for each model are displayed in the three chosen cardiac phases defined by the three rows: from top to bottom are end-systolic phase, diastasis phase and end-diastolic phase. The colored legend (bottom, center) defines values of endocardial displacement.

Patient A and Patient B (see Section 4.1) reconstructions is shown in Figure 4.18: the evolution remains the same with decreasing volumes for systolic contraction and increasing for ventricular filling.
The comparison between techniques highlights the more fluctuating evolution of a standard reconstruction technique, defined in Chapter 2, with respect to MSMorph technique in two variants, defined in Section 3.3, applied to Patient A. Especially, as observed for the LV reconstruction volumes in the previous section, MSMorph II over MSMorph III has less fluctuations: the tendency shows that more information are incorporated in the model reconstruction technique, less are the fluctuations observed in the time evolution of volumes in the models. However, the MSMorph III technique results in slight fluctuations, as also represented by the application of this variant to the ventricle reconstruction of Patient B, which shows much higher ventricular volumes, even if the patient is younger with respect to Patient A. For Patient B, evident RV dilation can be observed.

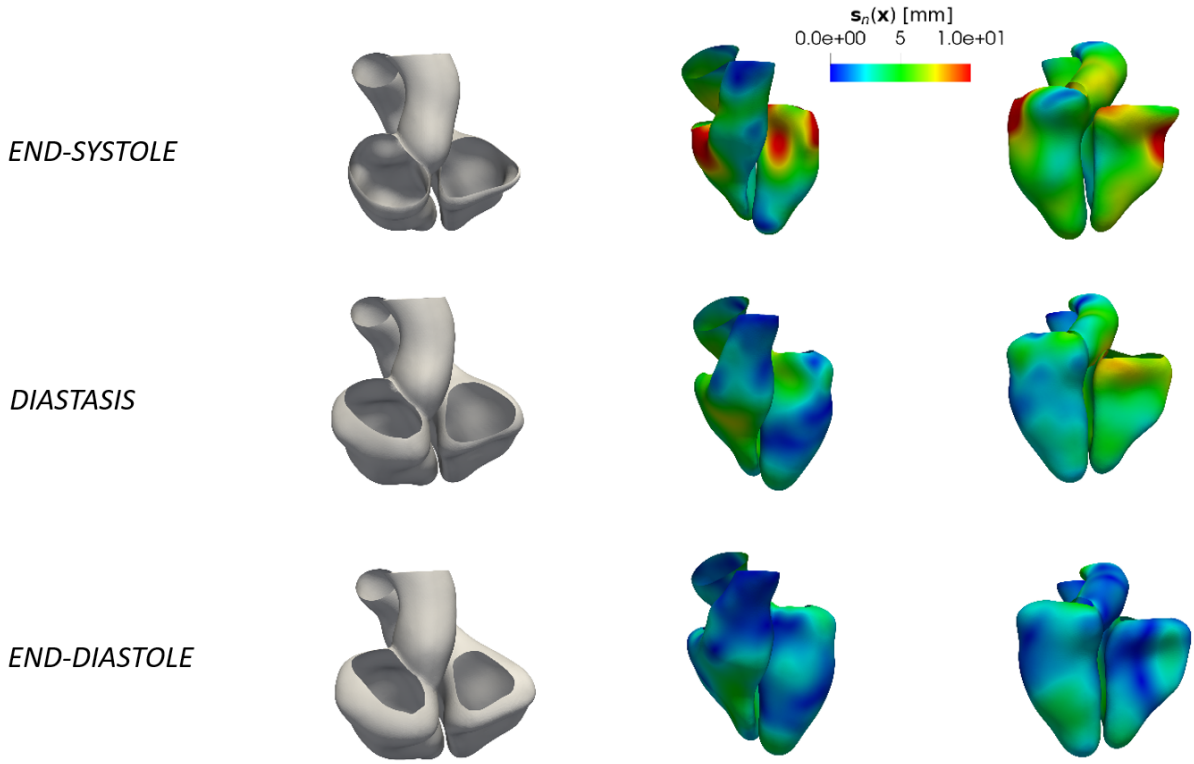

Figure 4.13: Patient A, biventricular model: morphology in a top view (left column) and the displacement field in two views (central and right columns). Models are displayed in the three chosen cardiac phases defined by the three rows: from top to bottom are end-systolic phase, diastasis phase and end-diastolic phase.

The difference in fluctuations can be also observed considering the evolution time of the RV flowrates: fluctuations are accentuated for SA-based technique, where the manual improvement is greater, while MSMorph technique results to generate models in which variations of volume over the cardiac cycle are attenuated, reflecting a more physiological scenario. A representation is given in Figure 4.19. The analysis of ventricular volumes is enriched as above mentioned by computation of clinically relevant parameters, that are compared with reference values found in literature. The clinical parameters obtained by reconstructions are listed in Table 4.2. All values listed are in accordance with references found in scientific literature for every technique that has been used to generate models, with a slight difference for ejection fraction (EF) in application of MSMorph II and MSMorph III. Reference parameters are listed in Table 4.3. The reference values are related to healthy ventricular values, then to be compared with values only of Patient A: the ventricular model of Patient B, affected by Tetralogy of Fallot as defined in Section 4.1, resulted to have greater ventricular volumes, as in the previous time analysis, and lower ejection fraction. This tendency has been found also in [93]: in this paper, mean

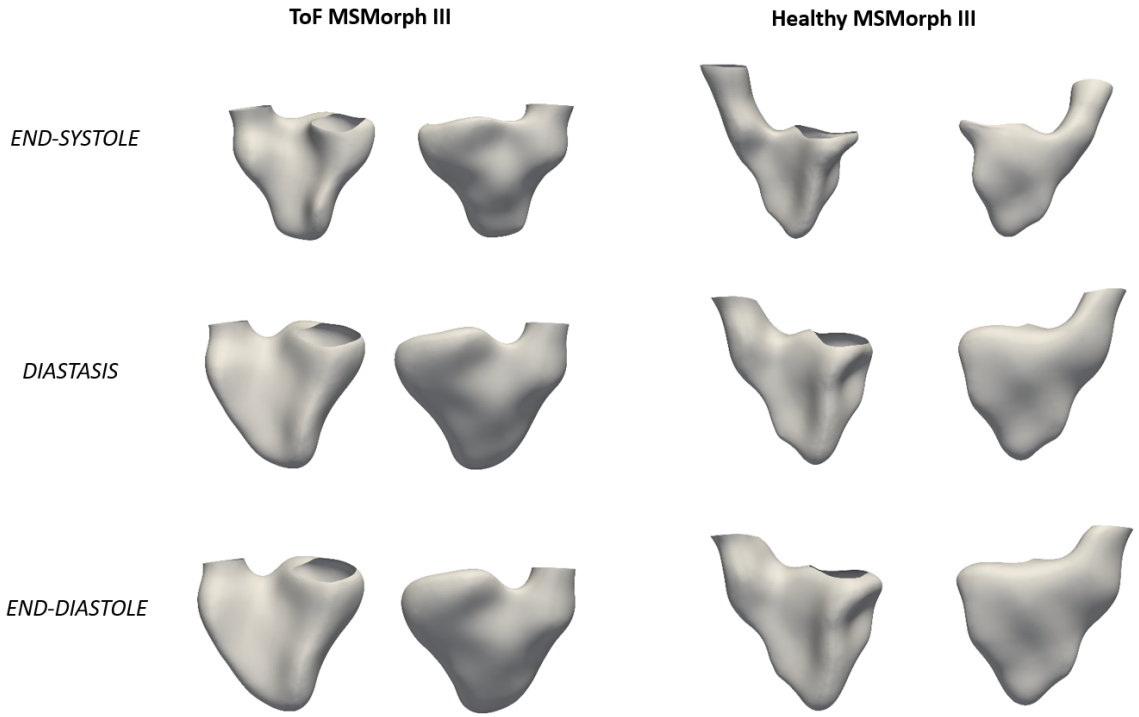

Figure 4.14: Morphology of RV surfaces related to Patient B (left) and Patient A (right), obtained with the same MSMorph III variant (see Section 3.3) at three specific phases of cardiac cycle: the first row represents the end-systolic reconstructions, the second row the reconstruction at diastasis phase, the third row displays the end-diastolic surfaces.

values of RVEDVi and RVESVi in ToF patients were obtained to be 216 ± 99 and 139 ± 88, while EF resulted as 40 ± 9. The parameters obtained in the ToF model of this work results in accordance with these values, with a slightly decreased valued for EF: it can be observed that reference values of ToF patients have huge variations with respect to healthy values and this can be addressed to the great variations in anomalies charachterizing these pathological hearts. Also, the RV dilation, as mentioned in Section 1.2, can alter the RV systolic function, resulting in a decreases value of ejection fraction: indeed, RV dilation has been confirmed by the morphological representation of the results above.

4.7. Analysis of accuracy and efficiency of the MSMorph technique

Analysis of accuracy and efficiency of Multi-Series Morphing technique (see Chapter 3) are carried out considering models obtained exclusively for Patient A, introduced in Section

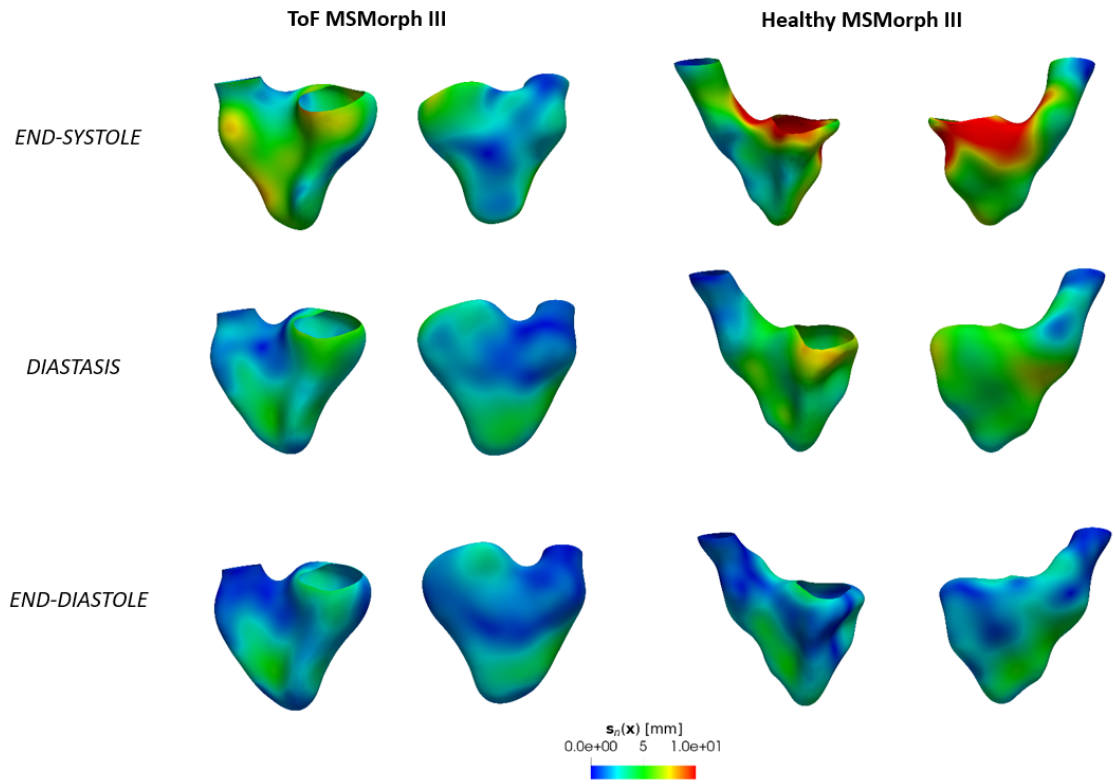

Figure 4.15: Displacement field of RV surfaces related to Patient B (left) and Patient A (right), obtained with the same MSMorph III variant (see Section 3.3) at three specific phases of cardiac cycle: the first row represents the end-systolic reconstructions, the second row the reconstruction at diastasis phase, the third row displays the end-diastolic surfaces.

4.1: indeed, analysis of the accuracy of MSMorph technique consists in comparison of the reconstructed models with respect to the gold standard contours, traced with completely manual segmentation, provided only for Patient A by Ing. Francesca Renzi, as specified in Section 4.1.
The efficiency of the MSMorph method was assessed instead by comparing the time used for the entire generation of contours and surfaces of Patient A, except the time for the manual generation of orifices of tricuspid and pulmonary valves in right ventricle. The comparison was based on the use of a standard reconstruction, described in Chapter 2, and MSMorph technique, explained in Chapter 3. Given these considerations, as the standard reconstruction technique was only applied to Patient A, this analysis is again referred only to this patient.

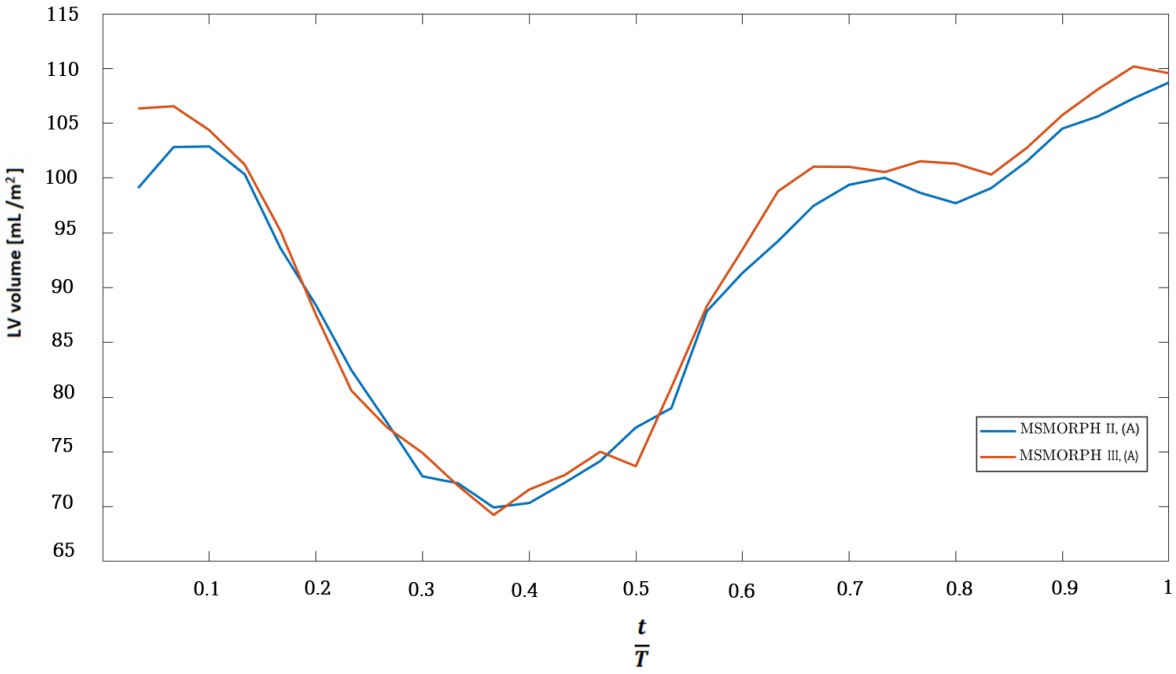

Figure 4.16: Time-evolution of LV volumes for MSMorph II and MSMorph III (see Section 3.3) applied to Patient (A), normalized by Body Surface Area (BSA). The x axis represents the acquisition times normalized by heartbeat duration (T). The legend represents the name of the technique applied, followed by the letter defining the patient in brackets.

4.7.1. Analysis of accuracy

Accounting for accuracy, it is important to note that contours manually traced for each slice and frame represent the gold standard technique for the reconstruction of the right ventricle: the manual operation allows very precise tracing, considering that all the anatomical knowledge permits to distinguish different structures that can be hidden in the MRI images. Indeed, the accuracy of contours reconstructions has impact in the overall accuracy of the final model: it needs to be aligned at best to the real anatomical shape of the ventricle. For this reason, the present analysis is carried out in comparison with this reference method.
Provided gold standard contours are represented in Figure 4.20.
Automatization of the segmentation procedure, introduced by the MSMorph technique (see Chapter 3) in the contours generation process, can be a powerful tool to decrease the total segmentation time, which represents the principal downside of manual approach combined to the inter-variability for the dependency on the user. Accuracy of the MSMorph technique was assessed by computation of two parameters:

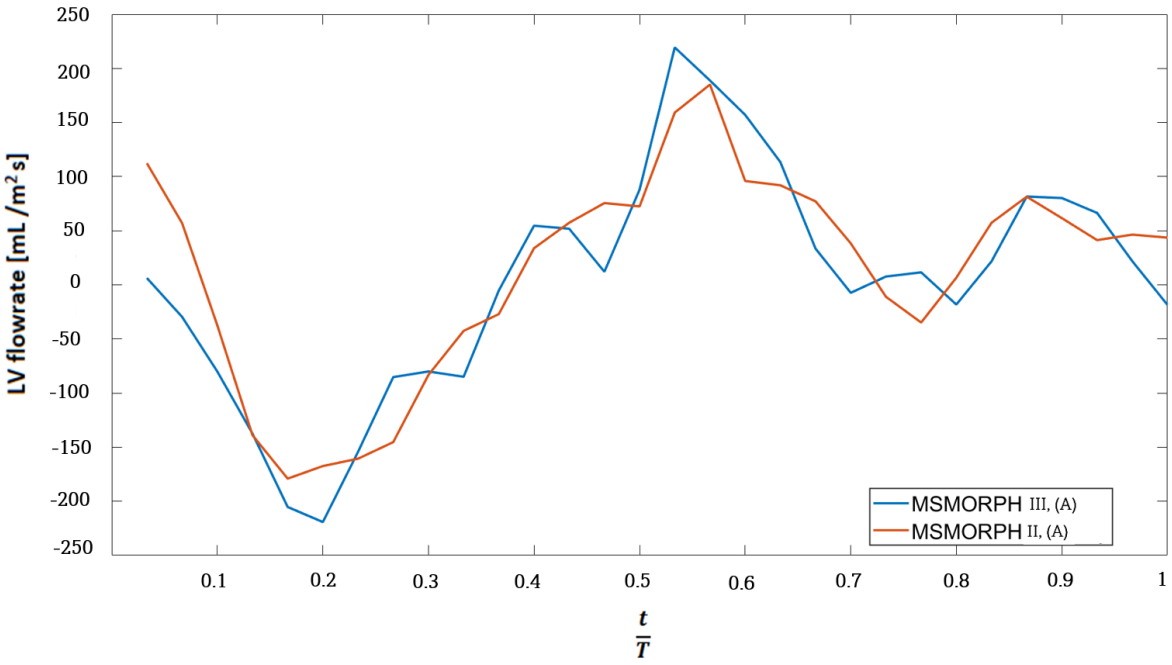

Figure 4.17: Time-evolution of LV flowrate for MSMorph II and MSMorph III (see Section 3.3) applied to Patient (A), normalized by Body Surface Area (BSA). The x axis represents the acquisition times normalized by heartbeat duration (T). The legend represents the name of the technique applied, followed by the letter defining the patient in brackets.

- Mean Square Distance (MSD) between the Gold Standard manual contours and the contours obtained in the MSMorph procedure: this value can assess the accuracy of the automatic registration of contours over cardiac cycle by use of one manually traced contour.
  For this work we identify as $\overline{\Gamma}_n$ the gols standard contours, representing the reference configuration, and with Γ_n we consider the semi-automatically obtained contours used for application of MSMorph variants of the technique.
  In this notation, the MSD definition, based on [84], is given by

$$MSD = \frac{1}{|\overline{\Gamma}_n|} \cdot \int_{\overline{\Gamma}_n} ||x - \widehat{x}||^2_{R^3} dx$$

  For MSD, given x $\in \overline{\Gamma}_n$, $\widehat{x}$ is defined as:

$$\widehat{x} = \underset{y \in \Gamma_n}{\text{argmin}} ||y - x||_{R^3}$$

- Time Average Mean Square Distance (TAMSD) between the Gold Standard manual contours and the endocardial surfaces obtained in MSMorph variants: this value can

Parameters	MSMorph II,(A)	MSMorph III,(A)	Mean (LL-UL) [51]
$EDVi[mL/m^2]$	108,7	109,5	86 (61–112)
$ESVi[mL/m^2]$	69,9	69,2	34 (14-53)
$SVi[mL/m^2]$	38,7	40,3	54 (40-68)
$EF[\%]$	35,6	36,7	60 (46-74)

Table 4.1: Patient (A), LV clinical parameters for MSMorph II and MSMorph III (see Section 3.3) variants. EDVi: End-Diastolic Volume indexed, as EDV normalized by BSA. ESVi: End-Systolic Volume indexed, as ESV normalized by BSA. SVi: Stroke Volume indexed, as SV normalized by BSA. In first row, the names of the technique applied are present, each followed by the letter defining the patient in brackets. The last slot on the right in first row instead represents the presentation of reference values composed of a Mean value and the corresponding Lower Limit (LL) and Upper Limit (UL), with the source cited.

Index	SA-based,(A)	MSMorph II,(A)	MSMorph III,(A)	MSMorph III,(B)
$EDVi[mL/m^2]$	94.1	92.5	90.2	178.7
$ESVi[mL/m^2]$	51.2	57.1	55.6	127.5
$SVi[mL/m^2]$	42.8	35.4	34.6	51.2
$EF[\%]$	45.5	38.3	38.3	28.6

Table 4.2: RV clinical parameters. EDVi: End-Diastolic Volume indexed, as EDV normalized by BSA. ESVi: End-Systolic Volume indexed, as ESV normalized by BSA. SVi: Stroke Volume indexed, as SV normalized by BSA. In first row, the names of the technique applied are present, each followed by the letter defining the patient in brackets. SA-based: standard reconstruction technique.

assess the accuracy of the generation of the surface using the morphing technique. TAMSD is computed between the gold standard contours $\overline{\Gamma}_n$ and the endocardial surfaces Λ_n obtained by MSMorph technique over the cardiac cycle: the discrepancy between them is defined, based on [84], as:

$$TAMSD(\overline{\Gamma}_n, \Lambda_n) = \frac{1}{T} \sum_{n=0}^{T/\tau_{cMRI}} \frac{1}{|\overline{\Gamma}_n|} \cdot \int_{\overline{\Gamma}_n} ||x - \widehat{x}||^2_{R^3} dx$$

where T represents the heartbeat duration and τ_{cMRI} the time resolution of cine-MRI.

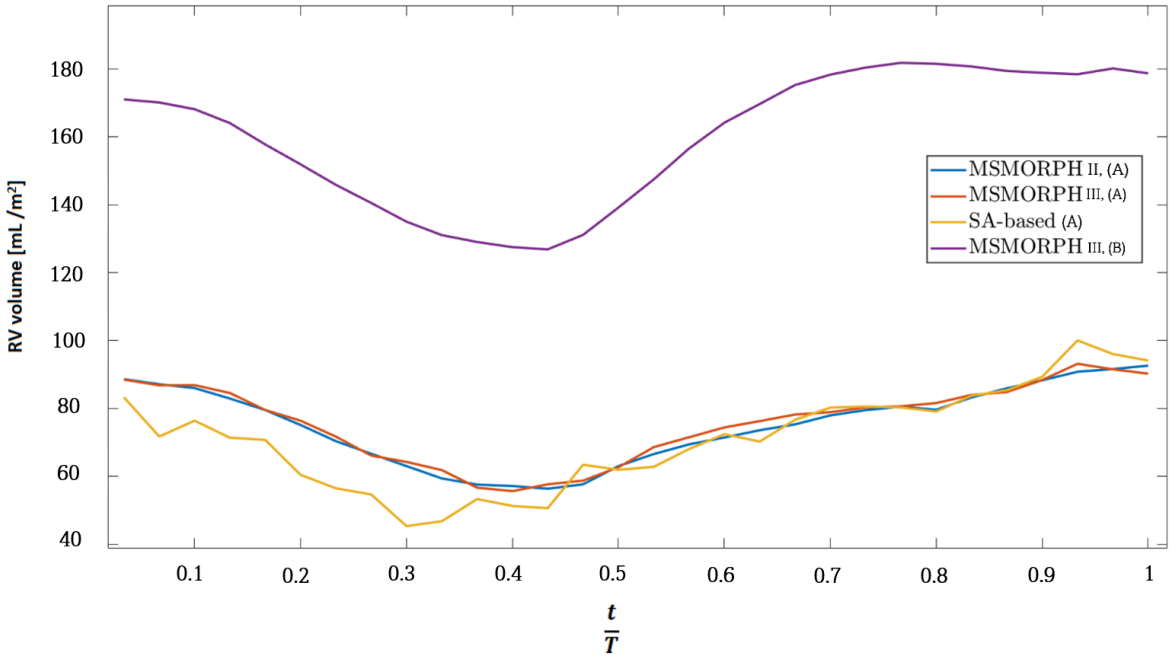

Figure 4.18: Time-evolution of RV volumes for each technique applied to Patient (A) and (B), normalized by Body Surface Area (BSA). The x axis represents the acquisition times normalized by heartbeat duration (T). The legend represents the name of the technique applied, followed by the letter defining the patient in brackets. SA-based: standard reconstruction technique.

For TAMSD, given x $\in \overline{\Gamma}_n$, $\widehat{x}$ is defined as:

$$\widehat{x} = \underset{y \in \Lambda_n}{\operatorname{argmin}} ||y - x||_{R^3}$$

Results for the parameters are displayed, as evolution in time of the MSD over the cardiac cycle in Figure 4.21 and values obtained for the square root of TAMSD for the different techniques used for RV reconstruction are shown in Table 4.4.

The time evolution of MSD shows that values decrease significantly in correspondence of the time frame of diastasis, where the manual tracing of the contour has been performed: MSD value in this phase does not reach a zero values as contours do not coincide, but the great decrease of this value represents how the manual tracing in both cases generated a similar result. The other values of MSD, both before and after diasiasis phase, increases since the error generated accumulates, but it is important to note that they reach at maximum the double value of the in-slice resolution of 1.15 mm. Incresead values of this parameter can be related to the difficulty of the automatic generation of contours to

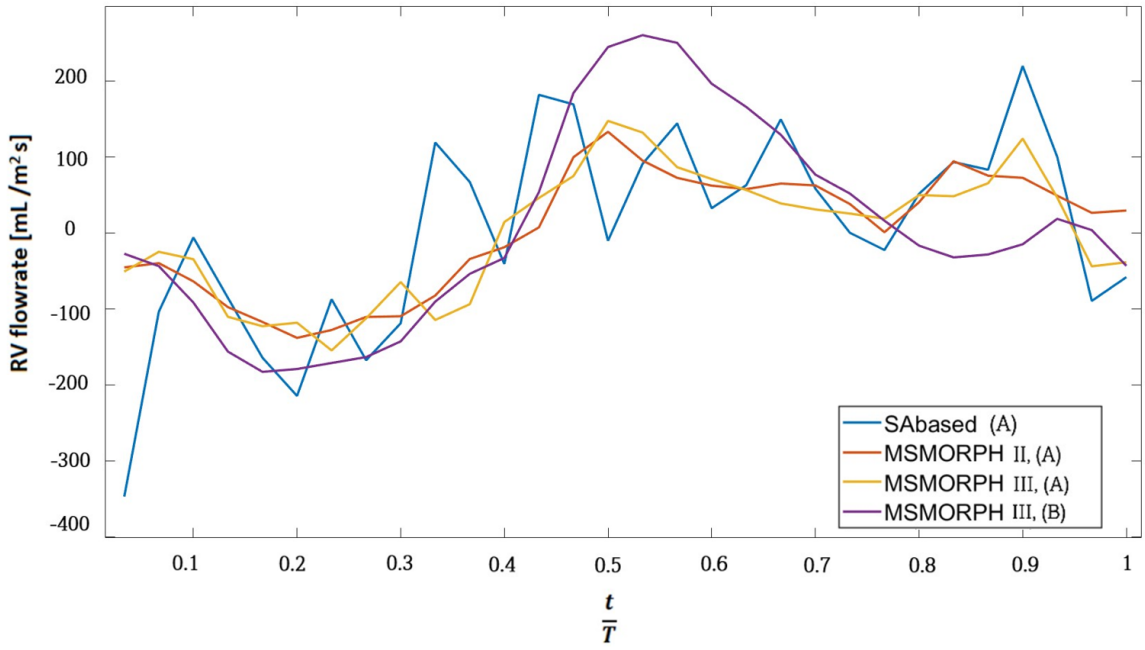

Figure 4.19: Time-evolution of RV volumes flowrate for each technique applied to Patient (A) and Patient (B). The x axis represents the acquisition times normalized by heartbeat duration (T). The legend represents the name of the technique applied, followed by the letter defining the patient in brackets. SA-based: standard reconstruction technique.

perfectly delineate the endocardium in case of trabeculations, that characterize the RV anatomical structure: an highly trabeculated structure in the MRI representation can results with an altered grey-level function with respect to structure in which trabeculations are absent. These variations result in the MRI image and can be instead caught with manual contouring.
Analyzing the discrepancy not between contours sets but between reference manual contours and morphed surfaces, TAMSD is instead computed. Values obtained are close to the in-slice resolution of 1.15 mm: the accuracy of all the reconstructed models with respect to the reference of manual contours set. Accuracy is comparable for the standard reconstruction (see Chapter 2) and MSMorph techniques that are characterized only by a slight improvement with respect to standard reconstruction technique. Accuracy is preserved with a greater efficiency, due to the decreased reconstruction time used for MSMorph technique, that is now analyzed in the following section.

4.7.2. Analysis of efficiency

Analysis of the reconstruction time employed in standard reconstruction technique, de-

Index	normal range [78]	mean ± SD [51]
$EDVi[mL/m^2]$	68-125	94±15
$ESVi[mL/m^2]$	25-63	44±11
$SVi[mL/m^2]$	34-67	51±13
$EF[\%]$	45-65	52±8

Table 4.3: Reference values of clinical parameters for right healthy ventricle. EDVi: End-Diastolic Volume indexed, as EDV normalized by BSA. ESVi: End-Systolic Volume indexed, as ESV normalized by BSA. SVi: Stroke Volume indexed, as SV normalized by BSA. The two columns represents reference ranges from different sources, cited in the description. SD: Standard Deviation.

SA-based	MSMorph III	MSMorph II
1.75 mm	1.61 mm	1.57 mm

Table 4.4: Values of square root of TAMSD computed for different techniques: SA-based corrresponds to a standard reconstruction technique (see Chapter 2), while MSMorph II and MSMorph III corresponds to variants of the MSMorph technique (see Chapter 3). These results are referred to Patient A, defined in Section 4.1.

scribed in Chapter 2 and MSMorph variants (see Section 3.3), applied to Patient A, defined in Section 4.1, is carried out. The reconstruction time is intended as the amount of time employed for the segmentation of medical images and for the achievement of the 3D surface that best fits the real anatomy. The generation of valve orifices, obtainment of epicardial and myocardial surfaces and the achievement of endocardial motion, delineated in Chapter 2, are not considered, as performed equally in all reconstruction techniques.

Making a comparison, the generation of all contours and of the final endocardial surfaces has the following durations in different techniques applied:

- Generation of contours with a standard reconstruction technique is performed with the use of MITK Workbench application combined with the manual adaptation of the resulting surface to be correspondent with respect to cine-MRI series, as described in Chapter 2.

  After having gained confidence with the software and with the anatomical features of the RV structure, the time implied in the reconstruction of the surface obtained by segmentation took a minimum of 15 minutes. Then the manual adaptation of the surfaces to all available cine-MRI images took a minimum duration of 45 minutes for each surface. Therefore, an optimum value of duration for the total reconstruction

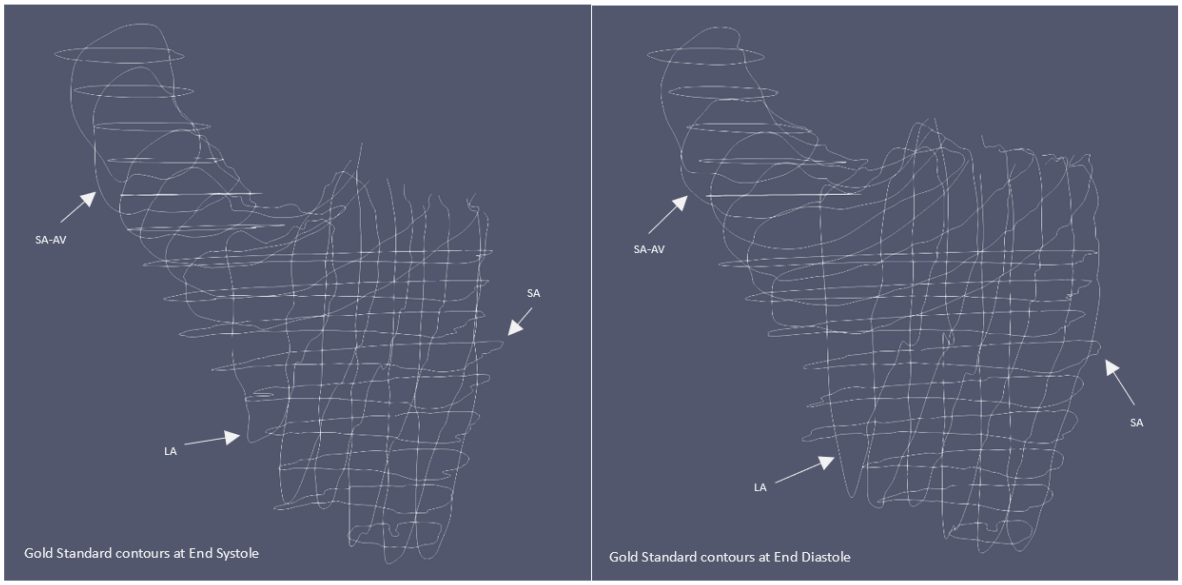

Figure 4.20: Visual representation of Gold Standard contours of Patient A at end-systolic (left) and end-diastolic (right) configurations: arrows indicate the type of cine-MRI series for segmentation. Long-Axis (LA) contours develops horizontally in parallel slices, Short-Axis (SA) has parallel contours developing vertically instead. Short-Axis Aortic Valve (SA-AV) contours are oblique, following the normal direction of the plane of aortic valve.

of the model with a standard procedure could be considered as 1 hour: the total amount of time implied resulted in 30 hours for the reconstruction of all the models along the whole cardiac cycle.

- Generation of contours with the MSMorph procedure is performed on each slice at a fixed frame by manual segmentation combined with automatic procedure of registration of contours to obtain the remaining ones and generation of the surfaces by morphing, as described in Chapter 3.

  In the present work, the time used for the manual segmentation of each slice at a fixed frame reached a maximum value of 1 hour for every cine-MRI series considered. It is important to underline that for the execution of the following registration algorithm a mask has been used: the process of mask generation is included in the considered time of 1 hour. This task requires less time as it implies the individuation of the portion of the grey-level function in which the transformation is applied to the contour. The mask should contain this portion along the entire cardiac cycle and it is generated for each slice on each cine-MRI series with less precision requested with respect to the contour delineation.

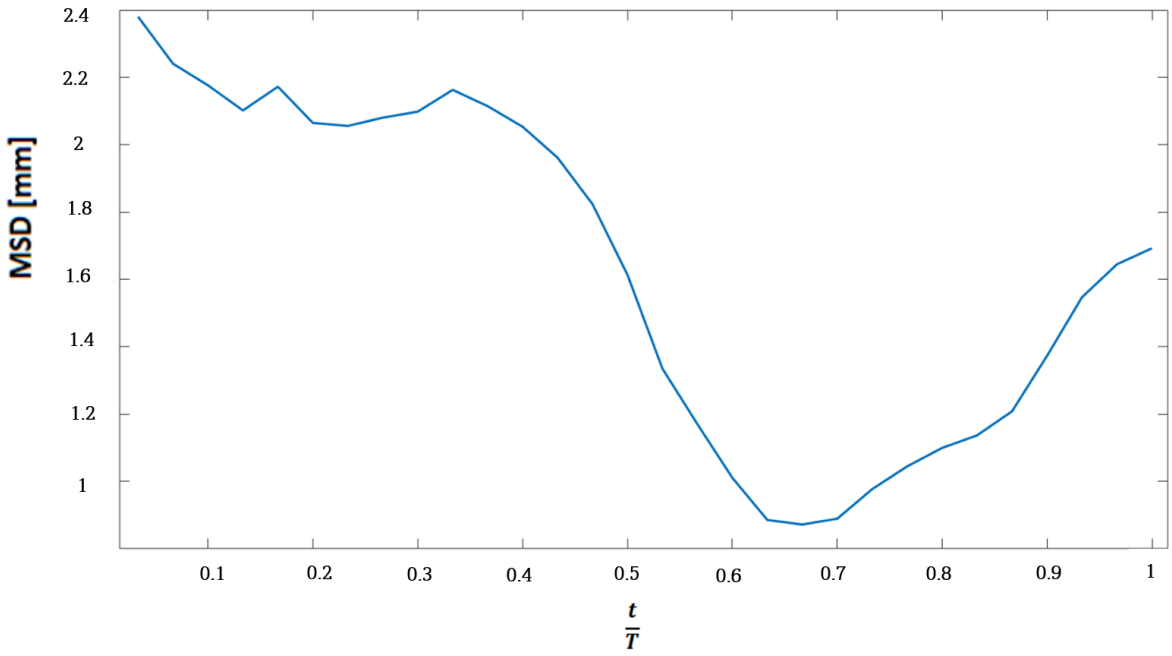

Figure 4.21: Time evolution of the Mean Square Distance along the cardiac cycle. The x axis represents the acquisition times normalized by heartbeat duration (T). These results are referred to Patient A (see Section 4.1).

The speed of the registration process, to obtain automatically the remaining contours, depends on the used machine: in this work, a virtual machine with 2 processor cores and 4GB of RAM has been used. The automatic generation of the contours with registration procedure took about 2 hours to be completed in cine-MRI series made of 6 slices, as Long-Axis and Short-Axis Aortic Valve acquisitions, while could take also 4 hours in case of Short Axis cine-MRI series that was made of 21 slices, of which only 15 were taken into account since the remaining ones did not contain information about RV structure. In particular, SA slices 1,2,3,4,20,21 were not considered in the reconstruction procedure as RV was not visible.

The surface reconstruction by morphing was very rapid as for each surface morphed with respect to a certain set of contours, a maximum time of 5 minutes was employed: this amount of time depends on the number of morphing iterations imposed by the user, that was found to be 10 and 8 respectively for MSMorph II and MSMorph III for right ventricle application. According to these considerations, the total amount of time for the reconstruction of all the surfaces during the entire cardiac cycle with the MSMorph Technique resulted in: 10.5 hours for MSMorph III and 13.5 hours for MSMorph II, as can be observed in Figure 4.22.

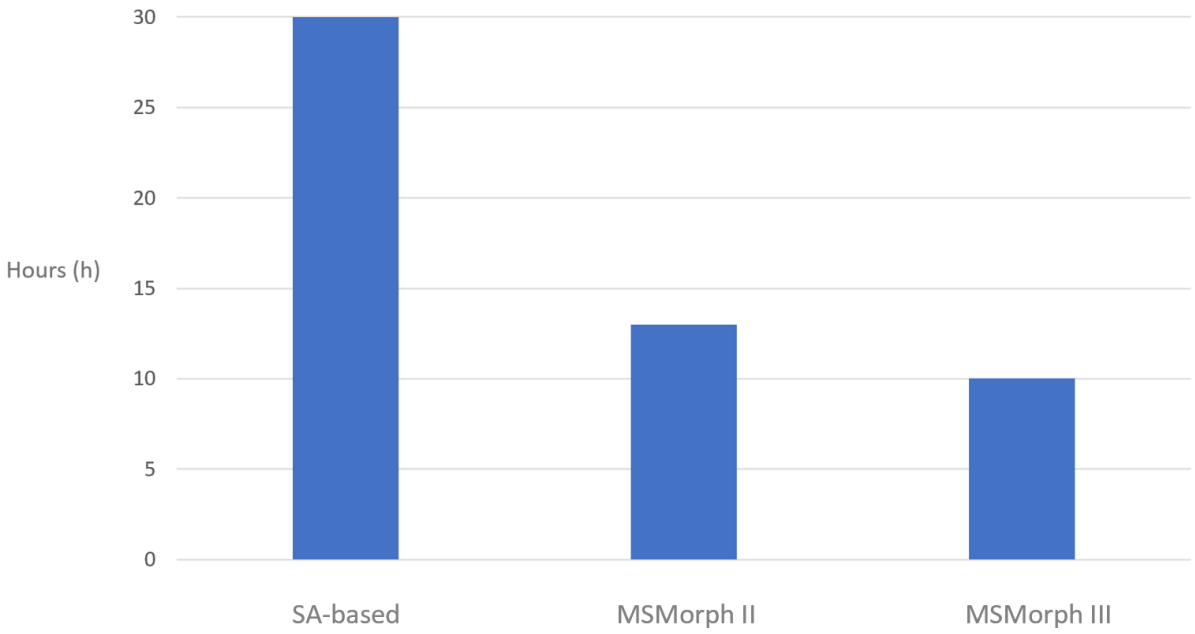

Figure 4.22: An illustrative graph representative of differences in reconstruction times for different techniques employed to reconstruct the right ventricle of Patient A (see Section 4.1).

With this observation, in the present work, the reconstruction time has been optimized by about 55%-65% with respect to the standard technique by using the MSMorph technique.

5 | Final remarks and limitations

In this work, the new reconstruction technique named Multi-Series Morphing (MSMorph) method was applied to obtain models of right and left cardiac ventricles by using merged information from different cine-MRI series. In particular, MSMorph II and MSMorph III variants of the technique were used, with different levels of merging of images, and compared with the use of a standard reconstruction techinque, which instead utilizes only short-axis MRI acquisitions. Indeed, for MSMorph variants application, other standard MRI images as Long-Axis but also specific acquisitions as the Short-Axis Aortic Valve cine-MRI series have been included, to reconstruct also right ventricle in a pathological case of Tetralogy of Fallot. The need for merging different cine-MRI images derives from the more complex shape, more difficult to segment and reconstruct, of the right ventricle (RV), with respect to left ventricle: the complexity of the morphology in the RV structure is given by a triangular shape with great cross-sectional variations along the longitudinal axis of the chamber. Also, complexity of RV increases in presence of pathological cases as Tetralogy of Fallot. Moreover, in clinical field less investigation was concentrated on right ventricle, if compared to left ventricle, but the crucial role of RV has been acknowledged in the recent years.
The major outcomes of the present work are:

- Multi-Series Morphing technique generates accurate models of morphology and wall motion of right ventricle for the entire cardiac cycle with use of merged information, provided by different acquisitions of time resolved MRI series: the comparison with models of healthy right ventricle obtained with standard reconstruction techniques, that use only one type of acquisitions, highlighted the efficiency of the MSMorph technique. Increased efficiency was exploited in the application of the MSMorph technique to obtain a biventricular model of an healthy patient: shape and motion of left ventricle have been obtained and considered for the possible effects on the right ventricle function due to ventricular interdependence.

- Multi-Series Morphing technique can be used to generated accurate models of morphology and wall motion of right ventricle of a patient affected by Tetralogy of Fallot

(ToF), since the technique relies on the merging of different cine-MRI series, some of which are specific for the monitoring of this pathological condition. From the reconstructions, RV dilation have been assessed by surface visualization and lowered wall motion with respect to healthy case have been obtained. Effects of ToF have been also assessed by computation of clinically relevant parameters.

- Multi-Series Morphing technique can generate models with accuracy comparable to contours obtained with a completely manual segmentation, representing the gold standard method for ventricles' reconstruction: efficiency of the MSMorph method is increased by the use of semi-automatic registration process for generation of endocardial contours, that allows to optimize the reconstruction time without loosing accuracy.

Besides, some limitations of the present work and possible further improvements are now discussed:

- Small cohort of patients has been analyzed: the patients considered were only two, that does not represent a number useful to generate robust results. Seen the improvement in terms of time efficiency given by the MSMorph technique with comparable accuracy, this possibility is favorable with respect to application of longer techniques.
- Multi-Series Morphing technique was used in only two variants: the use of MSMorph I variant for cardiac reconstruction can give better results in terms of accuracy but increasing the reconstruction time due to necessity to segment also Rotational-TV cine-MRI series.
- The work is limited to a morphological reconstruction with achievement of displacement, without performing image-driven CFD simulations: the use of the wall motion to simulate cardiac blood dynamics in cardiac ventricles can be useful and simpler with respect to FSI. Simulations can be generated on the biventricular model for assessment of the ventricular interdependence.
- Use of cine-MRI series that were not of standard clinical practice: the SA-AV used in application of right and left reconstruction are specific acquisitions for examination of the pathological follow-up of Tetralogy of Fallot. The use, when at disposal, of these acquisitions can be relevant for the reconstruction of the complex shape of RV.

Bibliography

[1] 3d slicer image computing platform. URL https://www.slicer.org/.

[2] Openstax anatphys fig.19.8 - ventricular muscle thickness - english labels by openstax, license: Cc by. source: book 'anatomy and physiology'. URL https://openstax.org/details/books/anatomy-and-physiology.

[3] Paraview. URL https://www.paraview.org/.

[4] The vascular modeling toolkit. URL http://www.vmtk.org/.

[5] The visualization toolkit (vtk). URL https://vtk.org/.

[6] World health organization. URL https://www.who.int/news-room/fact-sheets/detail/cardiovascular-diseases-(cvds).

[7] Autodesk meshmixer. URL https://meshmixer.com/.

[8] URL https://www.mitk.org/wiki/The_Medical_Imaging_Interaction_Toolkit_(MITK).

[9] X. Alba, R. M. Figueras i Ventura, K. Lekadir, C. Tobon-Gomez, C. Hoogendoorn, and A. F. Frangi. Automatic cardiac lv segmentation in mri using modified graph cuts with smoothness and interslice constraints. *Magnetic resonance in medicine*, 72(6):1775–1784, 2014.

[10] V. S. Aleem A, Akbar Samad AB. Emerging variants of sars-cov-2 and novel therapeutics against coronavirus (covid-19). 2023.

[11] R. S. Alipour Symakani, W. J. van Genuchten, L. M. Zandbergen, S. Henry, Y. J. Taverne, D. Merkus, W. A. Helbing, and B. Bartelds. The right ventricle in tetralogy of fallot: adaptation to sequential loading. 2023. doi: https://doi.org/10.3389/fped.2023.1098248.

[12] M. Ammar, S. Mahmoudi, M. A. Chikh, and A. Abbou. Endocardial border detection in cardiac magnetic resonance images using level set method. *Journal of digital imaging*, 25:294–306, 2012.

[13] A. Ammari, R. Mahmoudi, B. Hmida, R. Saouli, and M. H. Bedoui. A review of approaches investigated for right ventricular segmentation using short-axis cardiac mri. *IET Image Processing*, 15(9):1845–1868, 2021.

[14] C. M. Augustin, A. Crozier, A. Neic, A. J. Prassl, E. Karabelas, T. Ferreira da Silva, J. F. Fernandes, F. Campos, T. Kuehne, and G. Plank. Patient-specific modeling of left ventricular electromechanics as a driver for haemodynamic analysis. *Europace : European pacing, arrhythmias, and cardiac electrophysiology : journal of the working groups on cardiac pacing, arrhythmias, and cardiac cellular electrophysiology of the European Society of Cardiology*, 2016. doi: https://doi.org/10.1093/europace/euw369.

[15] I. B. Ayed, H.-m. Chen, K. Punithakumar, I. Ross, and S. Li. Max-flow segmentation of the left ventricle by recovering subject-specific distributions via a bound of the bhattacharyya measure. *Medical image analysis*, 16(1):87–100, 2012.

[16] S. Bae, S. R. Kim, M.-N. Kim, W. J. Shim, and S.-M. Park. Impact of cardiovascular disease and risk factors on fatal outcomes in patients with covid-19 according to age: a systematic review and meta-analysis. 2021. doi: https://doi.org/10.1136/heartjnl-2020-317901.

[17] F. Bailliard and R. H. Anderson. Tetralogy of fallot. *Orphanet journal of rare diseases*, 2009. doi: https://doi.org/10.1186/1750-1172-4-2.

[18] R. Battani, C. Corsi, A. Sarti, C. Lamberti, T. Piva, and R. Fattori. Estimation of right ventricular volume without geometrical assumptions utilizing cardiac magnetic resonance data. pages 81 – 84, 10 2003. ISBN 0-7803-8170-X. doi: 10.1109/CIC.2003.1291095.

[19] J. Bernal-Ramirez, M. C. Díaz-Vesga, M. Talamilla, A. Méndez, C. Quiroga, J. A. Garza-Cervantes, A. Lázaro-Alfaro, C. Jerjes-Sanchez, M. Henríquez, G. García-Rivas, et al. Exploring functional differences between the right and left ventricles to better understand right ventricular dysfunction. *Oxidative Medicine and Cellular Longevity*, 2021, 2021.

[20] N. K. Bodhey, P. Beerbaum, S. Sarikouch, S. Kropf, P. Lange, F. Berger, R. H. Anderson, and T. Kuehne. Functional analysis of the components of the right ventricle in the setting of tetralogy of fallot. 2008. doi: https://doi.org/10.1161/CIRCIMAGING.108.783795.

[21] D. Bos, N. Guberina, S. Zensen, M. Opitz, M. Forsting, and A. Wetter. Radiation

exposure in computed tomography. 2023. doi: https://doi.org/10.3238/arztebl.m2022.0395.

[22] M. Bucelli, A. Zingaro, P. C. Africa, I. Fumagalli, L. Dede', and A. Quarteroni. A mathematical model that integrates cardiac electrophysiology, mechanics, and fluid dynamics: Application to the human left heart. *nternational journal for numerical methods in biomedical engineering*, 2023. doi: https://doi.org/10.1002/cnm.3678.

[23] G. D. Buckberg, J. I. Hoffman, H. C. Coghlan, and N. C. Nanda. Ventricular structure-function relations in health and disease: Part i. the normal heart. *European journal of cardio-thoracic surgery : official journal of the European Association for Cardio-thoracic Surgery*, 2015. doi: https://doi.org/10.1093/ejcts/ezu278.

[24] E. Carmel and D. Cohen-Or. Warp-guided object-space morphing. *Visual Computer*, 13(9):465, 1997.

[25] L. Cavigli, M. Focardi, M. Cameli, G. E. Mandoli, S. Mondillo, and F. D'Ascenzi. The right ventricle in "left-sided" cardiomyopathies: The dark side of the moon. *Trends in Cardiovascular Medicine*, 31(8):476–484, 2021. ISSN 1050-1738. doi: https://doi.org/10.1016/j.tcm.2020.10.003. URL `https://www.sciencedirect.com/science/article/pii/S1050173820301262`.

[26] D. Collia, L. Zovatto, G. Tonti, and G. Pedrizzetti. Comparative analysis of right ventricle fluid dynamics. 2021. doi: https://doi.org/10.3389/fbioe.2021.667408.

[27] C. Constantinides, Y. Chenoune, N. Kachenoura, E. Roullot, E. Mousseaux, A. Herment, and F. Frouin. Semi-automated cardiac segmentation on cine magnetic resonance images using gvf-snake deformable models. *The MIDAS Journal-Cardiac MR Left Ventricle Segmentation Challenge*, 77, 2009.

[28] E. Criseo. Computational hemodynamics for pulmonary valve replacement by means of a reduced fluid-structure interaction model. Master's thesis, Politecnico di Milano, 2022.

[29] M. Dandel. Heart–lung interactions in covid-19: Prognostic impact and usefulness of bedside echocardiography for monitoring of the right ventricle involvement. *Heart Failure Reviews*, 27(4):1325–1339, 2022.

[30] N. Das and S. Das. A review on right ventricle cardiac mri segmentation. *Computer Methods in Biomechanics and Biomedical Engineering: Imaging & Visualization*, 11(4):1348–1358, 2023.

[31] H. El-Rewaidy and A. S. Fahmy. Segmentation of the right ventricle in mr images

using dual active shape model in the bookstein coordinates. In *2015 IEEE 12th International Symposium on Biomedical Imaging (ISBI)*, pages 1320–1323. IEEE, 2015.

[32] M. Fedele and A. Quarteroni. Polygonal surface processing and mesh generation tools for the numerical simulation of the cardiac function. *International journal for numerical methods in biomedical engineering*, 37, 2021. doi: https://doi.org/10.1002/cnm.3435.

[33] A. Fetzer, S. Zelzer, T. Schroeder, H.-P. Meinzer, and M. Nolden. An interactive 3d segmentation for the medical imaging interaction toolkit (mitk). *Proc. MICCAI Interactive Medical Image Computing*, pages 1–11, 2014.

[34] T. G. Flohr, R. Raupach, and H. Bruder. Cardiac ct: how much can temporal resolution, spatial resolution, and volume coverage be improved? *Journal of cardiovascular computed tomography*, 2009. doi: https://doi.org/10.1016/j.jcct.2009.04.004.

[35] N. Forsch, S. Govil, J. C. Perry, S. Hegde, A. A. Young, J. H. Omens, and A. D. McCulloch. Computational analysis of cardiac structure and function in congenital heart disease: Translating discoveries to clinical strategies. *Journal of computational science*, 2021. doi: https://doi.org/10.1016/j.jocs.2020.101211.

[36] M. K. Friedberg and A. N. Redington. Right versus left ventricular failure: differences, similarities, and interactions. *Circulation*, 129(9):1033–1044, 2014.

[37] I. Fumagalli, M. Fedele, C. Vergara, S. Ippolito, F. Nicolò, C. Antona, R. Scrofani, A. Quarteroni, et al. An image-based computational hemodynamics study of the systolic anterior motion of the mitral valve. 2020. doi: https://doi.org/10.1016/j.compbiomed.2020.103922.

[38] K. Gilbert, W. Bai, C. Mauger, P. Medrano-Gracia, A. Suinesiaputra, A. M. Lee, M. M. Sanghvi, N. Aung, S. K. Piechnik, S. Neubauer, et al. Independent left ventricular morphometric atlases show consistent relationships with cardiovascular risk factors: A uk biobank study. *Scientific Reports*, 2019. doi: https://doi.org/10.1038/s41598-018-37916-6.

[39] A. Goshtasby and D. A. Turner. Segmentation of cardiac cine mr images for extraction of right and left ventricular chambers. *IEEE transactions on medical imaging*, 14(1):56–64, 1995.

[40] M. D. Grant, R. D. Mann, S. D. Kristenson, R. M. Buck, J. D. Mendoza, J. M. Reese, D. W. Grant, and E. A. Roberge. Transthoracic echocardiography: Beginner's guide

with emphasis on blind spots as identified with ct and mri. 2021. doi: https://doi.org/10.1148/rg.2021200142.

[41] C. R. Greyson. Evaluation of right ventricular function. *Current Cardiology Reports*, 2011.

[42] N. Groun, M. Villalba-Orero, E. Lara-Pezzi, E. Valero, J. Garicano-Mena, and S. Le Clainche. A novel data-driven method for the analysis and reconstruction of cardiac cine mri. 2022. doi: https://doi.org/10.1016/j.compbiomed.2022.106317.

[43] S. Y. Ho. Anatomy and myoarchitecture of the left ventricular wall in normal and in disease. *European Journal of Echocardiography*, 10(8):iii3–iii7, 12 2009. ISSN 1525-2167. doi: 10.1093/ejechocard/jep159. URL `https://doi.org/10.1093/ejechocard/jep159`.

[44] H. Hu, H. Liu, Z. Gao, and L. Huang. Hybrid segmentation of left ventricle in cardiac mri using gaussian-mixture model and region restricted dynamic programming. *Magnetic resonance imaging*, 31(4):575–584, 2013.

[45] J. Hu, L. Liu, and G. Wang. Dual laplacian morphing for triangular meshes. *Computer Animation and Virtual Worlds*, 18(4-5):271–277, 2007.

[46] S. Huang, J. Liu, L. C. Lee, S. K. Venkatesh, L. L. S. Teo, C. Au, and W. L. Nowinski. An image-based comprehensive approach for automatic segmentation of left ventricle from cardiac short axis cine mr images. *Journal of digital imaging*, 24: 598–608, 2011.

[47] D. G. Hurrell, R. A. Nishimura, S. T. Higano, C. P. Appleton, G. K. Danielson, D. R. Holmes Jr, and A. J. Tajik. Value of dynamic respiratory changes in left and right ventricular pressures for the diagnosis of constrictive pericarditis. *Circulation*, 93(11):2007–2013, 1996.

[48] V. Jani, L. Li, M. Craft, F. Veronesi, N. Khoo, D. Danford, D. Muraru, and S. Kutty. Semi-automated quantification of tricuspid valve dynamics and structure in tetralogy of fallot and hypoplastic left heart syndrome using three-dimensional echocardiography. *Echo Research & Practice*, 10(1):10, 2023.

[49] M.-P. Jolly. Automatic segmentation of the left ventricle in cardiac mr and ct images. *International Journal of Computer Vision*, 70(2):151–163, 2006.

[50] K. U. Juergens and R. Fischbach. Left ventricular function studied with mdct. *European radiology*, 16:342–357, 2006.

[51] N. Kawel-Boehm, S. J. Hetzel, B. Ambale-Venkatesh, G. Captur, C. J. Francois, M. Jerosch-Herold, M. Salerno, S. D. Teague, E. Valsangiacomo-Buechel, R. J. Van der Geest, et al. Reference ranges ("normal values") for cardiovascular magnetic resonance (cmr) in adults and children: 2020 update. *Journal of cardiovascular magnetic resonance*, 22(1):1–63, 2020.

[52] J. R. Kent, W. E. Carlson, and R. E. Parent. Shape transformation for polyhedral objects. *ACM SIGGRAPH Computer Graphics*, 26(2):47–54, 1992.

[53] P. L. Kerkhof, P. M. van de Ven, B. Yoo, R. A. Peace, G. R. Heyndrickx, and N. Handly. Ejection fraction as related to basic components in the left and right ventricular volume domains. *International journal of cardiology*, 255:105–110, 2018.

[54] J. Y. Kim, Y. J. Suh, K. Han, Y. J. Kim, and B. W. Choi. Cardiac ct for measurement of right ventricular volume and function in comparison with cardiac mri: A meta-analysis. *Korean journal of radiology*, 2020. doi: https://doi.org/10.3348/kjr.2019.0499.

[55] W. Kim, J. G. Kwak, S. Cho, and W.-H. Kim. Ten years follow-up of dilatation of aortic structures in fallot type anomalies. 2023.

[56] S. Klein and M. Staring. *elastix the manual*.

[57] S. Klein, M. Staring, K. Murphy, M. A. Viergever, and J. P. W. Pluim. elastix: A toolbox for intensity-based medical image registration. *IEEE Transactions on Medical Imaging*, 29(1):196–205, 2010. doi: 10.1109/TMI.2009.2035616.

[58] G. Kovacs, A. Berghold, S. Scheidl, and H. Olschewski. Pulmonary arterial pressure during rest and exercise in healthy subjects: a systematic review. *European Respiratory Journal*, 34(4):888–894, 2009. ISSN 0903-1936. doi: 10.1183/09031936.00145608. URL `https://erj.ersjournals.com/content/34/4/888`.

[59] U. Kurkure, A. Pednekar, R. Muthupillai, S. D. Flamm, and I. A. Kakadiaris. Localization and segmentation of left ventricle in cardiac cine-mr images. *IEEE transactions on biomedical engineering*, 56(5):1360–1370, 2008.

[60] F. Lazarus and A. Verroust. Three-dimensional metamorphosis: a survey. *The Visual Computer*, 14(8-9):373–389, 1998.

[61] H. Lester and S. R. Arridge. A survey of hierarchical non-linear medical image registration. *Pattern recognition*, 32(1):129–149, 1999.

[62] W. C. Little and J. K. Oh. Echocardiographic evaluation of diastolic function can be used to guide clinical care. *Circulation*, 120(9):802–809, 2009.

[63] N. Liu, W. Strugnell, R. Slaughter, R. Riley, S. Crozier, S. Wilson, F. Liu, B. Appleton, A. Trakic, and Q. Wei. Right ventricle extraction by low level and model-based algorithm. In *2005 IEEE Engineering in Medicine and Biology 27th Annual Conference*, pages 1607–1610, 2005. doi: 10.1109/IEMBS.2005.1616745.

[64] J. Lötjönen and T. Mäkelä. Elastic matching using a deformation sphere. In *International Conference on Medical Image Computing and Computer-Assisted Intervention*, pages 541–548. Springer, 2001.

[65] X. Lu, Y. Wang, B. Georgescu, A. Littman, and D. Comaniciu. Automatic delineation of left and right ventricles in cardiac mri sequences using a joint ventricular model. In *Functional Imaging and Modeling of the Heart: 6th International Conference, FIMH 2011, New York City, NY, USA, May 25-27, 2011. Proceedings 6*, pages 250–258. Springer, 2011.

[66] Y.-L. Lu, K. A. Connelly, A. J. Dick, G. A. Wright, and P. E. Radau. Automatic functional analysis of left ventricle in cardiac cine mri. *Quantitative imaging in medicine and surgery*, 3(4):200, 2013.

[67] M. Lynch, O. Ghita, and P. F. Whelan. Segmentation of the left ventricle of the heart in 3-d+ t mri data using an optimized nonrigid temporal model. *IEEE Transactions on Medical Imaging*, 27(2):195–203, 2008.

[68] J. Maintz and M. A. Viergever. A survey of medical image registration. *Medical Image Analysis*, 2(1):1–36, 1998. ISSN 1361-8415. doi: https://doi.org/10.1016/S1361-8415(01)80026-8. URL `https://www.sciencedirect.com/science/article/pii/S1361841501800268`.

[69] T. Mansi, I. Voigt, B. Leonardi, X. Pennec, S. Durrleman, M. Sermesant, H. Delingette, A. M. Taylor, Y. Boudjemline, G. Pongiglione, et al. A statistical model for quantification and prediction of cardiac remodelling: application to tetralogy of fallot. 2011. doi: https://doi.org/10.1109/TMI.2011.2135375.

[70] S. C. Mitchell, J. G. Bosch, B. P. Lelieveldt, R. J. Van der Geest, J. H. Reiber, and M. Sonka. 3-d active appearance models: segmentation of cardiac mr and ultrasound images. *IEEE transactions on medical imaging*, 21(9):1167–1178, 2002.

[71] O. Moolan-Feroze, M. Mirmehdi, and M. Hamilton. Right ventricle segmentation

using a 3d cylindrical shape model. In *2016 IEEE 13th International Symposium on Biomedical Imaging (ISBI)*, pages 44–48. IEEE, 2016.

[72] F. Odille, A. Bustin, S. Liu, B. Chen, P.-A. Vuissoz, J. Felblinger, and L. Bonnemains. Isotropic 3 d cardiac cine mri allows efficient sparse segmentation strategies based on 3 d surface reconstruction. *Magnetic resonance in medicine*, 79(5): 2665–2675, 2018.

[73] J. A. Oscanoa, M. J. Middione, C. Alkan, M. Yurt, M. Loecher, S. S. Vasanawala, and D. B. Ennis. Deep learning-based reconstruction for cardiac mri: A review. 2023. doi: https://doi.org/10.3390/bioengineering10030334.

[74] Y. Ou, J. Doshi, G. Erus, and C. Davatzikos. Multi-atlas segmentation of the cardiac mr right ventricle. *Proceedings of 3D Cardiovascular Imaging: A MICCAI Segmentation Challenge*, 2012.

[75] A. Pednekar, U. Kurkure, R. Muthupillai, S. Flamm, and I. A. Kakadiaris. Automated left ventricular segmentation in cardiac mri. *IEEE Transactions on Biomedical Engineering*, 53(7):1425–1428, 2006.

[76] P. Peng, K. Lekadir, A. Gooya, L. Shao, S. E. Petersen, and A. F. Frangi. A review of heart chamber segmentation for structural and functional analysis using cardiac magnetic resonance imaging. 2016. doi: https://doi.org/10.1007/s10334-015-0521-4.

[77] K. Penska, L. Folio, and R. Bunger. Medical applications of digital image morphing. *Journal of digital imaging*, 20:279–283, 2007.

[78] S. E. Petersen, N. Aung, M. M. Sanghvi, F. Zemrak, K. Fung, J. M. Paiva, J. M. Francis, M. Y. Khanji, E. Lukaschuk, A. M. Lee, et al. Reference ranges for cardiac structure and function using cardiovascular magnetic resonance (cmr) in caucasians from the uk biobank population cohort. *Journal of cardiovascular magnetic resonance*, 19(1):1–19, 2017.

[79] C. Petitjean and J.-N. Dacher. A review of segmentation methods in short axis cardiac mr images. 2011. doi: https://doi.org/10.1016/j.media.2010.12.004.

[80] K. Punithakumar, M. Noga, I. B. Ayed, and P. Boulanger. Right ventricular segmentation in cardiac mri with moving mesh correspondences. *Computerized Medical Imaging and Graphics*, 43:15–25, 2015.

[81] S. Queirós, D. Barbosa, B. Heyde, P. Morais, J. L. Vilaça, D. Friboulet, O. Bernard,

and J. D'hooge. Fast automatic myocardial segmentation in 4d cine cmr datasets. *Medical image analysis*, 18(7):1115–1131, 2014.

[82] S. Rao, P. Madueme, D. Podberesky, and M. J. Cartoski. Cardiac magnetic resonance imaging and computed tomography for the pediatric cardiologist. *Progress in Pediatric Cardiology*, 58:101273, 2020. ISSN 1058-9813. doi: https://doi.org/10.1016/j.ppedcard.2020.101273. URL `https://www.sciencedirect.com/science/article/pii/S1058981320301429`. Pediatric Echocardiography.

[83] R. A. Rehman I. *Anatomy, Thorax, Heart*. StatPearls.

[84] F. Renzi, C. Vergara, M. Fedele, V. Giambruno, A. Quarteroni, G. Puppini, and G. B. Luciani. Accurate and efficient 3d reconstruction of right heart shape and motion from multi-series cine-mri. 06 2023. doi: 10.1101/2023.06.28.546872.

[85] J. Ringenberg, M. Deo, V. Devabhaktuni, D. Filgueiras-Rama, G. Pizarro, B. Ibañez, O. Berenfeld, P. Boyers, and J. Gold. Automated segmentation and reconstruction of patient-specific cardiac anatomy and pathology from in vivo mri. *Measurement Science and Technology*, 23(12):125405, 2012.

[86] J. Ringenberg, M. Deo, D. Filgueiras-Rama, G. Pizarro, B. Ibañez, R. Peinado, J. L. Merino, O. Berenfeld, and V. Devabhaktuni. Effects of fibrosis morphology on reentrant ventricular tachycardia inducibility and simulation fidelity in patient-derived models. *Clinical Medicine Insights. Cardiology*, 2014. doi: https://doi.org/10.4137/CMC.S15712.

[87] d. V. B. D. B. S. P. N. V. M. A. L. T. Sander, J. Reconstruction and completion of high-resolution 3d cardiac shapes using anisotropic cmri segmentations and continuous implicit neural representations. 2023. doi: https://doi.org/10.1016/j.compbiomed.2023.107266.

[88] W. P. Santamore and L. J. Dell'Italia. Ventricular interdependence: significant left ventricular contributions to right ventricular systolic function. *Progress in cardiovascular diseases*, 40(4):289–308, 1998.

[89] M. Santarelli, V. Positano, C. Michelassi, M. Lombardi, and L. Landini. Automated cardiac mr image segmentation: theory and measurement evaluation. *Medical engineering & physics*, 25(2):149–159, 2003.

[90] J. Sanz, D. Sánchez-Quintana, E. Bossone, H. J. Bogaard, and R. Naeije. Anatomy, function, and dysfunction of the right ventricle: Jacc state-of-the-art review. 2019.

[91] J. Schaerer, C. Casta, J. Pousin, and P. Clarysse. A dynamic elastic model for

segmentation and tracking of the heart in mr image sequences. *Medical Image Analysis*, 14(6):738–749, 2010.

[92] A. Seraphim, K. D. Knott, J. Augusto, A. N. Bhuva, C. Manisty, and J. C. Moon. Quantitative cardiac mri. *Journal of magnetic resonance imaging*, 2020. doi: https://doi.org/10.1002/jmri.26789.

[93] F. H. Sheehan, S. Ge, G. W. Vick III, K. Urnes, W. S. Kerwin, E. L. Bolson, T. Chung, J. P. Kovalchin, D. J. Sahn, M. Jerosch-Herold, et al. Three-dimensional shape analysis of right ventricular remodeling in repaired tetralogy of fallot. *The American journal of cardiology*, 101(1):107–113, 2008.

[94] L. Shmuylovich, C. S. Chung, and S. J. Kovács. Point: Left ventricular volume during diastasis is the physiological in vivo equilibrium volume and is related to diastolic suction. *Journal of applied physiology*, 109(2):606–608, 2010.

[95] H. Stubbs, A. MacLellan, S. Lua, H. Dormand, and C. Church. The right ventricle under pressure: Anatomy and imaging in sickness and health. *Journal of anatomy*, 2023. doi: https://doi.org/10.1111/joa.13654.

[96] P. Thévenaz and M. Unser. Optimization of mutual information for multiresolution image registration. *IEEE transactions on image processing*, 9(12):2083–2099, 2000.

[97] H. C. Van Assen, M. G. Danilouchkine, A. F. Frangi, S. Ordás, J. J. Westenberg, J. H. Reiber, and B. P. Lelieveldt. Spasm: a 3d-asm for segmentation of sparse and arbitrarily oriented cardiac mri data. *Medical image analysis*, 10(2):286–303, 2006.

[98] P. M. van Dam, J. P. Gordon, M. M. Laks, and N. G. Boyle. Development of new anatomy reconstruction software to localize cardiac isochrones to the cardiac surface from the 12 lead ecg. *Journal of Electrocardiology*, 48(6):959–965, 2015.

[99] J. P. van der Ven, E. van den Bosch, A. J. Bogers, and W. A. Helbing. Current outcomes and treatment of tetralogy of fallot. 2019. doi: https://doi.org/10.12688/f1000research.17174.1.

[100] L. Velho, A. C. Frery, and J. Gomes. *Image processing for computer graphics and vision*. Springer Science & Business Media, 2009.

[101] B. Villard, V. Grau, and E. Zacur. Surface mesh reconstruction from cardiac mri contours. *Journal of Imaging*, 4(1), 2018. ISSN 2313-433X. doi: 10.3390/jimaging4010016. URL `https://www.mdpi.com/2313-433X/4/1/16`.

[102] B. Villard, V. Grau, and E. Zacur. Surface mesh reconstruction from cardiac mri contours. *Journal of Imaging*, 4(1):16, 2018.

[103] Y. Wang, Y. Zhang, W. Xuan, E. Kao, P. Cao, B. Tian, K. Ordovas, D. Saloner, and J. Liu. Fully automatic segmentation of 4d mri for cardiac functional measurements. *Medical physics*, 46(1):180–189, 2019.

[104] X. Yang, S. Y. Yeo, Y. Su, C. Lim, M. Wan, L. Zhong, and R. San Tan. Right ventricle segmentation by temporal information constrained gradient vector flow. In *2013 IEEE International Conference on Systems, Man, and Cybernetics*, pages 2551–2555. IEEE, 2013.

List of Figures

List of Tables

Acknowledgements

I would like to express my sincere gratitude to my advisor Prof. Christian Vergara and my co-advisor Ing. Francesca Renzi for their assistance at every stage of the research project.
I would like to deeply thank my parents, whom without this would have not been possible.
I am deeply grateful also to my sister Camilla: even if being often far from home, she managed to make me feel as she was always very close to me.
I would like to express my heartfelt thanks to Alessandro, who helped me throughout the entire university journey with all the love possible, sharing with me all good but also bad moments with unwavering support.
I would also like to thank my special friend Clarissa, who always helped me with kind words, which strengthen my soul.
I wish to show my appreciation to Chiara and Vittorio: from the very first days of this growth path, they have been true friends and source of joy.
A thought is for Pamela and also for ENPA in the section of Monza e Brianza: they showed me great comprehension in the last intense period of this path. With them, all my animal friends, especially my cats, that have always been in my heart.